



Data-Driven Retrospective Cost Adaptive Control for Flight Control Applications

Syed Aseem Ul Islam,* Tam W. Nguyen,† Ilya V. Kolmanovsky,‡ and Dennis S. Bernstein§
 University of Michigan, Ann Arbor, Michigan 48109

<https://doi.org/10.2514/1.G005778>

Unlike fixed-gain robust control, which trades off performance with modeling uncertainty, direct adaptive control uses partial modeling information for online tuning. The present paper combines retrospective cost adaptive control (RCAC), a direct adaptive control technique for sampled-data systems, with online system identification based on recursive least squares (RLS) with variable-rate forgetting (VRF). The combination of RCAC and RLS-VRF constitutes data-driven RCAC (DDRCAC), where the online system identification is used to construct the target model, which defines the retrospective performance variable. This paper investigates the ability of RLS-VRF to provide the modeling information needed for the target model, especially non-minimum-phase (NMP) zeros. DDRCAC is applied to single-input, single-output and multiple-input, multiple-output numerical examples with unknown NMP zeros, as well as several flight control problems, namely, unknown transition from minimum phase to NMP lateral dynamics, flexible modes, flutter, and nonlinear planar missile dynamics.

Nomenclature

E	= performance-variable selection matrix	$R_z, R_u, R_{\Delta u}$	= $E_z^T E_z, E_u^T E_u, E_{\Delta u}^T E_{\Delta u}$
$E_z, E_u, E_{\Delta u}$	= performance, control, and control-move weighting	r_k	= command
FIA	= frozen input argument	s	= Laplace transform variable
I_l	= $l \times l$ identity matrix	T_s	= sample time
k	= step	t	= time
\bar{k}	= fixed step with respect to \mathbf{q}	$u(t)$	= control
l	= dimension of $w(t)$ and w_k	u_k	= sampled control
$l_y, l_{\theta_c}, l_{\theta_m}, l_{\bar{\theta}}$	= dimensions of $\tilde{y}_k, \theta_{c,k}, \theta_{m,k}$, and $\bar{\theta}_k$	\bar{u}	= saturation level for recursive least squares-based adaptive control
m	= dimension of $u(t)$ and u_k	$v(t)$	= sensor noise
n	= dimension of $x(t)$	vec	= column-stacking operator
n_c	= controller window length	v_k	= sampled sensor noise
p	= dimension of $y(t), y_k, y_{w,k}, y_{u,k}$, and $y_{0,k}$	$w(t)$	= disturbance
$p_{c,0}$	= retrospective cost adaptive control and data-driven retrospective cost adaptive control tuning parameter	$\bar{w}_{k,i}$	= constant disturbance during intersample subinterval
$p_{m,0}$	= recursive least squares-based identification tuning parameter	$x(t)$	= state
Q_{wv}	= disturbance and sensor noise covariance matrix for linear-quadratic-Gaussian design	$y(t)$	= noisy measurement
Q_{xu}	= state and control weight matrix for linear-quadratic-Gaussian design	y_k	= sampled noisy measurement
q	= dimension of $y_{z,k}$ and r_k	\tilde{y}_k	= input vector of controller
\mathbf{q}	= forward-shift operator	$y_{z,k}$	= performance variable
$\mathbb{R}(\mathbf{q})_{\text{prop}}^{l_1 \times l_2}$	= $l_1 \times l_2$ proper, discrete-time transfer functions	$y_0(t)$	= noise-free system output
$\mathbb{R}(s)_{\text{prop}}^{l_1 \times l_2}$	= $l_1 \times l_2$ proper, transfer functions	$y_{0,k}$	= noise-free sampled output due to $u(t)$ and $w(t)$
$\mathbb{R}[\mathbf{z}]_{\text{prop}}^{l_1 \times l_2}$	= $l_1 \times l_2$ polynomial matrix in \mathbf{z}	\mathbf{z}	= Z-transform variable
$\mathbb{R}(\mathbf{z})_{\text{prop}}^{l_1 \times l_2}$	= $l_1 \times l_2$ proper, discrete-time transfer functions	z_k	= command-following error and adaptation variable
		η	= recursive least squares-based identification window length
		$\theta_{c,k}$	= controller coefficient vector
		$\theta_{m,k}$	= model coefficient vector
		$\bar{\theta}_k$	= minimizer of recursive least squares with variable-rate forgetting
		$\lambda_{c,k}$	= recursive least squares-based adaptive control variable-rate forgetting factor
		$\lambda_{m,k}$	= recursive least squares-based identification variable-rate forgetting factor
		σ_{max}	= maximum singular value
		τ_d	= denominator window length for variable-rate forgetting
		τ_n	= numerator window length for variable-rate forgetting
		\otimes	= Kronecker product
		$\ \cdot\ _{\infty}, \ \cdot\ , \cdot $	= H_{∞} norm, L_2 norm, absolute value
		\setminus, \cup	= set minus, set union
		$\mathbf{1}[\cdot]$	= step function that is 0 for negative arguments and 1 otherwise
		$\mathbf{1}_{l_1 \times l_2}$	= $l_1 \times l_2$ matrix of 1 s

Received 8 November 2020; revision received 31 March 2021; accepted for publication 1 April 2021; published online 11 August 2021. Copyright © 2021 by the American Institute of Aeronautics and Astronautics, Inc. All rights reserved. All requests for copying and permission to reprint should be submitted to CCC at www.copyright.com; employ the eISSN 1533-3884 to initiate your request. See also AIAA Rights and Permissions www.aiaa.org/randp.

*Graduate Student, Aerospace Engineering, 1320 Beal Avenue; aseemisl@umich.edu (Corresponding Author).

†Post-Doctoral Researcher, Aerospace Engineering, 1320 Beal Avenue; twnguyen@umich.edu.

‡Professor, Aerospace Engineering, 1320 Beal Avenue; ilya@umich.edu. Associate Fellow AIAA.

§Professor, Aerospace Engineering, 1320 Beal Avenue; dsbaero@umich.edu.

I. Introduction

IN DIRECT adaptive control, the controller gains are updated in response to the actual dynamics of the controlled system. Unlike fixed-gain robust control, which trades off performance with prior modeling uncertainty, direct adaptive control uses partial modeling information for online self-tuning. Direct adaptive control is especially of interest for time-varying systems [1,2]. The theory of direct adaptive control has been extensively developed [3–6], and numerous successful applications to aerospace systems have been reported [7,8]. The research challenge in direct adaptive control is to determine the minimal modeling information needed to facilitate fast, accurate, and reliable control.

As an alternative to direct adaptive control, indirect adaptive control performs online identification to update the required modeling information for use by a fixed-gain controller ([4] pp. 397, 467 and [5] Chap. 7). The combination of online identification and fixed-gain control is justified by the certainty equivalence principle ([9 p. 2738]). Indirect adaptive control is advantageous for applications where the required modeling information is either difficult or impossible to obtain before operation due, for example, to unpredictable changes in the dynamics of the controlled system. By further reducing the dependence on prior modeling, indirect adaptive control facilitates control under extremely limited a priori modeling information. Indirect adaptive control can thus be viewed as a further step in the evolution of control from strong model dependence to model-free control.

Model-free control is a longstanding goal in control theory, and the challenges are far from trivial. In particular, data-driven control [10,11] seeks to circumvent the need for a model using data. Furthermore, the interplay between identification and control is a longstanding problem in control theory [12–14]. This interplay is addressed by dual control, where the objective is to determine probing signals that enhance the speed and accuracy of the concurrent identification [15–17].

The present paper focuses on retrospective cost adaptive control (RCAC), which is a direct adaptive control technique for discrete-time and sampled-data systems [18–20]. The modeling information required by RCAC resides in the target model, which serves as an essential model of the closed-loop transfer function from the virtual external control perturbation to the retrospective performance variable. As shown in [20], the essential modeling information for discretized single-input, single-output (SISO) plants includes the sign of the leading numerator coefficient, the relative degree, and all non-minimum-phase (NMP) zeros. Numerical examples show that, under sufficiently aggressive tuning, RCAC may cancel unmodeled NMP zeros [21].

The goal of the present paper is to extend RCAC by incorporating online model identification; this method is called *data-driven RCAC* (DDRCAC). DDRCAC depends on system identification performed concurrently with controller adaptation, where the modeling details are extracted from the identified model in order to construct the target model. Because RCAC is based on recursive least squares (RLS) to update the controller coefficients, RLS is also used for system identification within DDRCAC. Unlike standard least squares, which uses constant-rate forgetting [22], online identification in the present paper takes advantage of RLS with variable-rate forgetting (VRF) [23].

Note that DDRCAC uses online identification to obtain the modeling information needed by RCAC, which is a direct adaptive control technique. Consequently, DDRCAC is neither a direct adaptive control technique, which requires limited but precise modeling information, nor an indirect adaptive control, which requires modeling information in accordance with certainty equivalence. DDRCAC can thus be viewed as a hybrid direct/indirect adaptive control method that uses online system identification to obtain approximate, limited modeling information required by a direct adaptive control algorithm.

To assist in analyzing the effectiveness of DDRCAC and to obtain deeper insight into the modeling information required by the target model, the present paper shows that the retrospective performance

variable can be decomposed into the sum of a performance term and a model-matching term. The performance term consists of a closed-loop transfer function, whereas the model-matching term involves the difference between a closed-loop transfer function and the target model driven by the virtual external control perturbation. A crucial insight arises from the observation that, at each step, RLS minimizes the magnitude of the retrospective performance variable by forcing the performance term and the model-matching term to have similar magnitudes but opposite signs. As the controller converges, the virtual external control perturbation, and thus the model-matching term, converges to zero, which, in turn, drives the performance term to zero. By preventing the performance term from diverging when the controller converges, this mechanism prevents RLS from converging to a controller that is destabilizing or has poor performance. The decomposition of the retrospective performance variable is used in this paper to elucidate the mechanism described above and diagnose the performance of DDRCAC.

As in all applications of system identification, persistency is needed to guarantee that the identified model captures the true system dynamics [24–26]. Persistency may be provided by the commands and disturbances, or it may be self-generated by the controller. Beyond persistency, because online identification and learning occur during closed-loop operation, the control input is correlated with the measurements due to disturbances and sensor noise. When RLS is used for closed-loop identification, as in the present paper, this correlation may obstruct *consistency* and thus lead to asymptotic bias in the parameter estimates [27–29]. Alternative identification methods, such as instrumental variables, provide consistency despite signal correlation, although at higher computational cost [30].

The present paper describes the elements of DDRCAC and investigates the effectiveness of this approach on numerical examples. These examples include synthetic examples that emphasize specific challenges as well as illustrative flight-control problems. The synthetic examples are focused on three key issues, namely, NMP zeros, consistency, and persistency. Because, as noted above, RCAC may cancel unmodeled NMP zeros, the highest priority is to extract information about the NMP zeros from the identified model; this information is embedded in the numerator of the identified model, which, in the case of a multiple-input, multiple-output (MIMO) system, is a matrix polynomial. These examples are motivated by the fact, as noted in [8], that the stability of finite transmission zeros is a standard assumption in output-feedback adaptive control. Furthermore, because lack of consistency may occur when RLS is used for closed-loop system identification, the effect of bias is examined. In particular, the bias arising from sensor noise within closed-loop system identification under DDRCAC is shown to be less severe than the bias arising from sensor noise within closed-loop system identification under fixed-gain control. Finally, in cases where the commands and disturbances provide limited persistency, these examples highlight self-generated persistency, that is, persistency due to the controller.

This paper applies DDRCAC to four flight-control examples. First, adaptive control is applied to roll-angle command following for a hypersonic aircraft that undergoes an unknown transition from minimum phase (MP) to NMP dynamics. Second, adaptive control is applied for pitch-rate command following of a flexible aircraft, which has 12 lightly damped modes. Third, adaptive control is applied for flutter suppression of the benchmark active control technology (BACT) wing. Finally, adaptive control is applied to normal-acceleration command following for a nonlinear planar missile.

II. Sampled-Data Adaptive-Control Architecture

All of the examples in this paper consider continuous-time systems under sampled-data control using discrete-time adaptive controllers. In particular, consider the adaptive control architecture shown in Fig. 1, where a realization of $G(s) \triangleq [G_u(s)G_w(s)]$ is given by

$$\dot{x}(t) = Ax(t) + Bu(t) + B_w w(t) \quad (1)$$

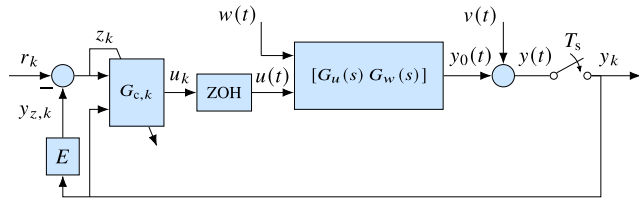


Fig. 1 Command following and disturbance rejection under sampled-data adaptive control. The objective is to follow commands r_k to the performance variable $y_{z,k} = Ey_k$. All sample-and-hold operations are synchronous.

$$y(t) = Cx(t) + D_u u(t) + v(t) \tag{2}$$

where $x(t) \in \mathbb{R}^n$ is the state, $u(t) \in \mathbb{R}^m$ is the control, $w(t) \in \mathbb{R}^l$ is the disturbance, $y(t) \in \mathbb{R}^p$ is the noisy measurement of the system output, $v(t) \in \mathbb{R}^p$ is the sensor noise, and A, B, B_w, C, D_u , are real matrices. Define

$$G_u(s) \triangleq C(sI_n - A)^{-1}B + D_u \tag{3}$$

$$G_w(s) \triangleq C(sI_n - A)^{-1}B_w + D_u \tag{4}$$

where $G_u \in \mathbb{R}(s)^{p \times m}_{prop}$ and $G_w \in \mathbb{R}(s)^{p \times l}_{prop}$ are proper $p \times m$ and $p \times l$ transfer functions, respectively. The disturbance $w(t)$ is matched if there exists $\bar{U} \in \mathbb{R}^{m \times m}$ such that $B_w = B\bar{U}$; otherwise, the disturbance is unmatched. The system output $y_0(t) \in \mathbb{R}^p$ is corrupted by sensor noise $v(t)$ and sampled to produce $y_k \in \mathbb{R}^p$. The sampling operation can be realized as $y_k \triangleq y_0(kT_s) + v_k$, where $v_k \triangleq v(kT_s) \in \mathbb{R}^p$ is the sampled sensor noise and $T_s \in \mathbb{R}$ is the sample time. In this paper the statistics of the sampled sensor noise v_k are specified. The performance variable is $y_{z,k} \triangleq Ey_k \in \mathbb{R}^q$, where the matrix $E \in \mathbb{R}^{q \times p}$ selects components of y_k or a linear combination of the components of y_k that are required to follow the command $r_k \in \mathbb{R}^q$. The command-following error is thus $z_k \triangleq r_k - y_{z,k} \in \mathbb{R}^q$. The inputs to the adaptive feedback controller $G_{c,k}$ are the measurement y_k and the command-following error z_k . The adaptive feedback controller produces the discrete-time control $u_k \in \mathbb{R}^m$ at each step k . The continuous-time control $u(t)$ is produced by applying a zero-order-hold operator to u_k . Note that z_k serves as the adaptation variable, as denoted by the diagonal line in Fig. 1 passing through $G_{c,k}$. The objective is to minimize the magnitude of the command-following error z_k in the presence of the disturbance $w(t)$ and sensor noise $v(t)$.

Figure 2 shows an equivalent representation of Fig. 1, where $w(t)$ and $y_{w,k}$ are related by the operator

$$y_{w,k} \triangleq \mathcal{G}[w(t)] = C \int_{(k-1)T_s}^{kT_s} e^{A(kT_s-\tau)} B_w w(\tau) d\tau \tag{5}$$

Note that Fig. 2 shows two transfer functions in feedback, namely, $G_d(\mathbf{q})$ and $EG_d(\mathbf{q})$, which are, respectively, the transfer functions from u_k to y_k and u_k to $y_{z,k}$. Furthermore, $G_d \in \mathbb{R}(\mathbf{q})^{p \times m}_{prop}$, where \mathbf{q} is the forward-shift operator, is the exact discretization of $G_u(s)$ using zero-order-hold and sampling operations. For details, see ([31] p. 11). Consequently,

$$y_k = \mathcal{G}[w(t)] + G_d(\mathbf{q})u_k + v_k \tag{6}$$

$$z_k = r_k - Ey_k \tag{7}$$

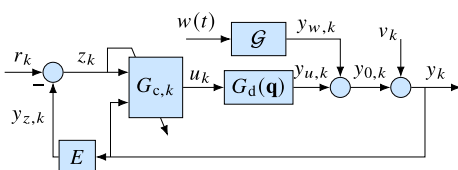


Fig. 2 Equivalent representation of Fig. 1. The exact discretization $G_d(\mathbf{q})$ of $G_u(s)$ operates on u_k to generate $y_{u,k}$.

Note that the argument \mathbf{q} of G_d in Eq. (6) reflects the fact that Eq. (6) is a time-domain equation whose solution depends on the initial conditions of the input-output system. Using the Z-transform variable \mathbf{z} in place of the forward-shift operator \mathbf{q} would account for the forced response of Eq. (6) but would implicitly assume zero initial conditions and thus would omit the free response. The distinction between \mathbf{z} and \mathbf{q} in accounting for initial conditions and the resulting free response is discussed in [32,33]. Since $G_d(\mathbf{z})$ and $G_d(\mathbf{q})$ have the same form, the argument has no effect on the algebraic properties of G_d such as poles and zeros.

To compute the intersample response of Eq. (5), the disturbance $w(t)$ is assumed to be piecewise constant within each subinterval of the interval kT_s to $(k+1)T_s$, where each subinterval has length $T_s/10$. In particular, letting $\bar{w}_{k,i}$ denote the approximate value of $w(t)$ for $t \in \left[\left(k + \frac{i}{10}\right)T_s, \left(k + \frac{i+1}{10}\right)T_s \right]$, for $i = 0, \dots, 9$, it follows that

$$y_{w,k+1} = C \int_{kT_s}^{(k+1)T_s} e^{A[(k+1)T_s-\tau]} B_w w(\tau) d\tau \tag{8}$$

$$\approx C \left[\int_{kT_s}^{kT_s + \frac{1}{10}T_s} e^{A[(k+1)T_s-\tau]} d\tau B_w \bar{w}_{k,0} + \dots + \int_{kT_s + \frac{9}{10}T_s}^{(k+1)T_s} e^{A[(k+1)T_s-\tau]} d\tau B_w \bar{w}_{k,9} \right] \tag{9}$$

$$= C \left[\int_{\frac{9}{10}T_s}^{T_s} e^{A\tau} d\tau B_w \bar{w}_{k,0} + \dots + \int_0^{\frac{1}{10}T_s} e^{A\tau} d\tau B_w \bar{w}_{k,9} \right] \tag{10}$$

Within each subinterval, the MATLAB function ODE45 is used to integrate the dynamics of $G(s)$. For all examples in this paper, the ODE45 relative and absolute tolerances are set to 2.22045×10^{-14} and 10^{-14} , respectively, which determine the variable step lengths during each subinterval. In the case where $w(t)$ is stochastic, the standard deviation of $\bar{w}_{k,i}$ is specified.

Figure 3 shows the intersample response of

$$G_w(s) = \frac{s-1}{s^2-3s+2}$$

where $\bar{w}_{k,i}$ is zero-mean, Gaussian white noise with standard deviation 1 simulated with $T_s = 0.01$ s/step. In all subsequent numerical examples, the intersample response is computed but not shown.

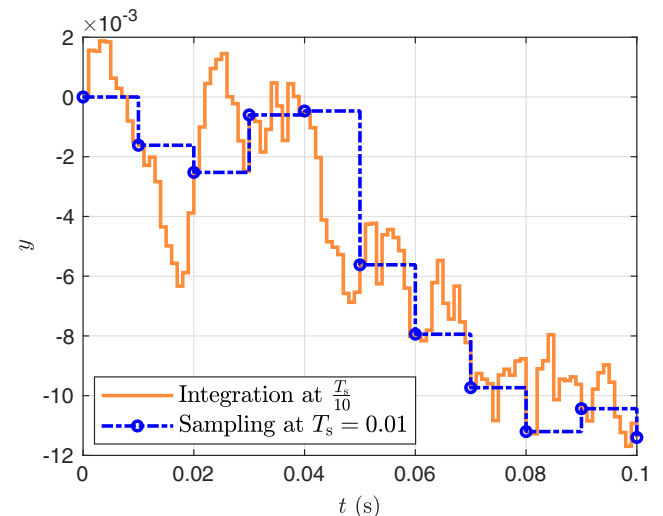


Fig. 3 Numerical integration of $G_w(s)$ using ODE45 within each subinterval of size $T_s/10$, where $T_s = 0.01$ s/step. The intersample response is plotted in orange, and the blue dash-dots show the sampled response.

Table 1 Special cases of $G_u(s)$ given by Eq. (11)

Case	a	b	c	n_d	Zeros
1	10	-30	-20	2	1 real NMP
2	10	-30	-20	0	1 real NMP
3	$10 + 10j$	$10 - 10j$	-20	2	2 complex NMP

For each case, the values of a, b, c, n_d and the type of zeros are shown.

Sections III–V consider SISO continuous-time transfer functions with $G_u(s) = G_w(s)$ of the form

$$G_u(s) = 10e^{-n_d T_s} \frac{(s-a)(s-b)(s-c) \prod_{i=1}^3 (s^2 + 2\bar{\zeta}_i \bar{\omega}_i s + \bar{\omega}_i^2)}{\prod_{i=1}^5 (s^2 + 2\zeta_i \omega_i s + \omega_i^2)} \quad (11)$$

where n_d is a nonnegative integer, the parameters a, b, c, n_d are given in Table 1, and $\bar{\zeta}_1 = 0.96, \bar{\zeta}_2 = 0.22, \bar{\zeta}_3 = 0.8, \bar{\omega}_1 = 54, \bar{\omega}_2 = 38, \bar{\omega}_3 = 8, \zeta_1 = 0.4, \zeta_2 = 0.15, \zeta_3 = 0.05, \zeta_4 = 0.06, \zeta_5 = 0.05, \omega_1 = 4, \omega_2 = 25, \omega_3 = 35, \omega_4 = 65, \text{ and } \omega_5 = 96$. The transfer function Eq. (11) with the parameters in Table 1 are used to investigate the performance of RCAC, recursive least squares-based identification (RLSID), and DDRCAC in later sections.

The time delay of $n_d T_s$, where n_d is a nonnegative integer, is included in $G_u(s)$ as $e^{-n_d T_s}$. Choosing the time delay to be a multiple of T_s facilitates investigation of the effect of uncertain discrete-time relative degree on the performance of the closed-loop discrete-time system. Note that Eq. (11) can be exactly discretized by separately considering the rational and exponential factors. In particular, the rational part of Eq. (11) is exactly discretized with a zero-order-hold (ZOH) discretization computed using MATLAB command `c2d`, whereas the exponential part of Eq. (11) is exactly discretized by the factor \mathbf{q}^{-n_d} in $G_d(\mathbf{q})$. Note that the exact discretization of Eq. (11) has relative degree $n_d + 1$.

For all examples in this paper, Eq. (11) is simulated by using a minimal realization whose initial state is zero. Hence, $E = 1, p = q = m = l = 1$, and $B = B_w$ in Eqs. (1) and (2).

III. Retrospective Cost Adaptive Control

A. Controller Structure and Definition of the Retrospective Performance Variable

Consider the strictly proper, discrete-time dynamic compensator

$$u_k = \sum_{i=1}^{n_c} P_{i,k} u_{k-i} + \sum_{i=1}^{n_c} Q_{i,k} \tilde{y}_{k-i} \quad (12)$$

where $k \geq 0, u_k \in \mathbb{R}^m$ is the requested control, n_c is the controller window length, $\tilde{y}_k \in \mathbb{R}^{l_y}$, and $Q_{1,k}, \dots, Q_{n_c,k} \in \mathbb{R}^{m \times l_y}$ and $P_{1,k}, \dots, P_{n_c,k} \in \mathbb{R}^{m \times m}$ are the numerator and denominator controller coefficient matrices, respectively. For convenience, a ‘‘cold’’ startup is assumed, where $Q_{1,0}, \dots, Q_{n_c,0}, P_{1,0}, \dots, P_{n_c,0}, u_{-n_c}, \dots, u_{-1}$, and $\tilde{y}_{-n_c}, \dots, \tilde{y}_{-1}$ are defined to be zero, and thus $u_0 = 0$. The controller (12) can be written as

$$u_k = \phi_{c,k} \theta_{c,k} \quad (13)$$

where

$$\phi_{c,k} \triangleq \begin{bmatrix} u_{k-1} \\ \vdots \\ u_{k-n_c} \\ \tilde{y}_{k-1} \\ \vdots \\ \tilde{y}_{k-n_c} \end{bmatrix}^T \otimes I_m \in \mathbb{R}^{m \times l_{\theta_c}} \quad (14)$$

is the controller regressor, $l_{\theta_c} \triangleq n_c m(m + l_y)$, and the controller coefficient vector is defined by

$$\theta_{c,k} \triangleq \text{vec}[P_{1,k} \ \cdots \ P_{n_c,k} \ Q_{1,k} \ \cdots \ Q_{n_c,k}] \in \mathbb{R}^{l_{\theta_c}} \quad (15)$$

In terms of \mathbf{q} , the controller (12) can be expressed as

$$u_k = G_{c,k}(\mathbf{q}) \tilde{y}_k \quad (16)$$

where

$$N_{c,k}(\mathbf{q}) \triangleq Q_{1,k} \mathbf{q}^{n_c-1} + \cdots + Q_{n_c,k} \quad (17)$$

$$D_{c,k}(\mathbf{q}) \triangleq I_m \mathbf{q}^{n_c} - P_{1,k} \mathbf{q}^{n_c-1} - \cdots - P_{n_c,k} \quad (18)$$

$$G_{c,k}(\mathbf{q}) \triangleq D_{c,k}^{-1}(\mathbf{q}) N_{c,k}(\mathbf{q}) \quad (19)$$

The signal \tilde{y}_k is constructed from z_k, y_k , and r_k . In the simplest case, $\tilde{y}_k = z_k$, whereas, when additional measurements are available, $\tilde{y}_k = [z_k^T \ y_k^T]^T$. Alternatively, feedforward action can be included by setting $\tilde{y}_k = [z_k^T \ r_k^T]^T$. More generally, the components of \tilde{y}_k can be arbitrary, fixed linear combinations of the components of z_k, y_k , and r_k . Fixed, nonlinear functions of z_k, y_k , and r_k can also be included in \tilde{y}_k ; however, this is outside the scope of this paper.

Next, define the filtered signals

$$u_{f,k} \triangleq G_f(\mathbf{q}) u_k \quad (20)$$

$$\phi_{f,k} \triangleq G_f(\mathbf{q}) \phi_{c,k} \quad (21)$$

where, for startup, $u_{f,k}$ and $\phi_{f,k}$ are initialized at zero and thus are computed as the forced responses of Eqs. (119) and (120), respectively. Unless specified otherwise, the same filter initialization is for all filters in the subsequent development. The $q \times m$ filter $G_f(\mathbf{q})$ has the form

$$G_f(\mathbf{q}) \triangleq D_f(\mathbf{q})^{-1} N_f(\mathbf{q}) \quad (22)$$

where

$$N_f(\mathbf{q}) \triangleq N_{f,0} \mathbf{q}^{n_f} + N_{f,1} \mathbf{q}^{n_f-1} + \cdots + N_{f,n_f} \quad (23)$$

$$D_f(\mathbf{q}) \triangleq I_q \mathbf{q}^{n_f} + D_{f,1} \mathbf{q}^{n_f-1} + \cdots + D_{f,n_f} \quad (24)$$

n_f is the filter window length, and $N_{f,0}, \dots, N_{f,n_f} \in \mathbb{R}^{q \times m}$ and $D_{f,1}, \dots, D_{f,n_f} \in \mathbb{R}^{q \times q}$ are the numerator and denominator coefficients of $G_f(\mathbf{q})$, respectively.

Equivalently, Eqs. (20) and (21) can be written as

$$u_{f,k} = -DU_{f,k} + NU_k \quad (25)$$

$$\phi_{f,k} = -D\Phi_{f,k} + N\Phi_{c,k} \quad (26)$$

where

$$U_{f,k} \triangleq \begin{bmatrix} u_{f,k-1} \\ \vdots \\ u_{f,k-n_f} \end{bmatrix} \in \mathbb{R}^{n_f q}, \quad U_k \triangleq \begin{bmatrix} u_k \\ \vdots \\ u_{k-n_f} \end{bmatrix} \in \mathbb{R}^{(n_f+1)m} \quad (27)$$

$$\Phi_{f,k} \triangleq \begin{bmatrix} \phi_{f,k-1} \\ \vdots \\ \phi_{f,k-n_f} \end{bmatrix} \in \mathbb{R}^{n_f q \times l_{\theta_c}}, \quad \Phi_{c,k} \triangleq \begin{bmatrix} \phi_{c,k} \\ \vdots \\ \phi_{c,k-n_f} \end{bmatrix} \in \mathbb{R}^{(n_f+1)m \times l_{\theta_c}} \quad (28)$$

$$\begin{aligned} N &\triangleq [N_{f,0} \quad \dots \quad N_{f,n_f}] \in \mathbb{R}^{q \times m(n_f+1)}, \\ D &\triangleq [D_{f,1} \quad \dots \quad D_{f,n_f}] \in \mathbb{R}^{q \times qn_f} \end{aligned} \quad (29)$$

Next, in order to update the controller coefficient vector (15), define the retrospective performance variable

$$\hat{z}_k(\theta_c) \triangleq z_k - (u_{f,k} - \phi_{f,k}\theta_c) \quad (30)$$

where z_k is given by Eq. (7) and θ_c is a generic variable for optimization. Note that $u_{f,k}$ depends on u_k and thus on the current controller coefficient vector $\theta_{c,k}$. The retrospective performance variable $\hat{z}_k(\theta_c)$ is used to determine the updated controller coefficient vector $\theta_{c,k+1}$ by minimizing a function of $\hat{z}_k(\theta_c)$. The optimized value of \hat{z}_k is thus given by

$$\hat{z}_k(\theta_{c,k+1}) = z_k - (u_{f,k} - \phi_{f,k}\theta_{c,k+1}) \quad (31)$$

which shows that the updated controller coefficient vector $\theta_{c,k+1}$ is “applied” retrospectively with the filtered controller regressor $\phi_{f,k}$. Furthermore, note that the filter $G_f(\mathbf{q})$ is used to obtain $\phi_{f,k}$ from ϕ_k by means of Eq. (21) but ignores past changes in the controller coefficient vector, as can be seen by the product $\phi_{f,k}\theta_{c,k+1}$ in Eq. (31). Consequently, the filtering used to construct Eq. (31) ignores changes in the controller coefficient vector over the window $[k - n_f, k]$. The effect of the actual time dependence of $\theta_{c,k}$ is analyzed in later sections.

Using Eqs. (25) and (26), Eq. (30) can be expressed as

$$\hat{z}_k(\theta_c) = z_k + D(U_{f,k} - \Phi_{f,k}\theta_c) - N(U_k - \Phi_{c,k}\theta_c) \quad (32)$$

In the case where $G_f(\mathbf{q})$ is a finite-impulse-response (FIR) transfer function, and thus $D = 0$, it follows from Eq. (32) that

$$\hat{z}_k(\theta_c) = z_k - NU_k + N\Phi_{c,k}\theta_c \quad (33)$$

To account for the control effort, define

$$z_{c,k}(\theta_c) \triangleq \begin{bmatrix} E_z \hat{z}_k(\theta_c) \\ E_u \phi_{c,k}\theta_c \end{bmatrix} \in \mathbb{R}^{q+r_1} \quad (34)$$

where the performance weighting $E_z \in \mathbb{R}^{q \times q}$ is nonsingular, and $E_u \in \mathbb{R}^{r_1 \times m}$ is the control weighting. If $E_u = 0$, then all expressions involving E_u in Eq. (34), as well as in all subsequent expressions, are omitted, and $r_1 = 0$. Using Eq. (30), it follows that Eq. (34) can be expressed as

$$z_{c,k}(\theta_c) = y_{c,k} - \phi_{f,k}\theta_c \quad (35)$$

where

$$y_{c,k} \triangleq \begin{bmatrix} E_z z_k - E_z u_{f,k} \\ 0_{r \times 1} \end{bmatrix} \in \mathbb{R}^{q+r_1}, \quad \phi_{f,k} \triangleq \begin{bmatrix} -E_z \phi_{f,k} \\ -E_u \phi_{c,k} \end{bmatrix} \in \mathbb{R}^{(q+r_1) \times l_{\theta_c}} \quad (36)$$

Using Eq. (34), define the retrospective cost

$$J_k(\theta_c) \triangleq \sum_{i=0}^k z_{c,i}(\theta_c)^T z_{c,i}(\theta_c) + (\theta_c - \theta_{c,0})^T P_{c,0}^{-1} (\theta_c - \theta_{c,0}) \quad (37)$$

and note that

$$z_{c,k}(\theta_c)^T z_{c,k}(\theta_c) = \hat{z}_k(\theta_c)^T R_z \hat{z}_k(\theta_c) + \theta_c^T \phi_{c,k}^T R_u \phi_{c,k} \theta_c \quad (38)$$

where $R_z \triangleq E_z^T E_z \in \mathbb{R}^{q \times q}$ is positive definite and $R_u \triangleq E_u^T E_u \in \mathbb{R}^{m \times m}$ is positive semidefinite. For all $k \geq 0$, the minimizer $\theta_{c,k+1}$ of Eq. (37) is given by the RLS solution [22]

$$P_{c,k+1} = P_{c,k} - P_{c,k} \phi_{f,k}^T (I_{q+r_1} + \phi_{f,k} P_{c,k} \phi_{f,k}^T)^{-1} \phi_{f,k} P_{c,k} \quad (39)$$

$$\theta_{c,k+1} = \theta_{c,k} + P_{c,k+1} \phi_{f,k}^T (y_{c,k} - \phi_{f,k} \theta_{c,k}) \quad (40)$$

Using the updated controller coefficient vector given by Eq. (40), the requested control at step $k + 1$ is given by

$$u_{k+1} = \phi_{c,k+1} \theta_{c,k+1} \quad (41)$$

Although $\theta_{c,0}$ can be chosen arbitrarily, $\theta_{c,0} = 0$ is chosen in all examples in order to reflect the absence of additional modeling information. Finally, $P_{c,0} = p_{c,0} I_{l_{\theta_c}}$, where $p_{c,0} \in (0, \infty)$ is a tuning parameter.

B. Decomposition of the Retrospective Performance Variable

This subsection shows that the retrospective performance variable can be decomposed into the sum of a performance term and a model-matching term. A more restrictive version of the results in this section is given in [34]. For simplicity, this section focuses on the case where $\tilde{y}_k \triangleq z_k$.

Because the optimized controller coefficient vector is time dependent, the retrospective performance variable defined by Eq. (30) must be modified to ignore the time dependence of $\theta_{c,k+1}$. To do this, the terms $u_{f,k} - \phi_{f,k}\theta_c$ in Eq. (30) are replaced by a filtered version of $u_k - \phi_{c,k}\theta_c$ in which the controller coefficient vector is constrained to be $\theta_{c,k+1}$ over the filtering window. By defining

$$\tilde{u}_k(\theta_c) \triangleq u_k - \phi_{c,k}\theta_c \quad (42)$$

the filtered signal $\tilde{u}_{f,k}(\theta_{c,k+1})$ is given by a fixed-input-argument (FIA) filter with input $\tilde{u}_k(\theta_{c,k+1})$ as defined in Appendix B. In particular, $\tilde{u}_{f,k}(\theta_{c,k+1})$ is defined to be the output of the FIA filter

$$\tilde{u}_{f,k}(\theta_{c,k+1}) \triangleq G_f(\mathbf{q}) \tilde{u}_k(\theta_{c,k+1}) \quad (43)$$

which ignores the change in the argument $\theta_{c,k+1}$ of \tilde{u}_k over the interval $[k - n_f, k]$ in accordance with retrospective optimization. Note that, by the definition of FIA filtering, the filtered signal $\tilde{u}_{f,k}(\theta_{c,k+1})$ is a function of the time-dependent controller coefficient vector $\theta_{c,k+1}$. Equivalently, Eq. (43) can be written as

$$\tilde{u}_{f,k}(\theta_{c,k+1}) = -D\tilde{U}_{f,k} + N\tilde{U}_k(\theta_{c,k+1}) \quad (44)$$

where

$$\begin{aligned} \tilde{U}_{f,k} &\triangleq \begin{bmatrix} \tilde{u}_{f,k-1}(\theta_{c,k}) \\ \vdots \\ \tilde{u}_{f,k-n_f}(\theta_{c,k-n_f+1}) \end{bmatrix} \in \mathbb{R}^{n_f q}, \\ \tilde{U}_k(\theta_c) &\triangleq \begin{bmatrix} \tilde{u}_k(\theta_c) \\ \vdots \\ \tilde{u}_{k-n_f}(\theta_c) \end{bmatrix} \in \mathbb{R}^{(n_f+1)m} \end{aligned} \quad (45)$$

Using Eq. (43), the definition Eq. (30) of $\hat{z}_k(\theta_c)$ is replaced by

$$\hat{z}_{\text{ext},k}(\theta_{c,k+1}) \triangleq z_k - \tilde{u}_{f,k}(\theta_{c,k+1}) \quad (46)$$

Using Eqs. (42), (44), and (45), it follows that Eq. (46) can be written as

$$\hat{z}_{\text{ext},k}(\theta_{c,k+1}) = z_k + D\tilde{U}_{f,k} - N(U_k - \Phi_{c,k}\theta_{c,k+1}) \quad (47)$$

Note that the difference between $\hat{z}_k(\theta_{c,k+1})$ given by Eq. (32) and $\hat{z}_{\text{ext},k}(\theta_{c,k+1})$ given by Eq. (47) is because $U_{f,k} - \Phi_{f,k}\theta_c$ in Eq. (32) is

replaced by $\tilde{u}_{f,k}$ in Eq. (47). Hence, $\hat{z}_{\text{ext},k}(\theta_{c,k+1})$ is not generally $\hat{z}_k(\theta_{c,k+1})$. However, if, for all k , $\theta_{c,k+1} = \theta_c$, then $\tilde{u}_{f,k}(\theta_{c,k+1}) = u_{f,k} - \phi_{c,k}\theta_c$, and thus $\hat{z}_{\text{ext},k}(\theta_{c,k+1}) = \hat{z}_k(\theta_c)$.

The following result presents the *retrospective performance-variable decomposition*, which shows that the retrospective performance variable is a combination of the closed-loop performance and the extent to which the updated closed-loop transfer function from $\tilde{u}_k(\theta_{c,k+1})$ to z_k matches the filter $G_f(\mathbf{q})$. Henceforth, $G_f(\mathbf{q})$ is called the *target model* because it serves as the target for the closed-loop transfer function from $\tilde{u}_k(\theta_{c,k+1})$ to z_k .

Proposition 1: Assume that, for all $k \geq 0$, $\tilde{y}_k \triangleq z_k$, and $G_d(\mathbf{q})$ and $G_f(\mathbf{q})$ are strictly proper. Then, for all $k \geq 0$,

$$\hat{z}_{\text{ext},k}(\theta_{c,k+1}) = z_{\text{opp},k}(\theta_{c,k+1}) + z_{\text{tmp},k}(\theta_{c,k+1}) \quad (48)$$

where the one-step predicted performance $z_{\text{opp},k}(\theta_{c,k+1})$ and the target-model matching performance $z_{\text{tmp},k}(\theta_{c,k+1})$ are defined by

$$z_{\text{opp},k}(\theta_{c,k+1}) \triangleq \tilde{G}_{z\tilde{w},k+1}(\mathbf{q}) \left(r_k - Ev_k - EG[w(t)] \right) \quad (49)$$

$$z_{\text{tmp},k}(\theta_{c,k+1}) \triangleq \left[\tilde{G}_{z\tilde{u},k+1}(\mathbf{q}) - G_f(\mathbf{q}) \right] \tilde{u}_k(\theta_{c,k+1}) \quad (50)$$

and

$$\tilde{G}_{z\tilde{w},k+1}(\mathbf{q}) \triangleq \left[I_q + EG_d(\mathbf{q})G_{c,k+1}(\mathbf{q}) \right]^{-1} \quad (51)$$

$$\tilde{G}_{z\tilde{u},k+1}(\mathbf{q}) \triangleq -\mathbf{q}^{n_c} \left[I_q + EG_d(\mathbf{q})G_{c,k+1}(\mathbf{q}) \right]^{-1} EG_d(\mathbf{q})D_{c,k+1}^{-1}(\mathbf{q}) \quad (52)$$

Proof: It follows from Eqs. (49) and (51) that

$$z_{\text{opp},k}(\theta_{c,k+1}) = r_k - Ev_k - EG[w(t)] - EG_d(\mathbf{q})G_{c,k+1}(\mathbf{q})z_{\text{opp},k}(\theta_{c,k+1}) \quad (53)$$

Furthermore, defining the FIA filter output (see Definition 8 in Appendix B)

$$\tilde{z}_{\text{tmp},k}(\theta_{c,k+1}) \triangleq \tilde{G}_{z\tilde{u},k+1}(\mathbf{q})\tilde{u}_k(\theta_{c,k+1}) \quad (54)$$

it follows from Eqs. (52) and (54) that

$$\tilde{z}_{\text{tmp},k}(\theta_{c,k+1}) = -EG_d(\mathbf{q})D_{c,k+1}^{-1}(\mathbf{q})\mathbf{q}^{n_c}\tilde{u}_k(\theta_{c,k+1}) - EG_d(\mathbf{q})G_{c,k+1}(\mathbf{q})\tilde{z}_{\text{tmp},k}(\theta_{c,k+1}) \quad (55)$$

Now, replacing $\mathbf{q}^{n_c}\tilde{u}_k(\theta_{c,k+1})$ with $\tilde{u}_{k+n_c}(\theta_{c,k+1})$ in Eq. (55) yields

$$\tilde{z}_{\text{tmp},k}(\theta_{c,k+1}) = -EG_d(\mathbf{q})D_{c,k+1}^{-1}(\mathbf{q})\tilde{u}_{k+n_c}(\theta_{c,k+1}) - EG_d(\mathbf{q})G_{c,k+1}(\mathbf{q})\tilde{z}_{\text{tmp},k}(\theta_{c,k+1}) \quad (56)$$

Combining Eqs. (53) and (54) yields

$$\begin{aligned} z_{\text{opp},k}(\theta_{c,k+1}) + \tilde{z}_{\text{tmp},k}(\theta_{c,k+1}) &= r_k - Ev_k - EG[w(t)] - EG_d(\mathbf{q})D_{c,k+1}^{-1}(\mathbf{q})\tilde{u}_{k+n_c}(\theta_{c,k+1}) \\ &\quad - EG_d(\mathbf{q})G_{c,k+1}(\mathbf{q}) \left[z_{\text{opp},k}(\theta_{c,k+1}) + \tilde{z}_{\text{tmp},k}(\theta_{c,k+1}) \right] \end{aligned} \quad (57)$$

Next, replacing k with $k + n_c$ in Eq. (42) and setting $\theta_c = \theta_{c,k+1}$ yields

$$\tilde{u}_{k+n_c}(\theta_{c,k+1}) = u_{k+n_c} - \phi_{c,k+n_c}\theta_{c,k+1} \quad (58)$$

Hence, using

$$\phi_{c,k+n_c}\theta_{c,k+1} = \sum_{i=1}^{n_c} P_{i,k+1}u_{k+n_c-i} + \sum_{i=1}^{n_c} Q_{i,k+1}z_{k+n_c-i}$$

it follows from Eq. (58) that

$$\tilde{u}_{k+n_c}(\theta_{c,k+1}) = u_{k+n_c} - \sum_{i=1}^{n_c} P_{i,k+1}u_{k+n_c-i} - \sum_{i=1}^{n_c} Q_{i,k+1}z_{k+n_c-i} \quad (59)$$

Using Eqs. (17) and (18), note that Eq. (60) can be written as

$$\tilde{u}_{k+n_c}(\theta_{c,k+1}) = D_{c,k+1}(\mathbf{q})u_k - N_{c,k+1}(\mathbf{q})z_k$$

which can be combined with Eq. (57) to obtain

$$\begin{aligned} z_{\text{opp},k}(\theta_{c,k+1}) + \tilde{z}_{\text{tmp},k}(\theta_{c,k+1}) &= r_k - Ev_k - EG[w(t)] - EG_d(\mathbf{q})u_k + EG_d(\mathbf{q})G_{c,k+1}(\mathbf{q})z_k \\ &\quad - EG_d(\mathbf{q})G_{c,k+1}(\mathbf{q}) \left[z_{\text{opp},k}(\theta_{c,k+1}) + \tilde{z}_{\text{tmp},k}(\theta_{c,k+1}) \right] \end{aligned} \quad (60)$$

Using Eqs. (6) and (7), it follows from Eq. (60) that

$$\begin{aligned} (I_q + EG_d(\mathbf{q})G_{c,k+1}(\mathbf{q})) \left[z_{\text{opp},k}(\theta_{c,k+1}) + \tilde{z}_{\text{tmp},k}(\theta_{c,k+1}) \right] &= (I_q + EG_d(\mathbf{q})G_{c,k+1}(\mathbf{q}))z_k \end{aligned} \quad (61)$$

which implies that

$$z_k = z_{\text{opp},k}(\theta_{c,k+1}) + \tilde{z}_{\text{tmp},k}(\theta_{c,k+1}) \quad (62)$$

Next, substituting Eq. (62) into Eq. (46) yields

$$\hat{z}_{\text{ext},k}(\theta_{c,k+1}) = z_{\text{opp},k}(\theta_{c,k+1}) + \tilde{z}_{\text{tmp},k}(\theta_{c,k+1}) - \tilde{u}_{f,k}(\theta_{c,k+1}) \quad (63)$$

Hence, substituting Eqs. (43) and (54) into Eq. (63) and using Eq. (50) yields

$$\begin{aligned} \hat{z}_{\text{ext},k}(\theta_{c,k+1}) &= z_{\text{opp},k}(\theta_{c,k+1}) + \tilde{G}_{z\tilde{u},k+1}(\mathbf{q})\tilde{u}_k(\theta_{c,k+1}) \\ &\quad - G_f(\mathbf{q})\tilde{u}_k(\theta_{c,k+1}) \\ &= z_{\text{opp},k}(\theta_{c,k+1}) + \left[\tilde{G}_{z\tilde{u},k+1}(\mathbf{q}) - G_f(\mathbf{q}) \right] \tilde{u}_k(\theta_{c,k+1}) \\ &= z_{\text{opp},k}(\theta_{c,k+1}) + z_{\text{tmp},k}(\theta_{c,k+1}) \end{aligned}$$

In the case where $\tilde{y}_k = z_k$, y_k , and u_k are scalar, that is, $l_y = q = p = m = 1$, Eqs. (51) and (52) have the form

$$\tilde{G}_{z\tilde{w},k+1}(\mathbf{q}) = \frac{D_d(\mathbf{q})D_{c,k+1}(\mathbf{q})}{D_d(\mathbf{q})D_{c,k+1}(\mathbf{q}) + EN_d(\mathbf{q})N_{c,k+1}(\mathbf{q})} \quad (64)$$

$$\tilde{G}_{z\tilde{u},k+1}(\mathbf{q}) = \frac{-\mathbf{q}^{n_c}EN_d(\mathbf{q})}{D_d(\mathbf{q})D_{c,k+1}(\mathbf{q}) + EN_d(\mathbf{q})N_{c,k+1}(\mathbf{q})} \quad (65)$$

where

$$G_d(\mathbf{q}) \triangleq \frac{N_d(\mathbf{q})}{D_d(\mathbf{q})} \quad (66)$$

C. Analysis of the Retrospective Performance-Variable Decomposition

Assuming $E_c = I$, $E_u = 0$, and using Eqs. (34) and (48), it follows from Eq. (37) that

$$J_k(\theta_{c,k+1}) = \sum_{i=0}^k \hat{z}_i^T(\theta_{c,i+1}) \hat{z}_i(\theta_{c,i+1}) + (\theta_{c,i+1} - \theta_{c,0})^T P_{c,0}^{-1} (\theta_{c,i+1} - \theta_{c,0}) \quad (67)$$

In the case where $p_{c,0}$ is large, using RLS to minimize Eq. (67) yields

$$\hat{z}_k(\theta_{c,k+1}) \approx 0 \quad (68)$$

Furthermore, it is observed numerically and shown in Example 1 that using RLS to minimize Eq. (68) yields

$$\hat{z}_{\text{ext},k}(\theta_{c,k+1}) \approx \hat{z}_k(\theta_{c,k+1}) \quad (69)$$

which, using Eq. (48), implies that

$$z_{\text{opp},k}(\theta_{c,k+1}) + z_{\text{tmp},k}(\theta_{c,k+1}) \approx 0 \quad (70)$$

that is,

$$z_{\text{opp},k}(\theta_{c,k+1}) \approx -z_{\text{tmp},k}(\theta_{c,k+1}) \quad (71)$$

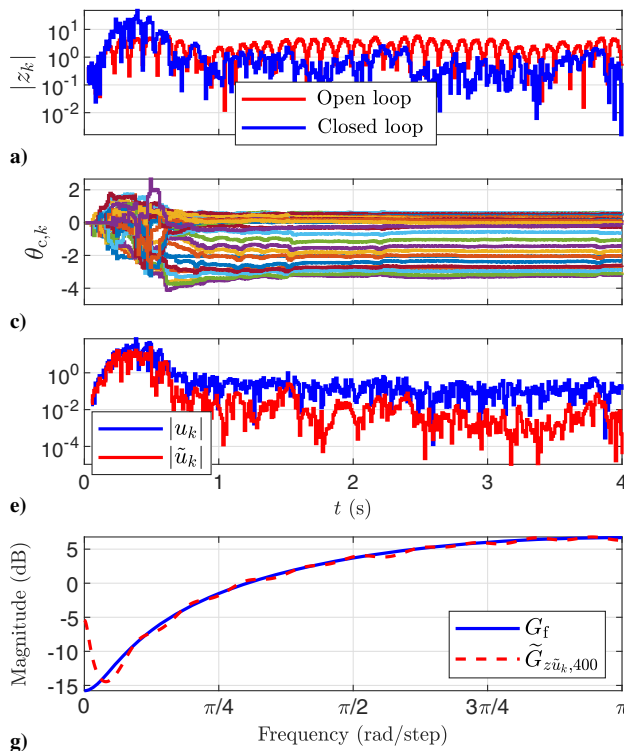
The following example illustrates this property.

Example 1: Minimization of $\hat{z}_{\text{ext},k}(\theta_{c,k+1})$ and its decomposition for a SISO system. Let

$$G_u(s) = \frac{100(s-10)(s+8)}{(s+11)(s^2-0.6s+900)} \quad (72)$$

and, for $T_s = 0.01$ s/step, let $G_d(\mathbf{q})$ denote the ZOH discretization of $G_u(s)$. Assume that the w is matched, that is, $G_u(s) = G_w(s)$, and let $\bar{w}_{k,i}$ be zero-mean, Gaussian white noise with standard deviation 1. For disturbance rejection with nonnoisy measurements, that is, with $r_k = 0$ and $v_k = 0$, adaptive control is applied with $E_z = 1$, $E_u = 0$, $E = 1$,

$$G_f(\mathbf{q}) = -0.9988 \frac{(\mathbf{q} - 1.1628)}{\mathbf{q}^2}$$



$n_c = 16$, and $p_{c,0} = 10$. Figures 4f and 4h show that, for all $0.04 \leq t \leq 0.7$, $z_{\text{opp},k}(\theta_{c,k+1})$ and $z_{\text{tmp},k}(\theta_{c,k+1})$ have large magnitudes and approximately sum to zero. In particular, Fig. 4h shows

$$\frac{|z_{\text{opp},k} + z_{\text{tmp},k}|}{|z_{\text{opp},k}| + |z_{\text{tmp},k}|}$$

which is small when $z_{\text{opp},k}(\theta_{c,k+1})$ and $z_{\text{tmp},k}(\theta_{c,k+1})$ have large magnitudes with opposite signs, and close to 1 when $z_{\text{opp},k}(\theta_{c,k+1})$ and $z_{\text{tmp},k}(\theta_{c,k+1})$ have small magnitudes. Figure 4g shows that $\tilde{G}_{z\tilde{u}_k,400}(\mathbf{q})$ and $G_f(\mathbf{q})$ have similar frequency responses, and thus the controller update promotes matching between the closed-loop transfer function $\tilde{G}_{z\tilde{u}_k,400}(\mathbf{q})$ and the target model $G_f(\mathbf{q})$.

Next, in order to compare $\hat{z}_k(\theta_{c,k+1})$ and $\hat{z}_{\text{ext},k}(\theta_{c,k+1})$ for the case where $G_f(\mathbf{q})$ is infinite-impulse-response (IIR), the simulation is repeated with

$$G_f(\mathbf{q}) = -0.9988 \frac{(\mathbf{q} - 1.1628)}{\mathbf{q}^2 + 0.1\mathbf{q} + 0.01}$$

Figure 5 shows that the error between $\hat{z}_k(\theta_{c,k+1})$ and $\hat{z}_{\text{ext},k}(\theta_{c,k+1})$ is less than 10^{-1} for all t . \diamond

Proposition 2: Assume that $\bar{\theta}_c \triangleq \lim_{k \rightarrow \infty} \theta_{c,k+1}$ exists and $\phi_{c,k+1}$ is bounded. Then $\lim_{k \rightarrow \infty} \tilde{u}_k(\theta_{c,k+1}) = 0$.

Proof: Equations (14) and (42) imply that

$$\tilde{u}_k(\theta_{c,k+1}) = \phi_{c,k}(\theta_{c,k} - \theta_{c,k+1})$$

Defining $\alpha = \sup_{k \geq 0} \sigma_{\max}(\phi_{c,k})$, it follows that

$$\begin{aligned} \|\tilde{u}_k(\theta_{c,k+1})\| &\leq \sigma_{\max}(\phi_{c,k}) \|\theta_{c,k} - \theta_{c,k+1}\| \\ &\leq \alpha \|\theta_{c,k} - \theta_{c,k+1}\| \end{aligned}$$

where σ_{\max} denotes the maximum singular value. Hence,

$$\lim_{k \rightarrow \infty} \|\tilde{u}_k(\theta_{c,k+1})\| \leq \alpha \lim_{k \rightarrow \infty} \|\theta_{c,k} - \theta_{c,k+1}\| = 0$$

\square

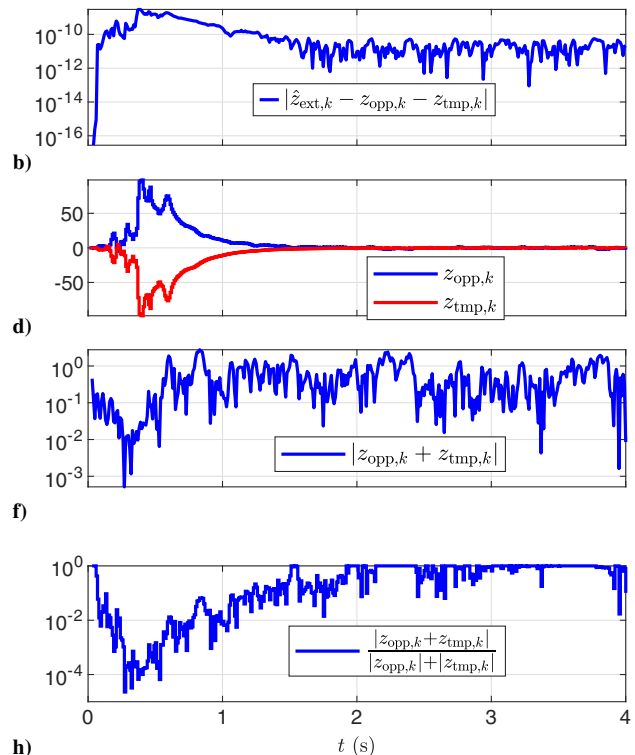


Fig. 4 Example 1: a) open- and closed-loop responses; b) $|\hat{z}_{\text{ext},k} - z_{\text{opp},k} - z_{\text{tmp},k}| < 3.01 \times 10^{-9}$ for all t , confirming Eq. (48).

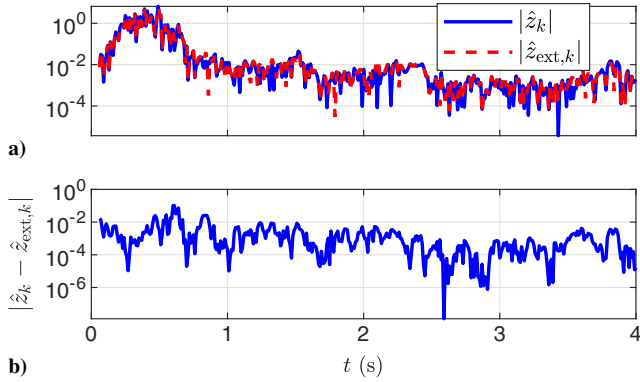


Fig. 5 Example 1: For an IIR $G_f(\mathbf{q})$, a) shows the absolute value of the retrospective cost variable and its extension, and b) shows the absolute error between the retrospective cost variable and its extension.

Proposition 5 and Eq. (50) suggest that the convergence of $\theta_{c,k}$ implies that $z_{\text{tmp},k}(\theta_{c,k+1})$ converges to zero, as illustrated in Fig. 4g. Therefore, Eq. (71) implies that $|z_{\text{opp},k}(\bar{\theta}_c)| \approx 0$, and thus, if $\theta_{c,k}$ converges, then the one-step predicted performance $|z_{\text{opp},k}(\bar{\theta}_c)|$ is small. This mechanism underlies the convergence of RCAC in Fig. 4 to a stabilizing controller that rejects the unknown disturbance. Note, however, that the convergence of $\theta_{c,k}$ and the consequent convergence of $\tilde{u}_k(\theta_{c,k+1})$ to zero do not imply that $z_{\text{tmp},k}(\theta_{c,k+1})$ converges to zero. In fact, Example 5 demonstrates that a poor choice of $G_f(\mathbf{q})$ may cause $z_{\text{tmp},k}(\theta_{c,k+1})$ to diverge while $\theta_{c,k}$ converges.

D. Feasibility of $G_f(\mathbf{q})$

The following definition concerns the case where there exists a controller parameter vector that exactly matches the transfer function $\tilde{G}_{z\tilde{u},k+1}(\mathbf{q})$ to $G_f(\mathbf{q})$.

Definition 1: Assume that, for all $k \geq 0$, $\tilde{y}_k = z_k \in \mathbb{R}^q$. Then, $G_f(\mathbf{q}) \in \mathbb{R}(\mathbf{q})_{\text{prop}}^{q \times m}$ is feasible if there exists $\theta_c = \text{vec}[P_1 \ \dots \ P_{n_c} \ Q_1 \ \dots \ Q_{n_c}] \in \mathbb{R}^{l_{\theta_c}}$ such that

$$\tilde{G}_{z\tilde{u}}(\mathbf{q}) = G_f(\mathbf{q}) \tag{73}$$

where

$$\tilde{G}_{z\tilde{u}}(\mathbf{q}) \triangleq -\mathbf{q}^{n_c} [I_q + EG_d(\mathbf{q})G_c(\mathbf{q})]^{-1} EG_d(\mathbf{q})D_c(\mathbf{q})^{-1} \tag{74}$$

with

$$D_c(\mathbf{q}) \triangleq I_m \mathbf{q}^{n_c} - P_1 \mathbf{q}^{n_c-1} - \dots - P_{n_c} \tag{75}$$

$$N_c(\mathbf{q}) \triangleq Q_1 \mathbf{q}^{n_c-1} + \dots + Q_{n_c} \tag{76}$$

$$G_c(\mathbf{q}) \triangleq D_c^{-1}(\mathbf{q})N_c(\mathbf{q}) \tag{77}$$

Definition 2: Let $\theta_{c,k}$ be given by Eq. (40), and $\tilde{G}_{z\tilde{u},k}(\mathbf{q})$ be given by Eq. (65). Then the asymptotic feasibility distance is

$$f_{\infty} \triangleq \limsup_{k \rightarrow \infty} \|\tilde{G}_{z\tilde{u},k}(\mathbf{q}) - G_f(\mathbf{q})\|_{\infty} \tag{78}$$

For the SISO case, the following result identifies several features of $\tilde{G}_{z\tilde{u}}(\mathbf{q})$ that are determined by $G_d(\mathbf{q})$.

Proposition 3: For all $k \geq 0$, assume that $\tilde{y}_k = z_k, y_k$, and u_k are scalar. Furthermore, let $\theta_c \in \mathbb{R}^{l_{\theta_c}}$ and $G_f(\mathbf{q}) \in \mathbb{R}(\mathbf{q})_{\text{prop}}$. Then the following statements hold:

- i) The leading numerator coefficient of $\tilde{G}_{z\tilde{u}}(\mathbf{q})$ is equal to the leading numerator coefficient of $-EG_d(\mathbf{q})$.
- ii) The relative degree of $\tilde{G}_{z\tilde{u}}(\mathbf{q})$ is equal to the relative degree of $G_d(\mathbf{q})$.
- iii) The zeros of $\tilde{G}_{z\tilde{u}}(\mathbf{q})$ consist of the zeros of $G_d(\mathbf{q})$ as well as n_c zeros at zero.

Proof: Since $\tilde{y}_k = z_k$ and u_k are scalar, it follows that E is scalar and the closed-loop transfer function (74) specializes to

$$\tilde{G}_{z\tilde{u}}(\mathbf{q}) = \frac{-\mathbf{q}^{n_c} EN_d(\mathbf{q})}{D_d(\mathbf{q})D_c(\mathbf{q}) + EN_d(\mathbf{q})N_c(\mathbf{q})} \tag{79}$$

which implies point (i). To prove point (ii), let d_d denote the degree of $D_d(\mathbf{q})$, and let $\xi \geq 0$ denote the relative degree of $G_d(\mathbf{q})$, so that the degree of $N_d(\mathbf{q})$ is $d_d - \xi$. Because the degree of $\mathbf{q}^{n_c} EN_d(\mathbf{q})$ is $n_c + d_d - \xi$ and the degree of $D_d(\mathbf{q})D_c(\mathbf{q}) + EN_d(\mathbf{q})N_c(\mathbf{q})$ is $n_c + d_d$, it follows that the relative degree of $\tilde{G}_{z\tilde{u}}(\mathbf{q})$ is ξ . Finally, point (iii) follows from the fact that the numerator of Eq. (79) is the numerator of $EG_d(\mathbf{q})$ multiplied by \mathbf{q}^{n_c} . \square

The following result, which is an immediate consequence of Proposition 4.4, provides necessary conditions for feasibility in the SISO case.

Proposition 4: For all $k \geq 0$, assume that $\tilde{y}_k = z_k, y_k$, and u_k are scalar. Furthermore, let $\theta_c \in \mathbb{R}^{l_{\theta_c}}$, let $G_f(\mathbf{q}) \in \mathbb{R}(\mathbf{q})_{\text{prop}}$, and assume that $G_f(\mathbf{q})$ is feasible. Then the following statements hold:

- i) The leading numerator coefficient of $G_f(\mathbf{q})$ is equal to the leading numerator coefficient of $-EG_d(\mathbf{q})$.
- ii) The relative degree of $G_f(\mathbf{q})$ is equal to the relative degree of $G_d(\mathbf{q})$.
- iii) The zeros of $G_f(\mathbf{q})$ consist of the zeros of $G_d(\mathbf{q})$, as well as n_c zeros at zero.

E. RCAC with Feasible and Infeasible $G_f(\mathbf{q})$ for SISO Systems

This subsection investigates the effect of feasible and infeasible target models on the convergence of $\theta_{c,k}$ given by Eq. (40). For all of the examples in this and the following subsection, let $G_u(s)$ be given by Eq. (72), and, for $T_s = 0.01$ s/step, let $G_d(\mathbf{q})$ denote the ZOH discretization of $G_u(s)$. In particular,

$$G_d(\mathbf{q}) = \frac{0.9988(\mathbf{q} - 1.1628)(\mathbf{q} - 0.7393)}{(\mathbf{q} - 0.9048)(\mathbf{q}^2 - 1.905\mathbf{q} + 0.994)} \tag{80}$$

Assume that w is matched, that is, $G_u(s) = G_w(s)$, and let $\bar{w}_{k,i}$ and v_k be zero-mean, Gaussian white noise with standard deviations 1 and 0.01, respectively. For various choices of the target model $G_f(\mathbf{q})$, the following examples consider disturbance rejection with noisy measurements with $r_k = 0, E_z = 1, E_u = 0$, and $E = 1$.

Example 2: Feasible $G_f(\mathbf{q})$. A linear-quadratic-Gaussian (LQG) controller $G_{\text{LQG}}(\mathbf{q})$ is designed for $G_d(\mathbf{q})$ given by Eq. (80) using the MATLAB command `lqg` with $Q_{xu} = I_4$ and $Q_{wv} = I_4$. The LQG controller

$$G_{\text{LQG}}(\mathbf{q}) \triangleq \frac{N_{\text{LQG}}(\mathbf{q})}{D_{\text{LQG}}(\mathbf{q})} \tag{81}$$

is used to construct

$$G_{f,\text{LQG}}(\mathbf{q}) = \frac{-\mathbf{q}^n N_d(\mathbf{q})}{D_d(\mathbf{q})D_{\text{LQG}}(\mathbf{q}) + N_d(\mathbf{q})N_{\text{LQG}}(\mathbf{q})} \tag{82}$$

The corresponding closed-loop target model is given by

$$G_{f,\text{LQG}}(\mathbf{q}) = \frac{-0.9988\mathbf{q}^3(\mathbf{q} - 1.1628)(\mathbf{q} - 0.7393)}{(\mathbf{q} - 0.8878)(\mathbf{q} - 0.2118)(\mathbf{q}^2 - 1.199\mathbf{q} + 0.3738)(\mathbf{q}^2 - 0.0926\mathbf{q} + 0.1148)} \tag{83}$$

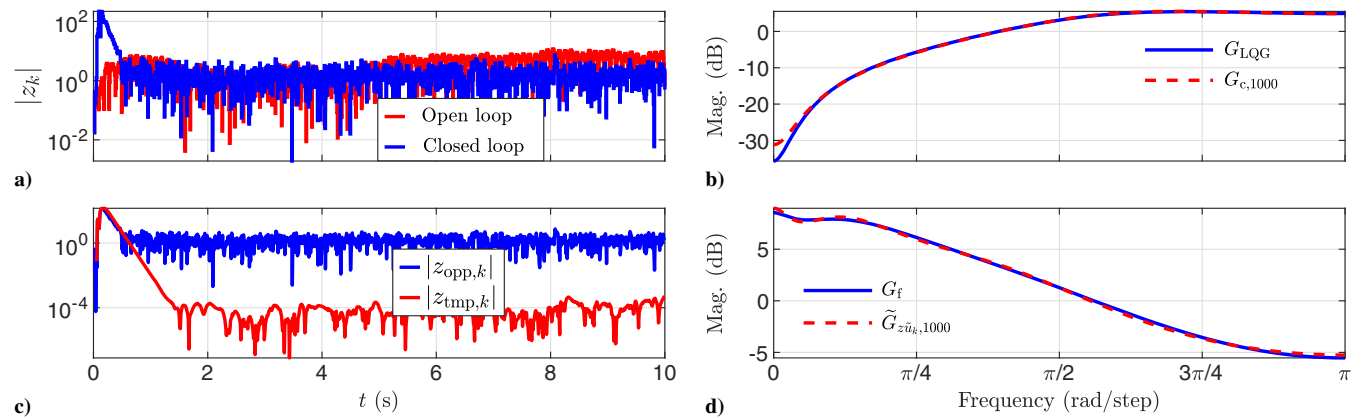


Fig. 6 Example 2: a) open- and closed-loop responses; b) frequency response of $G_{LQG}(\mathbf{q})$ and $G_{c,1000}(\mathbf{q})$; c) $|z_{opp,k}|$ and $|z_{tmp,k}|$; d) frequency response of $G_f(\mathbf{q})$ and $\tilde{G}_{z\tilde{u},1000}(\mathbf{q})$.

Note that Eq. (83) is feasible by construction. Since $G_{f,LQG}(\mathbf{q})$ is feasible, Proposition 3 implies that its leading numerator coefficient -0.9988 and relative degree 1 are the same as those of $-EG_d(\mathbf{q})$ and that its zeros $0, 0.7393$ and 1.1628 are the zeros of $G_d(\mathbf{q})$ as well as $n = 3$ zeros at zero. Next, adaptive control is applied with $G_f(\mathbf{q}) = G_{f,LQG}(\mathbf{q})$, $p_{c,0} = 10^7$, and $n_c = n = 3$. Figure 6d shows that $\tilde{G}_{z\tilde{u},1000}(\mathbf{q})$ and $G_f(\mathbf{q})$ have similar frequency responses, which is consistent with the fact that $G_{f,LQG}(\mathbf{q})$ is feasible. Moreover, Fig. 6b shows that $G_{c,1000}(\mathbf{q})$ and $G_{LQG}(\mathbf{q})$ have similar frequency responses, which suggests that the adaptive controller approximately converges to the LQG controller. \diamond

Example 3: Robustness to infeasible $G_f(\mathbf{q})$. To investigate the robustness of the feasible target model Eq. (83), the target model is chosen to be various infeasible perturbations of the feasible target model given by

$$G_f(\mathbf{q}) = \alpha_{LNC} G_{f,LQG}(\mathbf{q}) \quad (84)$$

$$G_f(\mathbf{q}) = \frac{1}{\alpha_{RD}} G_{f,LQG}(\mathbf{q}) \quad (85)$$

$$G_f(\mathbf{q}) = \frac{-0.9988\mathbf{q}^3(\mathbf{q} - 1.1628)(\mathbf{q} - \alpha_{MP})}{(\mathbf{q} - 0.8878)(\mathbf{q} - 0.2118)(\mathbf{q}^2 - 1.199\mathbf{q} + 0.3738)(\mathbf{q}^2 - 0.0926\mathbf{q} + 0.1148)} \quad (86)$$

$$G_f(\mathbf{q}) = \frac{-0.9988\mathbf{q}^3(\mathbf{q} - \alpha_{NMP})(\mathbf{q} - 0.7393)}{(\mathbf{q} - 0.8878)(\mathbf{q} - 0.2118)(\mathbf{q}^2 - 1.199\mathbf{q} + 0.3738)(\mathbf{q}^2 - 0.0926\mathbf{q} + 0.1148)} \quad (87)$$

which reflect uncertainty in α_{LNC} , α_{RD} , α_{MP} , and α_{NMP} , respectively. Note that Eqs. (84–87) are equal to Eq. (83) for the nominal values $\alpha_{LNC} = 1$, $\alpha_{RD} = 0$, $\alpha_{MP} = 0.7393$, and $\alpha_{NMP} = 1.1628$, respectively.

The suppression metric g_s is defined as the ratio of the root-mean-square of the last 1000 subinterval steps of the open-loop response and the closed-loop response in dB. The case $g_s > 0$ corresponds to disturbance suppression relative to the response of the open-loop system. Simulations where either $g_s \leq 0$ or the output of the closed-loop system diverges are indicated as failures.

To investigate the closed-loop performance with an off-nominal target model, α_{LNC} , α_{RD} , α_{MP} , and α_{NMP} are varied from their nominal values, and RCAC is applied with $n_c = n = 3$, $p_{c,0} = 1000$, for $0 \leq t \leq 20$ s. Figure 7 shows that the adaptive controller can be applied with the target models (84–87), where α_{LNC} , α_{MP} , and α_{NMP} are off-nominal. In particular, Fig. 7 shows the suppression metric g_s and asymptotic feasibility distance f_∞ for target models with various sources of infeasibility. Figures 7a and 7e show g_s and f_∞ , respectively, for Eq. (84), where $\alpha_{LNC} \in [-0.5, 6]$, which shows that infeasibility due to the sign of the leading numerator coefficient of the target model causes failure. However, the adaptive controller is robust to infeasibility due to the magnitude of the leading numerator coefficient of the target model. Figures 7b and 7f show g_s and f_∞ , respectively, for Eq. (85), where $\alpha_{RD} \in \{0, 1, 2, 3\}$, which shows that infeasibility due to the relative degree of target model causes failure. Figures 7c and 7g show g_s and f_∞ , respectively, for Eq. (87), where

$\alpha_{MP} \in [-1.2, 1.2]$, which shows that the adaptive controller is robust to infeasibility due to an incorrectly modeled MP zero in the target model. However, note that the adaptive controller fails when an MP zero of $G_d(\mathbf{q})$ is replaced with a positive NMP zero in the target

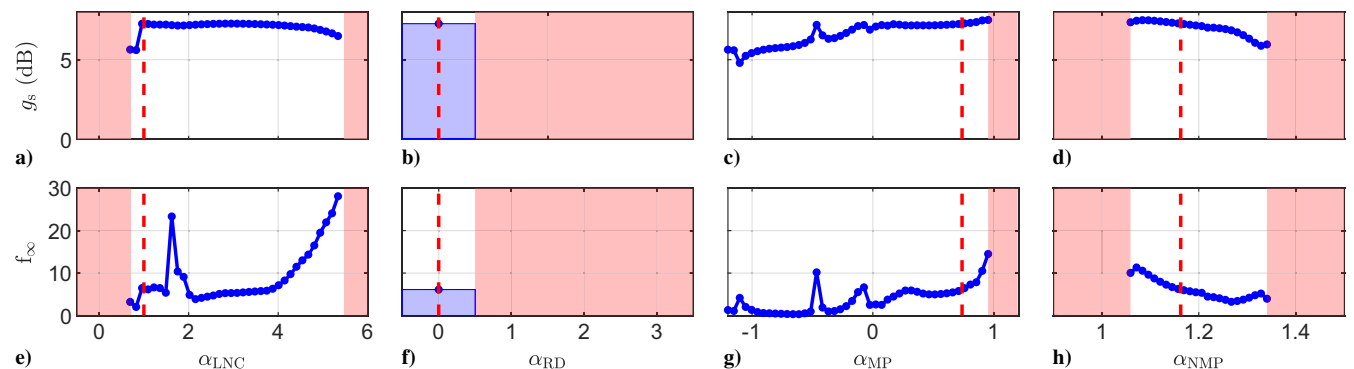


Fig. 7 Example 3: For $G_f(\mathbf{q})$ given by Eqs. (84–87), a–d) show g_s , and e–h) show f_∞ . The dashed lines indicate nominal values of α_{LNC} , α_{RD} , α_{MP} , and α_{NMP} ; the shaded regions indicate values for which $g_s \leq 0$.

model. Figures 7d and 7h show g_s and f_∞ , respectively, for Eq. (87), where $\alpha_{\text{NMP}} \in [0.9, 1.5]$, which shows that the adaptive controller is robust to infeasibility due to an incorrectly modeled NMP zero in the target model. Note that the adaptive controller fails when $\alpha_{\text{NMP}} < 1$ in the target model (87), that is, when the NMP zero in the feasible target model (83) is replaced with an MP zero. \diamond

F. Construction of $G_f(\mathbf{q})$ for SISO Systems

Example 3 shows that RCAC can reject disturbances with an infeasible $G_f(\mathbf{q})$ as long as $G_f(\mathbf{q})$ shares certain properties with $-EG_d(\mathbf{q})$, as described by the following definition.

Definition 3: Assume that $EG_d(\mathbf{q})$ is SISO, and let $G_f(\mathbf{q})$ be a proper SISO transfer function. Then $G_f(\mathbf{q})$ is *quasi-feasible* if the following statements hold:

- i) The leading numerator coefficients of $G_f(\mathbf{q})$ and $-EG_d(\mathbf{q})$ have the same sign.
- ii) $G_f(\mathbf{q})$ and $-EG_d(\mathbf{q})$ have the same relative degree.
- iii) $G_f(\mathbf{q})$ and $-EG_d(\mathbf{q})$ have the same NMP zeros.

Note that a quasi-feasible target model may be feasible; however, most quasi-feasible target model are infeasible

Definition 4: The *nominal target model* is the minimal-order, quasi-feasible FIR target model whose leading numerator coefficient is equal to the leading numerator coefficient of $-EG_d(\mathbf{q})$.

Note that the nominal target model is uniquely defined. Furthermore, the nominal target model may be feasible; however, in most cases, the nominal target model is infeasible. The rationale for choosing the nominal target model to be FIR is the fact that the target location for each closed-loop pole is the center of the open unit disk. For details, see [20]. Note that the nominal target model for $-EG_d(\mathbf{q})$, with $G_d(\mathbf{q})$ given by Eq. (80), is

$$G_{f,n}(\mathbf{q}) = -0.9988 \frac{\mathbf{q} - 1.1628}{\mathbf{q}^2} \tag{88}$$

The following example investigates the efficacy of the nominal target model when the required modeling information is uncertain.

Example 4: Robustness to perturbations from the nominal target model. To investigate the robustness of the nominal target model, first consider the case where $G_f(\mathbf{q})$ given by Eq. (88). Figure 8 shows the suppression metric g_s and the asymptotic feasibility distance f_∞ for this choice of target model, marked with the vertical red dashed lines.

Next, the target model is chosen to be a perturbation of the nominal target model given by the off-nominal target models

$$G_f(\mathbf{q}) = \alpha_{\text{LNC}} G_{f,n}(\mathbf{q}) \tag{89}$$

$$G_f(\mathbf{q}) = -0.9988 \frac{\mathbf{q} - 1.1628}{\mathbf{q}^{2+\alpha_{\text{RD}}}} \tag{90}$$

$$G_f(\mathbf{q}) = -0.9988 \frac{\mathbf{q} - \alpha_{\text{NMP}}}{\mathbf{q}^2} \tag{91}$$

which reflect uncertainty in α_{LNC} , α_{RD} , and α_{NMP} , respectively. Note that Eqs. (89), (90), and (91) are equal to $G_{f,n}(\mathbf{q})$ for the nominal values $\alpha_{\text{LNC}} = 1$, $\alpha_{\text{RD}} = 0$, and $\alpha_{\text{NMP}} = 1.1628$, respectively. To investigate the closed-loop performance with an off-nominal target model, α_{LNC} , α_{RD} , and α_{NMP} are varied from their nominal values, and adaptive control is applied with $n_c = 10$, $p_{c,0} = 1000$, for $0 \leq t \leq 20$ s. Figure 8 shows that the adaptive controller can be applied with the target models $G_{f,\text{LNC}}(\mathbf{q})$ and $G_{f,\text{NMP}}(\mathbf{q})$, where α_{LNC} and α_{NMP} are off-nominal. \diamond

Example 4 suggests that $G_f(\mathbf{q})$ can be constructed as

$$G_f(\mathbf{q}) = -G_\xi \frac{\prod_{i=1}^{N_z} (\mathbf{q} - \alpha_{z,i})}{\mathbf{q}^{N_z + \xi}} \tag{92}$$

where G_ξ , $\alpha_{z,i}$, N_z , ξ , are the leading numerator coefficient, all NMP zeros, number of NMP zeros, and relative degree of $EG_d(\mathbf{q})$, respectively. Note that the minus sign in Eq. (92) is due to the minus sign in Eq. (7).

Example 5: Unmodeled NMP zeros and the retrospective performance-variable decomposition. Let $G_f(\mathbf{q}) = -(0.9988/\mathbf{q})$, which has the same leading numerator coefficient and relative degree as $-EG_d(\mathbf{q})$; however, it does not have the NMP zero of $G_d(\mathbf{q})$. Adaptive control is applied with $E_z = 1$, $E_u = 0$, $E = 1$, $n_c = 16$, and $p_{c,0} = 1000$.

As shown by Examples 1 and 2, the minimization of the retrospective performance variable $\hat{z}_k(\theta_{c,k+1})$ leads to matching between $\tilde{G}_{z\tilde{u},k+1}(\theta_{c,k+1})$ and $G_f(\mathbf{q})$. Figure 9h shows that this is what happens for this example as well. Because Eq. (65) has an NMP zero at 1.1628 rad/step and $G_f(\mathbf{q})$ does not, the optimization attempts to cancel this NMP zero using the denominator of Eq. (65). This results in a controller pole at the NMP zero as shown in Fig. 9g, which results in a hidden instability, demonstrated by the lack of divergence of $|z_k|$ and the exponential divergence of $|u_k|$, as shown in Figs. 9e and 9a, respectively.

Additionally, as shown in Fig. 9b, the spectral radius of $D_u(\mathbf{q})D_c(\mathbf{q}) + N_u(\mathbf{q})N_c(\mathbf{q})$, which is the denominator polynomial of all closed-loop transfer functions, converges to a value greater than 1, which shows that all the closed-loop transfer functions are unstable. However, since $G_f(\mathbf{q})$ is asymptotically stable, and $|z_k|$ and $\tilde{u}_k(\theta_{c,k+1})$ remain small, it follows from Eq. (46) that $\hat{z}_{\text{ext},k}(\theta_{c,k+1})$ remains small, as shown in Fig. 9d. This in turn implies that $z_{\text{opp},k}(\theta_{c,k+1}) \approx -z_{\text{tmp},k}(\theta_{c,k+1})$, which can be seen in Fig. 9f. \diamond

G. MIMO Example

To investigate the role of the target model $G_f(\mathbf{q})$ in MIMO case, note that the closed-loop transfer function from r_k to y_k is given by

$$\tilde{G}_{yr}(\mathbf{q}) = [I_p + G_d(\mathbf{q})G_c(\mathbf{q})]^{-1} G_d(\mathbf{q})G_c(\mathbf{q}) \tag{93}$$

$$= G_d(\mathbf{q})[I_m + G_c(\mathbf{q})G_d(\mathbf{q})]^{-1} G_c(\mathbf{q}) \tag{94}$$

$$= G_d(\mathbf{q})G_c(\mathbf{q})[I_p + G_d(\mathbf{q})G_c(\mathbf{q})]^{-1} \tag{95}$$

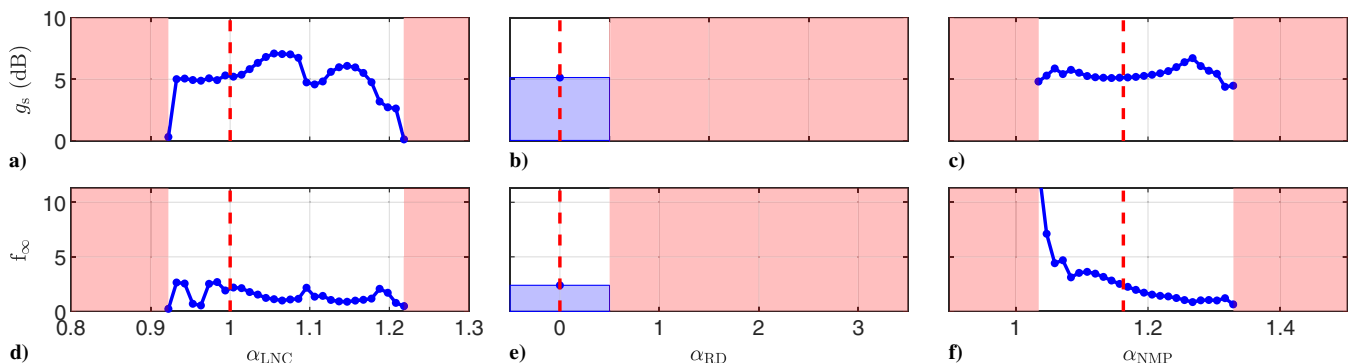


Fig. 8 Example 4: For $G_f(\mathbf{q})$ given by Eqs. (89–91), a–c) show g_s , and d–f) show f_∞ . The dashed lines indicate nominal values of α_{LNC} , α_{RD} , and α_{NMP} ; the shaded regions indicate values for which $g_s \leq 0$.

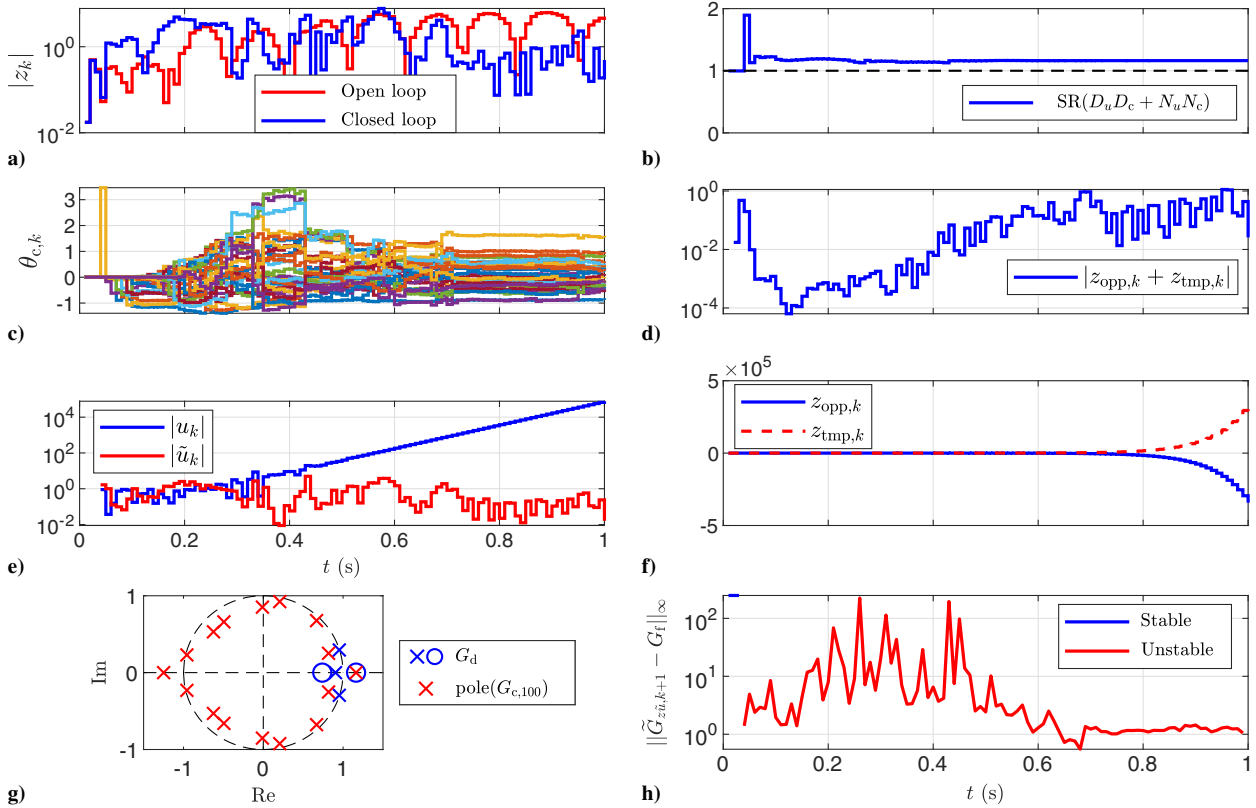


Fig. 9 Example 5: a) open- and closed-loop responses; b) spectral radius of $D_u D_c + N_u N_c$; h) $\|\tilde{G}_{z\bar{u},k+1}(\mathbf{q}) - G_f(\mathbf{q})\|_\infty$, coded by color for the stability of $\tilde{G}_{z\bar{u},k+1}(\mathbf{q})$.

assume that $G_d(\mathbf{q})$ and $G_c(\mathbf{q})$ have full normal rank, and consider the definitions and propositions in Appendix A. Note that, if $G_d(\mathbf{q})$ is square, then Proposition 8 implies that $\text{CZ}(G_d, G_c)$ and $\text{CZ}(G_c, G_d)$ are both empty. Alternatively, consider the case where $p \neq m$, and thus $G_d(\mathbf{q})$ in Fig. 2 is rectangular. Note that both products $G_d G_c \in \mathbb{R}(\mathbf{q})_{\text{prop}}^{p \times p}$ and $G_c G_d \in \mathbb{R}(\mathbf{q})_{\text{prop}}^{m \times m}$ appear in Eqs. (93–95). In particular, in the case where $m > p$, $G_c(\mathbf{q})G_d(\mathbf{q})$ is up-squared, and thus $\text{CZ}(G_c, G_d)$ is empty, whereas $G_d(\mathbf{q})G_c(\mathbf{q})$ is down-squared, and thus $\text{CZ}(G_d, G_c)$ may be nonempty. On the other hand, in the case $m < p$, $G_d(\mathbf{q})G_c(\mathbf{q})$ is up-squared, and thus $\text{CZ}(G_d, G_c)$ is empty, whereas $G_c(\mathbf{q})G_d(\mathbf{q})$ is down-squared, and thus $\text{CZ}(G_c, G_d)$ may be nonempty. As shown in the next example, cascade zeros of the down-squared loop transfer function may be cancelled by RCAC.

Example 6: Cancellation of an NMP cascade zero. Consider $G_u(s)$ and $G_w(s)$ given by Eqs. (3) and (4) with

$$A = \begin{bmatrix} -80 & 0 & 0 & 0 \\ 0 & -20 & 0 & 0 \\ -80 & 0 & -10 & -40 \\ -80 & 0 & 40 & -10 \end{bmatrix}, \quad B = \begin{bmatrix} -1.8 & 1.35 & -0.85 \\ 1.02 & -0.22 & -1.12 \\ 0.13 & -0.59 & 2.53 \\ 0.71 & -0.29 & 1.66 \end{bmatrix},$$

$$B_w = \begin{bmatrix} 0 \\ 1 \\ 0 \\ 0 \end{bmatrix} \quad (96)$$

$$C = \begin{bmatrix} 1.31 & -0.87 & 0.79 & -8.33 \\ -1.26 & -2.18 & -1.33 & -6.45 \end{bmatrix}, \quad D = 0_{2 \times 3} \quad (97)$$

and $T_s = 0.01$ s/step. Note that A is asymptotically stable. Let (A_d, B_d, C_d, D_d) be a minimal realization of $G_d(\mathbf{q})$. The objective

is to reject the effect of a white, zero-mean, Gaussian disturbance on both components of $y_k = [y_{1,k} \ y_{2,k}]^T$, and thus $E = I_2$. For Eqs. (96) and (97), $EG_d(\mathbf{q})$ has no transmission zeros and no NMP channel zeros. Let $\bar{w}_{k,i}$ and v_k be zero-mean, Gaussian white noise with standard deviations 1 and 0.001, respectively. Using the Markov parameters $H_1 = C_d B_d$ and $H_2 = C_d A_d B_d$ of $G_d(\mathbf{q})$, let

$$G_f(\mathbf{q}) = -\frac{H_1}{\mathbf{q}} - \frac{H_2}{\mathbf{q}^2} \quad (98)$$

This choice of $G_f(\mathbf{q})$ ensures that u_k is not restricted to a subspace of \mathbb{R}^m , where $m = 3$, as shown in [35]. With $G_f(\mathbf{q})$ given by Eq. (98) and $p_{c,0} = 10^3$, $E_z = I_2$, $E_u = 0$, $n_c = 20$, Fig. 10 shows that a controller pole cancels an NMP cascade zero of $(G_d, G_{c,509})$ at 1.168 rad/step, which causes the control u_k to diverge. Note that $G_d(\mathbf{q})G_{c,509}(\mathbf{q})$ does not have a transmission zero at 1.168 rad/step due to pole-zero cancellation, and thus the zero at 1.168 rad/step is an evanescent NMP zero of $(G_d, G_{c,509})$. \diamond

IV. Online Identification Using Recursive Least Squares

This section investigates the performance of RLS for online, closed-loop identification. The goal is to estimate key features of the open-loop transfer function $-EG_d(\mathbf{q})$ from u_k to z_k needed to construct $G_f(\mathbf{q})$, which, as shown in Sec. III, serves as the target model for $\tilde{G}_{z\bar{u},k}(\mathbf{q})$. Because closed-loop identification may lead to biased estimates, open-loop identification is also considered in order to provide a baseline comparison.

A. Recursive Least Squares-Based Identification

In this subsection, RLSID is used to identify $EG_d(\mathbf{q})$. The transfer function $EG_d(\mathbf{q})$ from u_k to $y_{z,k}$ is given by

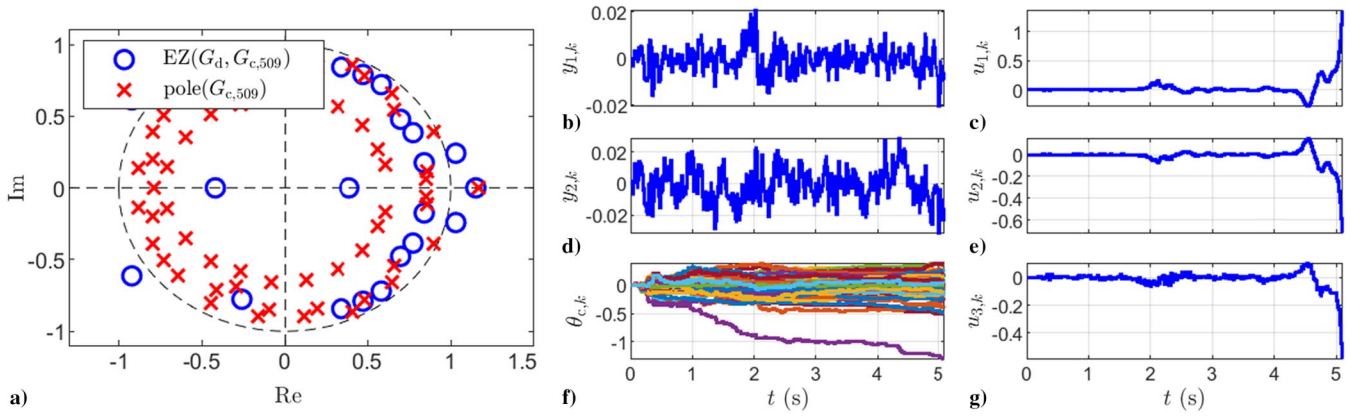


Fig. 10 Example 6: a) $EZ(G_d, G_{c,509})$ and controller poles, where an NMP element of $CZ(G_d, G_{c,509})$ is cancelled by a controller pole. b,d) Closed-loop response; c,e,g) all components of u_k diverge; f) $\theta_{c,k}$.

$$EG_d(\mathbf{q}) = (I_q \mathbf{q}^n + F_1 \mathbf{q}^{n-1} + \dots + F_n)^{-1} (G_0 \mathbf{q}^n + G_1 \mathbf{q}^{n-1} + \dots + G_n) \quad (99)$$

where $G_0, \dots, G_n \in \mathbb{R}^{q \times m}$, and $F_1, \dots, F_n \in \mathbb{R}^{q \times q}$ are the numerator and denominator coefficients of the transfer function, respectively.

Consider the sampled-data identification architecture shown in Fig. 11, which is based on Fig. 2.

Since E is known, $y_{z,k} = Ey_k$ can be computed internally by RLSID. Furthermore, at each step k , the requested control input u_k and the measurement y_k are assumed to be available. To identify $EG_d(\mathbf{q})$, a model of the form

$$y_{z,k} = - \sum_{i=1}^{\eta} F_{i,k} y_{z,k-i} + \sum_{i=0}^{\eta} G_{i,k} u_{k-i} \quad (100)$$

is fit to data where η is the RLSID window length, and $G_{0,k}, \dots, G_{\eta,k} \in \mathbb{R}^{q \times m}$, and $F_{1,k}, \dots, F_{\eta,k} \in \mathbb{R}^{q \times q}$ are numerator and denominator coefficient matrices that are to be estimated.

Next, note that Eq. (100) can be written as

$$y_{z,k} = \phi_{m,k} \theta_{m,k} \quad (101)$$

where

$$\phi_{m,k} \triangleq \begin{bmatrix} -y_{z,k-1} \\ \vdots \\ -y_{z,k-\eta} \\ u_k \\ \vdots \\ u_{k-\eta} \end{bmatrix}^T \otimes I_q \in \mathbb{R}^{q \times l_{\theta_m}} \quad (102)$$

$$\theta_{m,k} \triangleq \text{vec} [F_{1,k} \dots F_{\eta,k} G_{0,k} \dots G_{\eta,k}] \in \mathbb{R}^{l_{\theta_m}} \quad (103)$$

is the model coefficient vector, and $l_{\theta_m} = \eta q^2 + (\eta + 1)qm$. The model-output error is defined by

$$z_{m,k}(\theta_m) \triangleq y_{z,k} - \phi_{m,k} \theta_m \quad (104)$$

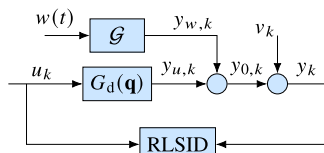


Fig. 11 Online identification using RLSID.

where θ_m is an argument for optimization of the form

$$\theta_m \triangleq \text{vec} [F_1 \dots F_{\eta} G_0 \dots G_{\eta}] \in \mathbb{R}^{l_{\theta_m}} \quad (105)$$

Next, to apply RLSID, note that the minimizer $\theta_{m,k+1}$ of the quadratic cost function

$$J_k(\theta_m) \triangleq \sum_{i=0}^k z_{m,i}(\theta_m)^T z_{m,i}(\theta_m) + (\theta_m - \theta_{m,0})^T P_{m,0}^{-1} (\theta_m - \theta_{m,0}) \quad (106)$$

is given recursively by

$$P_{m,k+1} = P_{m,k} - P_{m,k} \phi_{m,k}^T (I_q + \phi_{m,k} P_{m,k} \phi_{m,k}^T)^{-1} \phi_{m,k} P_{m,k} \quad (107)$$

$$\theta_{m,k+1} = \theta_{m,k} + P_{m,k+1} \phi_{m,k}^T (y_{z,k} - \phi_{m,k} \theta_{m,k}) \quad (108)$$

Note that $\theta_{m,0} = 0$ is chosen to reflect the absence of additional modeling information, and $P_{m,0} = p_{m,0} I_{l_{\theta_m}}$, where $p_{m,0} \in (0, \infty)$ is a tuning parameter. As shown by Example 7, the regularization term $(\theta_m - \theta_{m,0})^T P_{m,0}^{-1} (\theta_m - \theta_{m,0})$ in Eq. (106), which is a required feature of RLS [36–39], causes the estimates to be biased. Although the regularization-induced bias can be minimized by choosing $p_{m,0}$ to be large, it cannot be entirely avoided. The RLSID model at step k is given by

$$EG_{d,k}(\mathbf{q}) \triangleq (I_q \mathbf{q}^{\eta} + F_{1,k} \mathbf{q}^{\eta-1} + \dots + F_{\eta,k})^{-1} (G_{0,k} \mathbf{q}^{\eta} + \dots + G_{\eta,k}) \quad (109)$$

Unless stated otherwise, for all of the examples in this paper RLSID is applied with a strictly proper model, which is enforced by removing u_k and $G_{0,k}$ from the definitions (102) and (103), respectively, and redefining $l_{\theta_m} = \eta q(q + m)$.

B. Relative Degree and Leading Numerator Coefficient of SISO Systems

In the case where u_k and $y_{z,k}$ are scalar, the transfer function $EG_d(\mathbf{q})$ from u_k to $y_{z,k}$ can be expressed as

$$EG_d(\mathbf{q}) = \frac{EN_d(\mathbf{q})}{D_d(\mathbf{q})} = \frac{G_0 \mathbf{q}^n + \dots + G_n}{\mathbf{q}^n + F_1 \mathbf{q}^{n-1} + \dots + F_n} \quad (110)$$

where n is the order of $EG_d(\mathbf{q})$, and $G_0, \dots, G_n \in \mathbb{R}$ and $F_1, \dots, F_n \in \mathbb{R}$ are numerator and denominator coefficients, respectively. The leading numerator coefficient of Eq. (110) is the leftmost nonzero coefficient of $EN_d(\mathbf{q})$, and the relative degree of Eq. (110) is $\xi \triangleq \text{deg } D_d(\mathbf{q}) - \text{deg } EN_d(\mathbf{q})$. Note that G_{ξ} is leading

numerator coefficient of $EG_d(\mathbf{q})$, and, in the case where $\xi \geq 1$, $G_0 = \dots = G_{\xi-1} = 0$.

C. Numerical Examples

For all of the examples in this section, let $G_u(s)$ be given by Case 1 in Table 1, and let $G_d(\mathbf{q})$ denote the ZOH discretization of $G(s)$ with $T_s = 0.03$ s/step, and $EG_d(\mathbf{q})$ is a SISO 12th-order transfer function with an NMP zero at 1.4901 rad/step. Furthermore, $G_0 = G_1 = G_2 = 0$ and $G_3 = 0.2972$, and thus the relative degree of $EG_d(\mathbf{q})$ is 3 and G_3 is its leading numerator coefficient. To assess the ability of RLSID to estimate the relative degree and leading numerator coefficient of $EG_d(\mathbf{q})$, $G_{i,k}$ and G_i are compared for $i = 1, 2, 3$. Furthermore, to assess the accuracy of the estimate of the NMP zero of $G_d(\mathbf{q})$, the smallest distance $d_{z,k}$ between the zeros of the RLSID model and the NMP zero of $EG_d(\mathbf{q})$ is computed at each step. To assess the accuracy of open- and closed-loop identification, let $\eta = 12$, which is the order of $EG_d(\mathbf{q})$. Each example in this section involves 100 trials for $0 \leq t \leq 1000$ s.

Example 7: Open-loop RLSID with no disturbance, no sensor noise, showing regularization-induced bias. Let the input u_k of $G_d(\mathbf{q})$ be zero-mean, Gaussian white noise with standard deviation 1, and let $\tilde{w}_{k,i} = 0$ and $v_k = 0$. To demonstrate the effect of regularization, RLSID is applied to the input-output data with two choices of $p_{m,0}$, namely, $p_{m,0} = 10^{-3}$ and $p_{m,0} = 10^4$, where $p_{m,0} = 10^{-3}$ and $p_{m,0} = 10^4$ correspond to large and small regularization, respectively. A detailed treatment of regularization-induced bias in RLS is found in [40]. The averaged results from 100 trials are shown in Fig. 12. As shown in Fig. 12, the errors in the estimates of the first three numerator coefficients and the NMP zero are larger for trials with larger regularization. \diamond

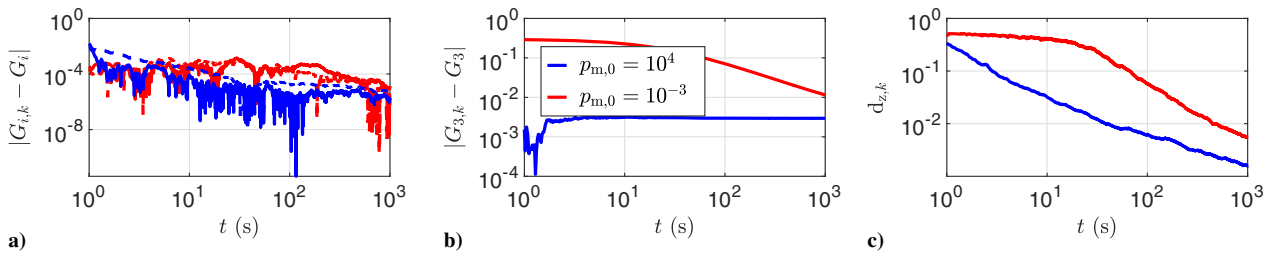


Fig. 12 Example 7: Regularization in RLSID. Averaged a) estimation errors for G_1, G_2 ; b) estimation error for G_3 ; and c) $d_{z,k}$. The accuracy of the identification is poor when the regularization is large.

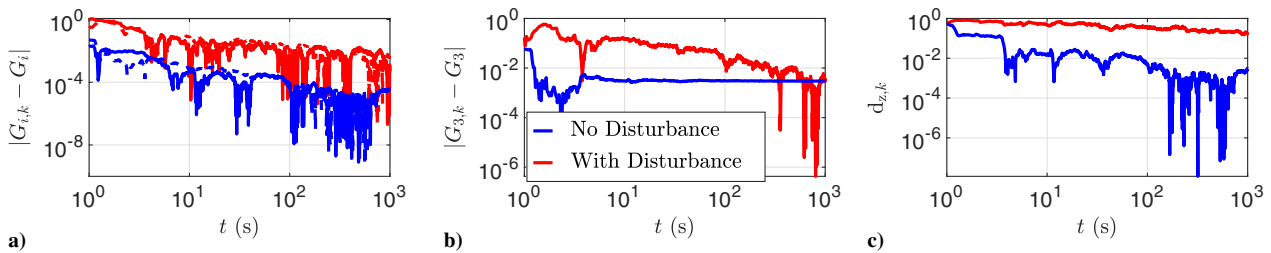


Fig. 13 Example 8: Disturbance and sensor noise in RLSID. Averaged a) estimation errors for G_1, G_2 ; b) estimation error for G_3 ; and c) $d_{z,k}$. Disturbance and sensor noise degrade identification accuracy.

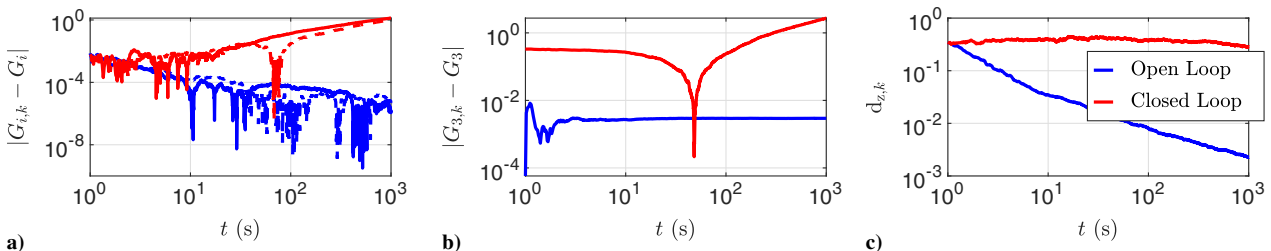


Fig. 14 Example 9: Closed-loop RLSID. Averaged a) estimation errors for G_1, G_2 ; b) estimation error for G_3 ; and c) $d_{z,k}$. The closed-loop identification accuracy is poor compared with open-loop identification.

Example 8: Open-loop RLSID with disturbance and sensor noise. Let the input u_k of $G_d(\mathbf{q})$ be zero-mean, Gaussian white noise with standard deviation 1; let and $p_{m,0} = 10^4$. To demonstrate the effect of disturbance and sensor noise, RLSID is applied to the input-output data, with $\tilde{w}_k = 0$, $v_k = 0$, and with $\tilde{w}_{k,i}$, v_k being zero-mean, Gaussian white noise with standard deviations 10,1, respectively. The averaged results from 100 trials are shown in Fig. 13. As shown in Fig. 13, the errors in the estimates of the first three numerator coefficients and the NMP zero are larger for the trials with disturbance and sensor noise present. \diamond

Example 9: Closed-loop RLSID with LQG Control. To demonstrate the effect of closed-loop control, RLSID is applied to the input-output data for open- and closed-loop scenarios. In particular, for open-loop simulations, u_k is zero-mean, Gaussian white noise with standard deviation 1, and for closed-loop simulations u_k is given by an LQG feedback controller designed using the MATLAB command `lqg` with $Q_{xu} = Q_{wv} = I_{13}$. Let $\tilde{w}_{k,i}$ and v_k be zero-mean, Gaussian white noise with standard deviations 0.05 and 0.005, respectively. For RLSID set $p_{m,0} = 10^4$. The averaged results from 100 trials are shown in Fig. 14. As shown in Fig. 14, the errors in the estimates of the first three numerator coefficients and the NMP zero are larger for closed-loop input-output data relative to open-loop input-output data. \diamond

V. Data-Driven Retrospective Cost Adaptive Control

This section describes DDRCAC [41], which combines RLSID with RLS-based adaptive control (RLSAC). The online identification uses RLS to fit an IIR model based on data $y_{z,k}$ and u_k collected during closed-loop operation. At each step, the identified IIR model is used to construct a time-dependent target model $G_{f,k}(\mathbf{q})$.

In particular, $G_{f,k}(\mathbf{q})$ is constructed as an FIR filter whose numerator is chosen to be the numerator of the latest identified IIR model. Note that this online technique for constructing $G_{f,k}(\mathbf{q})$ is a variation of the offline technique described in Sec. III, where $G_f(\mathbf{q})$ was constructed using only the NMP zeros of $EG_d(\mathbf{q})$. This approach avoids the need to compute NMP zeros during online operation and can be used in the MIMO case, where the numerator of the RLSID model is a $q \times m$ polynomial matrix. This target model is then used by RLSAC to update the coefficients of an IIR controller. For DDRCAC, both RLS implementations use VRF, as given by the following result [23].

Proposition 5: For all $k \geq 0$, let $\bar{y}_k \in \mathbb{R}^{l_y}$, $\phi_k \in \mathbb{R}^{l_y \times l_\phi}$, $\lambda_k \in (0, 1]$, and define $\rho_k \triangleq \prod_{j=0}^k \lambda_j$. Let $\bar{\theta}_0 \in \mathbb{R}^{l_\theta}$, and let $\bar{P}_0 \in \mathbb{R}^{l_\theta \times l_\theta}$ be positive definite. Furthermore, for all $k \geq 0$, denote the minimizer of

$$J_k(\bar{\theta}) \triangleq \sum_{i=0}^k \frac{\rho_i}{\rho_i} (\bar{y}_i - \phi_i \bar{\theta})^T (\bar{y}_i - \phi_i \bar{\theta}) + \rho_k (\bar{\theta} - \bar{\theta}_0)^T \bar{P}_0^{-1} (\bar{\theta} - \bar{\theta}_0) \quad (111)$$

where $\bar{\theta} \in \mathbb{R}^{l_\theta}$, by $\bar{\theta}_{k+1} \triangleq \underset{\bar{\theta} \in \mathbb{R}^{l_\theta}}{\text{argmin}} J_k(\bar{\theta})$. Then, for all $k \geq 0$, $\bar{\theta}_{k+1}$ is given by

$$\bar{P}_{k+1} = \frac{1}{\lambda_k} \bar{P}_k - \frac{1}{\lambda_k} \bar{P}_k \phi_k^T (\lambda_k I_{l_y} + \phi_k \bar{P}_k \phi_k^T)^{-1} \phi_k \bar{P}_k \quad (112)$$

$$\bar{\theta}_{k+1} = \bar{\theta}_k + \bar{P}_{k+1} \phi_k^T (\bar{y}_k - \phi_k \bar{\theta}_k) \quad (113)$$

For RLSID and RLSAC, a technique for specifying λ_k is given later in this section.

A. Recursive Least Squares-Based Identification

To identify $EG_d(\mathbf{q})$, an IIR model of the form Eq. (100) is fit to data. Since E is known, $y_{z,k} = Ey_k$ can be computed internally by RLSID. Using Proposition 6, for all $k \geq 0$ the model coefficient vector $\theta_{m,k}$ is updated recursively using

$$P_{m,k+1} = \frac{1}{\lambda_{m,k}} P_{m,k} - \frac{1}{\lambda_{m,k}} P_{m,k} \phi_{m,k}^T (\lambda_{m,k} I_q + \phi_{m,k} P_{m,k} \phi_{m,k}^T)^{-1} \phi_{m,k} P_{m,k} \quad (114)$$

$$\theta_{m,k+1} = \theta_{m,k} + P_{m,k+1} \phi_{m,k}^T (y_{z,k} - \phi_{m,k} \theta_{m,k}) \quad (115)$$

where $\phi_{m,k}$ and $\theta_{m,k}$ are given by Eqs. (102) and (103), respectively, and $P_{m,0} \in \mathbb{R}^{l_{a_m} \times l_{a_m}}$ is positive definite. The RLSID model at step k is given by

$$EG_{d,k}(\mathbf{q}) = (I_q \mathbf{q}^n + F_{1,k} \mathbf{q}^{n-1} + \dots + F_{\eta,k})^{-1} (G_{0,k} \mathbf{q}^n + \dots + G_{\eta,k}) \quad (116)$$

B. Recursive Least Squares-Based Adaptive Control

Define the strictly proper dynamic compensator

$$u_k \triangleq \text{sat}_{\bar{u}}(\phi_{c,k} \theta_{c,k}) \quad (117)$$

where $\phi_{c,k}$ and $\theta_{c,k}$ are given by Eqs. (14) and (15), respectively. The definition (117) represents an IIR controller whose output is saturated componentwise by the scalar saturation function $\text{sat}_{\bar{u}}$ defined by

$$\text{sat}_{\bar{u}}(x_i) \triangleq \begin{cases} x_i, & |x_i| < \bar{u}_i, \\ \text{sign}(x_i) \bar{u}_i, & |x_i| \geq \bar{u}_i \end{cases} \quad (118)$$

Next, define the filtered signals

$$u_{f,k} \triangleq G_{f,k}(\mathbf{q}) u_k \quad (119)$$

$$\phi_{f,k} \triangleq G_{f,k}(\mathbf{q}) \phi_{c,k} \quad (120)$$

where, for startup, $u_{f,k}$ and $\phi_{f,k}$ are initialized at zero and thus are computed as the forced responses of Eqs. (119) and (120), respectively, and where $G_{f,k}(\mathbf{q})$ is the time-dependent target model constructed using the updated numerator coefficients $G_{0,k+1}, \dots, G_{\eta,k+1}$ of the model (100). In particular,

$$G_{f,k}(\mathbf{q}) \triangleq - \sum_{i=0}^{\eta} G_{i,k+1} \frac{1}{\mathbf{q}^i} \quad (121)$$

which has the same form as Eq. (92) except that Eq. (121) is time varying, generalizes to MIMO systems, and includes all of the zeros of $EG_{d,k}(\mathbf{q})$. In the case where $q = m = 1$, it follows from $G_{0,k} = \dots = G_{\xi-1,k} = 0$ and $G_{\xi,k} = G_{\xi}$ that Eq. (121) and $-EG_d(\mathbf{q})$ have the same leading numerator coefficient and relative degree. Note that, at each step k , the numerator of Eq. (121) is chosen to be the numerator of Eq. (116). If there exists $k \geq 0$ such that $G_{0,k} = \dots = G_{\eta,k} = 0_{q \times m}$, then $G_{f,k}(\mathbf{q})$ is chosen to be

$$G_{f,k}(\mathbf{q}) \triangleq -\mathbf{1}_{q \times m} \quad (122)$$

The retrospective performance variable is defined to be

$$\hat{z}_k(\theta_c) \triangleq z_k - u_{f,k} + \phi_{f,k} \theta_c \quad (123)$$

Using Eqs. (121) and (122), Eq. (123) can be expressed as

$$\hat{z}_k(\theta_c) \triangleq z_k - N_k U_k + N_k \Phi_{c,k} \theta_c \quad (124)$$

where

$$N_k \triangleq \begin{cases} [-\mathbf{1}_{q \times m} 0 \dots 0], & G_{0,k+1} = \dots = G_{\eta,k} = 0, \\ [-G_{0,k+1} \dots -G_{\eta,k+1}], & \text{otherwise} \end{cases} \quad (125)$$

$N_k \in \mathbb{R}^{q \times (\eta+1)m}$, \bar{u}_k and $\bar{\phi}_{c,k}$ are given by Eqs. (27) and (28) with $n_f = \eta$, respectively, and $G_{0,k+1}, \dots, G_{\eta,k+1} \in \mathbb{R}^{q \times m}$ are the numerator coefficients of the RLSID model. Note that, by performing the RLSID update at step k before the RLSAC update, it follows thus the estimated numerator coefficients $G_{0,k+1}, \dots, G_{\eta,k+1}$ are available for constructing N_k at step k .

Next, define the controller cost variable

$$z_{c,k}(\theta_c) \triangleq \begin{bmatrix} E_z \hat{z}_k(\theta_c) \\ E_u \phi_{c,k} \theta_c \\ E_{\Delta u} (\phi_{c,k} \theta_c - u_k) \end{bmatrix} \in \mathbb{R}^{q+r_1+r_2} \quad (126)$$

where the performance weighting $E_z \in \mathbb{R}^{q \times q}$ is nonsingular and $E_u \in \mathbb{R}^{r_1 \times m}$, $E_{\Delta u} \in \mathbb{R}^{r_2 \times m}$ are the control weighting and control-move weighting, respectively. If $E_u = 0$ and $E_{\Delta u} = 0$, then $r_1 = 0$ and $r_2 = 0$, respectively, and all expressions involving E_u and $E_{\Delta u}$ are omitted from Eq. (126), as well as from all subsequent expressions. Note that

$$z_{c,k}(\theta_c)^T z_{c,k}(\theta_c) = \hat{z}_k(\theta_c)^T R_z \hat{z}_k(\theta_c) + \theta_c^T \phi_{c,k}^T R_u \phi_{c,k} \theta_c + (\phi_{c,k} \theta_c - u_k)^T \phi_{c,k}^T R_{\Delta u} \phi_{c,k} (\phi_{c,k} \theta_c - u_k) \quad (127)$$

where $R_z \triangleq E_z^T E_z \in \mathbb{R}^{q \times q}$ is positive definite, and $R_u \triangleq E_u^T E_u \in \mathbb{R}^{m \times m}$, $R_{\Delta u} \triangleq E_{\Delta u}^T E_{\Delta u} \in \mathbb{R}^{m \times m}$ are positive semidefinite.

Using Proposition 6, for all $k \geq 0$ the controller coefficient vector $\theta_{c,k}$ is updated recursively using

$$P_{c,k+1} = \frac{1}{\lambda_{c,k}} P_{c,k} - \frac{1}{\lambda_{c,k}} P_{c,k} \phi_{fc,k}^T (\lambda_{c,k} I_{q+r_1+r_2} + \phi_{fc,k} P_{c,k} \phi_{fc,k}^T)^{-1} \phi_{fc,k} P_{c,k} \quad (128)$$

$$\theta_{c,k+1} = \theta_{c,k} + P_{c,k+1} \phi_{fc,k}^T (y_{c,k} - \phi_{fc,k} \theta_{c,k}) \quad (129)$$

where

$$y_{c,k} \triangleq \begin{bmatrix} E_z z_k - E_z N_k \bar{U}_k \\ 0 \\ -E_{\Delta u} u_k \end{bmatrix} \in \mathbb{R}^{q+r_1+r_2},$$

$$\phi_{fc,k} \triangleq \begin{bmatrix} -E_z N_k \Phi_{c,k} \\ -E_u \phi_{c,k} \\ -E_{\Delta u} \phi_{c,k} \end{bmatrix} \in \mathbb{R}^{(q+r_1+r_2) \times l_{\theta_c}} \quad (130)$$

and $P_{c,0} \in \mathbb{R}^{l_{\theta_c} \times l_{\theta_c}}$ is positive definite.

For all of the examples in this paper, $\theta_{m,k}$ and $\theta_{c,k}$ are initialized as 0, and thus Eq. (122) is invoked at startup. This assumption reflects the absence of additional prior modeling information; however, $\theta_{m,k}$ and $\theta_{c,k}$ can be initialized based on any available modeling information. To initialize RLSAC and RLSID, $P_{c,0} = p_{c,0} I_{l_{\theta_c}}$ and $P_{m,0} = p_{c,0} I_{l_{\theta_m}}$ are chosen, where, for convenience, $p_{c,0} > 0$ is a common tuning parameter.

C. Data-Dependent Variable Rate Forgetting

For data-dependent VRF, set

$$\lambda_{m,k} = \frac{1}{1 + \varepsilon e(z_{m,k-\tau_d}, \dots, z_{m,k}) \mathbf{1}[e(z_{m,k-\tau_d}, \dots, z_{m,k})]} \quad (131)$$

$$\lambda_{c,k} = \frac{1}{1 + \varepsilon e(z_{c,k-\tau_d}, \dots, z_k) \mathbf{1}[e(z_{c,k-\tau_d}, \dots, z_k)]} \quad (132)$$

where

$$e(x_{k-\tau_d}, \dots, x_k) \triangleq \frac{\sqrt{\frac{1}{\tau_n} \sum_{i=k-\tau_n}^k x_i^T x_i}}{\sqrt{\frac{1}{\tau_d} \sum_{i=k-\tau_d}^k x_i^T x_i}} - 1.2 \quad (133)$$

“ $\mathbf{1}$ ” is the step function that is 0 for negative arguments and 1 for nonnegative arguments, and $e(0, \dots, 0) \triangleq 0$. In Eqs. (131–133), $\varepsilon \geq 0$, $0 < \tau_n < \tau_d$ are numerator and denominator window lengths, respectively. If the sequence $x_{k-\tau_d}, \dots, x_k$ is zero-mean noise, then the numerator and denominator of Eq. (133) approximate the average standard deviation of the noise over the intervals $[k - \tau_n, k]$ and $[k - \tau_d, k]$, respectively. In particular, by choosing $\tau_d \gg \tau_n$, it follows that the denominator of Eq. (133) approximates the long-term-average standard deviation of x_k , whereas the numerator of Eq. (133) approximates the short-term-average standard deviation of x_k . Consequently, the case $e(x_{k-\tau_d}, \dots, x_k) > 0$ implies that the short-term-average standard deviation of x_k is greater than the long-term-average standard deviation of x_k plus a threshold of 0.2. The function $e(x_{k-\tau_d}, \dots, x_k)$ used in VRF suspends forgetting when the short-term-average standard deviation of x_k drops below 1.2 times the long-term-average standard deviation of x_k . This technique thus prevents forgetting in RLSID and RCAC due to zero-mean sensor noise with constant standard deviation rather than due to the magnitude of the noise-free identification error and command-following error.

A list of parameters to be selected for DDRCAC is presented in Table 2.

Table 2 Tuning parameters that need to be selected for DDRCAC

Parameter	Description	Selection
η	Model window length	Integer ≥ 1 (1–10)
n_c	Controller window length	Integer ≥ 1 (2–40)
E_u	Control weighting	scaled $m \times m$ identity
$E_{\Delta u}$	Control move weighting	scaled $m \times m$ identity
\bar{u}	Control saturation-limit vector	95% actuator saturation limit
$p_{c,0}$	Initial RLS covariance scaling for RLSAC and RLSID	$p_{c,0} > 0$
ε	Forgetting parameter	$0 \leq \varepsilon < 1$ (0.001–0.2)
τ_n, τ_d	Forgetting window lengths	Integers $\tau_d > \tau_n$ ($\tau_n \in [1-400]$, $\tau_d \sim 3\tau_n$)

D. Numerical Examples

This subsection demonstrates DDRCAC, which uses no prior knowledge of $EG_d(\mathbf{q})$ and thus, in particular, no prior knowledge of the leading numerator coefficient, NMP zeros, or relative degree of $EG_d(\mathbf{q})$. Unless stated otherwise, all of the examples in this subsection use the same tuning parameters, namely, $p_{c,0} = 10^3$, $\eta = 4$, $n_c = 20$, $E = 1$, $E_z = 1$, $E_u = 0.1$, $E_{\Delta u} = 0$, $\varepsilon = 0.001$, $\tau_n = 200$, $\tau_d = 600$, and $\bar{u} = 1$. Furthermore, for all of the examples in this section $\tilde{y}_k \triangleq z_k$. As in Sec. IV.C, the ability of RLSID to estimate the leading numerator coefficient and relative degree of $EG_d(\mathbf{q})$ is investigated by comparing the first ξ numerator coefficients of the RLSID model and $EG_d(\mathbf{q})$. For all of the examples in this subsection, RLSID and RLSAC are applied with a strictly proper RLSID model and target model, respectively, which is enforced by removing u_k and $G_{0,k}$ from the definitions (102) and (103), respectively, redefining $l_{\theta_m} = \eta q(q + m)$ and

$$N_k \triangleq \begin{cases} [-\mathbf{1}_{q \times m} 0 \cdots 0], & G_{0,k+1} = \cdots = G_{\eta,k} = 0, \\ [-G_{1,k+1} \cdots -G_{\eta,k+1}], & \text{otherwise} \end{cases} \quad (134)$$

where $N_k \in \mathbb{R}^{q \times \eta m}$.

Example 10: Interaction between RLSID and RLSAC. Let

$$G_u(s) = \frac{100(s-10)(s+30)}{(s+10)(s^2-10s+1000)} \quad (135)$$

which is unstable and NMP, and, for $T_s = 0.01$ s/step, let $G_d(\mathbf{q})$ denote the ZOH discretization of $G_u(s)$. Then the NMP zero, leading numerator coefficient, and relative degree of $G_d(\mathbf{q})$ are 1.1056 rad/step, $G_\xi = G_1 = 1.079$, and $\xi = 1$, respectively. Let $\bar{w}_{k,i} = 0$, and let v_k be zero-mean, Gaussian white noise with standard deviation 0.001.

For command following with $r_k = \sin 0.23T_s k$, control is applied using an LQG controller designed for (A_d, B_d, C_d, D_d) augmented with a model of the harmonic command, using the MATLAB command `lqg`, with weights $Q_{xu} = Q_{wv} = I_6$. Figures 15a and 15c show the response and control u_k for the LQG controller, respectively. RLSID with VRF given by Eqs. (114) and (115) is used for closed-loop identification with the time-invariant LQG controller, as shown in Figs. 15e and 15h. In this case, the leading numerator coefficient and NMP zero of $G_d(\mathbf{q})$ are estimated poorly, as shown by Figs. 15g and 15h.

Next, adaptive control is applied with $\eta = 10$, where Figs. 15k and 15m show that, at $t \approx 0.1$ s, the leading numerator coefficient is correctly estimated, but the estimate of the NMP zero of $G_d(\mathbf{q})$ is erroneous. The initially poor RLSID model at $t \approx 0.1$ s results in a poor, infeasible target model, which induces a large transient response in $y_{z,k}$ and u_k for $0 \leq t \leq 1$ s. The additional persistency of this transient response, however, facilitates subsequent identification of the NMP zero of $G_d(\mathbf{q})$ at $t \approx 0.85$ s, as shown in Fig. 15g. Note that $\theta_{m,k}$ is converged for $t > 0.41$ s, and thus the time-dependent target model is also converged. With the converged time-dependent target model, Fig. 15g shows that RLS with VRF facilitates further adaptation of $\theta_{c,k}$ for $t > 0.41$ s, and $\theta_{c,k}$ is converged for $t > 1$ s. This

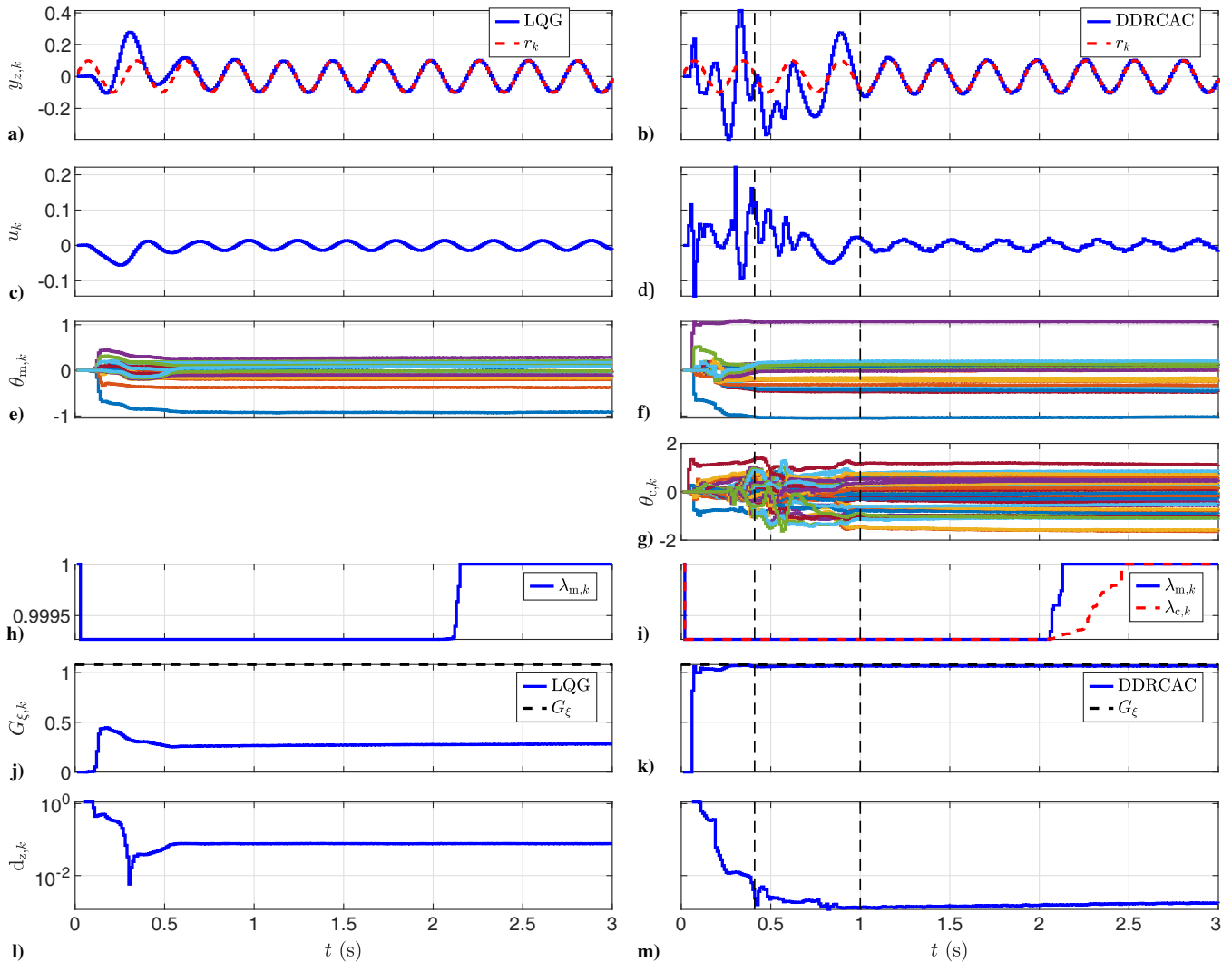


Fig. 15 Example 10: RLSID with LQG yields biased estimates of G_ξ and the NMP zero of $G_d(\mathbf{q})$; for adaptive control, the biases in (k) and (m) are smaller. The vertical dashed lines denote the settling times of $\theta_{m,k}$ and $\theta_{c,k}$.

example thus illustrates mutually beneficial interaction between RLSID and RLSAC. \diamond

Example 11: RCAC, DDRCAC, and $\hat{z}_k(\theta_{c,k+1})$ decomposition. Let $G_u(s)$ be given by Case 2 in Table 1 with $T_s = 0.01$ s/step. To avoid numerical issues arising from the need for multiple discretized systems, the disturbance w_k is assumed to be constant within each sampling interval $[kT_s, (k + 1)T_s)$. Because $G_u(s)$ is lightly damped, high-precision arithmetic is used to compare the left- and right-hand sides of Eq. (48).

For disturbance rejection, let $r_k = 0$, and let w_k and v_k be zero-mean, Gaussian white noise with standard deviations 0.1 and 0.001, respectively. Three scenarios are considered, namely, i) RCAC with the nominal target model

$$G_f(\mathbf{q}) = -0.153 \frac{(\mathbf{q} - 1.1078)}{\mathbf{q}^2}$$

which assumes knowledge of the true leading numerator coefficient, NMP zeros, and relative degree of $EG_d(\mathbf{q})$; ii) RCAC with the off-nominal target model

$$G_f(\mathbf{q}) = -0.35 \frac{(\mathbf{q} - 1.2)}{\mathbf{q}^2}$$

where the leading numerator coefficient is erroneous by a factor of 2.29 and the NMP zero is erroneous by a factor of 1.08; and iii) DDRCAC. RCAC is applied with $n_c = 20$, $E_u = 0.1$, $E_z = 1$,

and $p_{c,0} = 10^3$, which are identical to the tuning parameters for DDRCAC specified above.

The first, second, and third columns of Fig. 16 correspond to scenarios (i), (ii), and (iii), respectively. Note that the closed-loop performance degrades significantly due to the use of the off-nominal target model. However, with no prior knowledge of the system dynamics, DDRCAC achieves closed-loop performance similar to RCAC with the nominal target model.

Figure 17 shows the RLSID coefficients $\theta_{m,k}$; the true and estimated leading numerator coefficients G_ξ and $G_{\xi,k}$, respectively; the VRF factors $\lambda_{m,k}$, $\lambda_{c,k}$; and the closest distance $d_{z,k}$ between the zeros of the RLSID model and the NMP zero of $EG_d(\mathbf{q})$. Note that RLSID approximates the leading numerator coefficient, NMP zero, and relative degree of $EG_d(\mathbf{q})$, and thus the time-dependent target model (121) approximates the nominal target model. \diamond

Example 12: Effect of sensor noise and $p_{c,0}$. Let $G_u(s)$ be given by Case 3 in Table 1 with $T_s = 0.01$ s/step. Then the NMP zeros, leading numerator coefficient, and relative degree of $G_d(\mathbf{q})$ are $\{1.106 \pm 0.106j\}$ rad/step, $G_\xi = 0.128$, and $\xi = 3$, respectively. Hence, $G_1 = 0$, $G_2 = 0$, and $G_{\xi,k} = G_3 = 0.128$. The time-dependent target model (121) has the same leading numerator coefficient and relative degree as $-EG_d(\mathbf{q})$, and is thus equal to the nominal target model, if $G_{0,k} = \dots = G_{\xi-1,k} = 0$ and $G_{\xi,k} = G_\xi$.

Let $r_k = 0$, let $\tilde{w}_{k,i}$ be Gaussian white noise with standard deviation 0.1 and mean 0.5, and consider three scenarios, where v_k is zero-mean, Gaussian white noise with standard deviations 0.001, 0.01, and 0.1; these scenarios correspond to the first, second, and

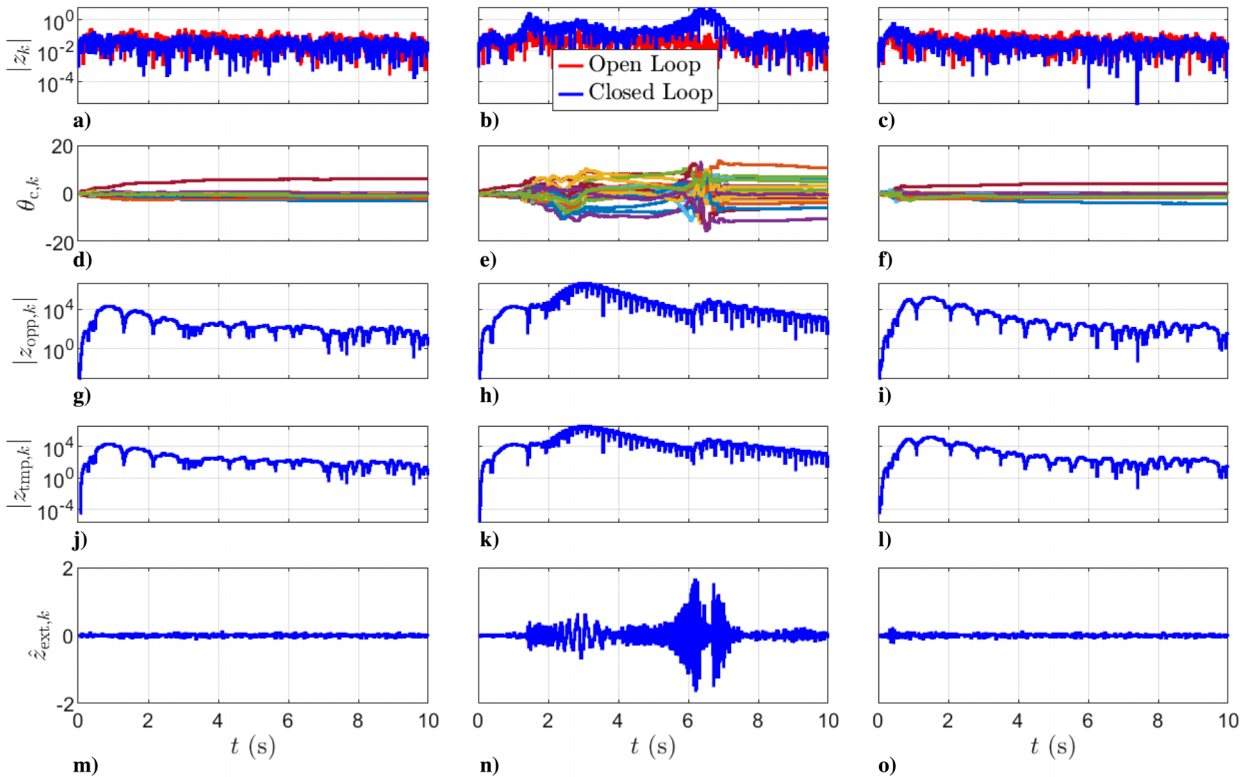


Fig. 16 Example 11: Columns 1–3 correspond to RCAC with the nominal target model, RCAC with an off-nominal target model, and DDRCAC. The performance of DDRCAC is similar to the performance RCAC in column 1.

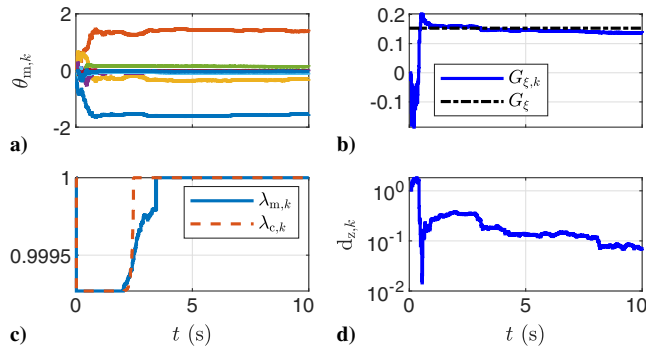


Fig. 17 Example 11: a) RLSID coefficients $\theta_{m,k}$; b) identified and true leading numerator coefficients, $G_{\xi,k}$, and G_{ξ} , respectively; c) forgetting factors $\lambda_{m,k}$ and $\lambda_{c,k}$ for RLSID and RLSAC, respectively; d) $d_{z,k}$.

third columns of Fig. 18, respectively. The measurement signal-to-noise ratio (SNR) is defined to be the ratio of the root-mean-square of the last 1000 subinterval steps of y_k to the root-mean-square of the last 1000 subinterval steps of v_k . Note that the suppression metric g_s decreases as SNR increases.

Next, to investigate the effect of $p_{c,0}$, three disturbance rejection scenarios with $r_k = 0$ are considered, where $p_{c,0}$ is 10, 10^2 , and 10^3 ; these scenarios correspond to the first, second, and third columns of Fig. 19, respectively. Note that, although the transient response of identified numerator coefficients increases with $p_{c,0}$, the level of asymptotic disturbance suppression is largely insensitive to the choice of $p_{c,0}$. \diamond

Example 13: Example 6 revisited using DDRCAC. As shown in Example 6, the control of nonsquare MIMO systems using RCAC can cause the creation of NMP cascade zeros of $(G_d, G_{c,k})$ that are cancelled by poles of $G_{c,k}$, leading to the divergence of u_k . DDRCAC is applied with $E_u = 0$, and thus the tuning parameters are identical to the RCAC tuning parameters in Example 6. As in Example 6, Fig. 20 shows that the controller gives rise to NMP cascade zeros. However, unlike Example 6, these NMP zeros are not cancelled by the controller, and thus u_k does not diverge. \diamond

Example 14: Time-varying relative degree and NMP zeros with abrupt and smooth transitions. Let $\bar{w}_{k,i}$ and v_k be zero-mean, Gaussian white noise with standard deviations 0.1 and 0.01, respectively, and $r_k = 0$. Let $G_1(s)$, $G_2(s)$, and $G_3(s)$ be given by Case 1, Case 2, and Case 3 in Table 1, respectively, with minimal realizations (A_1, B_1, C_1, D_1) , (A_2, B_2, C_2, D_2) , and (A_3, B_3, C_3, D_3) , respectively. Furthermore, at each intersample time step $t = (k/10)T_s$, let $G_u(s)$ be given by Eqs. (1) and (2) with

$$\begin{aligned} A(t) &\triangleq f(A_2, A_1, A_3, t), & B_w(t) = B(t) &\triangleq f(B_2, B_1, B_3, t), \\ C(t) &\triangleq f(C_2, C_1, C_3, t), & D(t) &\triangleq f(D_2, D_1, D_3, t) \end{aligned} \quad (136)$$

$$f(M_1, M_2, M_3, t) \triangleq \begin{cases} M_1, & t \leq 10 \text{ s}, \\ M_2, & 10 < t \leq 15 \text{ s}, \\ M_2 + (M_2 - M_1) \frac{t - 10}{5}, & 15 < t \leq 20 \text{ s}, \\ M_3, & t > 20 \text{ s} \end{cases} \quad (137)$$

Note that, at $t = 10$ s the relative degree of the discretization of Eq. (136) changes from 1 to 3, and during $15 \leq t < 20$ s, the dynamics of the discretization of Eq. (136) smoothly transition from a single real NMP zero at 1.1078 rad/step to a pair of complex NMP zeros at $\{1.106 \pm 0.106j\}$ rad/step.

Figure 21 shows that the adaptive controller rejects the disturbance despite the unknown, abrupt, and smooth transitions in the dynamics Eq. (136). Note that in Fig. 21f, $G_{\xi,k}$ is equal to $G_{1,k}$ for $t \leq 10$ s and equal to $G_{3,k}$ for $t > 10$ s. Furthermore, note that $G_{\xi-1,k}$, $G_{\xi-2,k}$ are undefined for $t \leq 10$ s, and are thus plotted for $t > 10$ s in Fig. 21d. \diamond

VI. Adaptive Flight Control

In this section, DDRCAC is applied to several flight-control problems, namely, i) roll control of a hypersonic aircraft with an

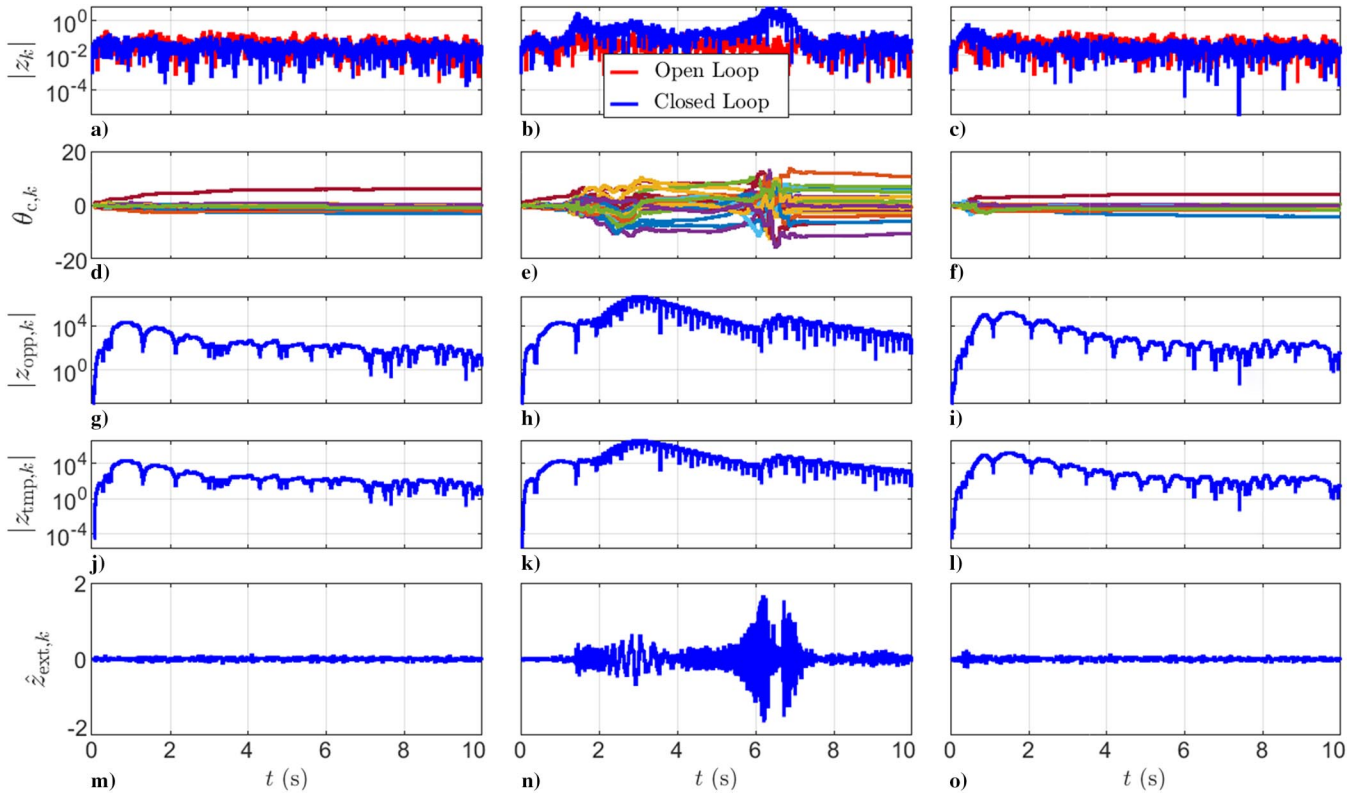


Fig. 18 Example 12: Columns 1–3 correspond to v_k with standard deviations 0.001, 0.01, and 0.1. The insets in (m), (n), and (o) show the full range of the transient response.

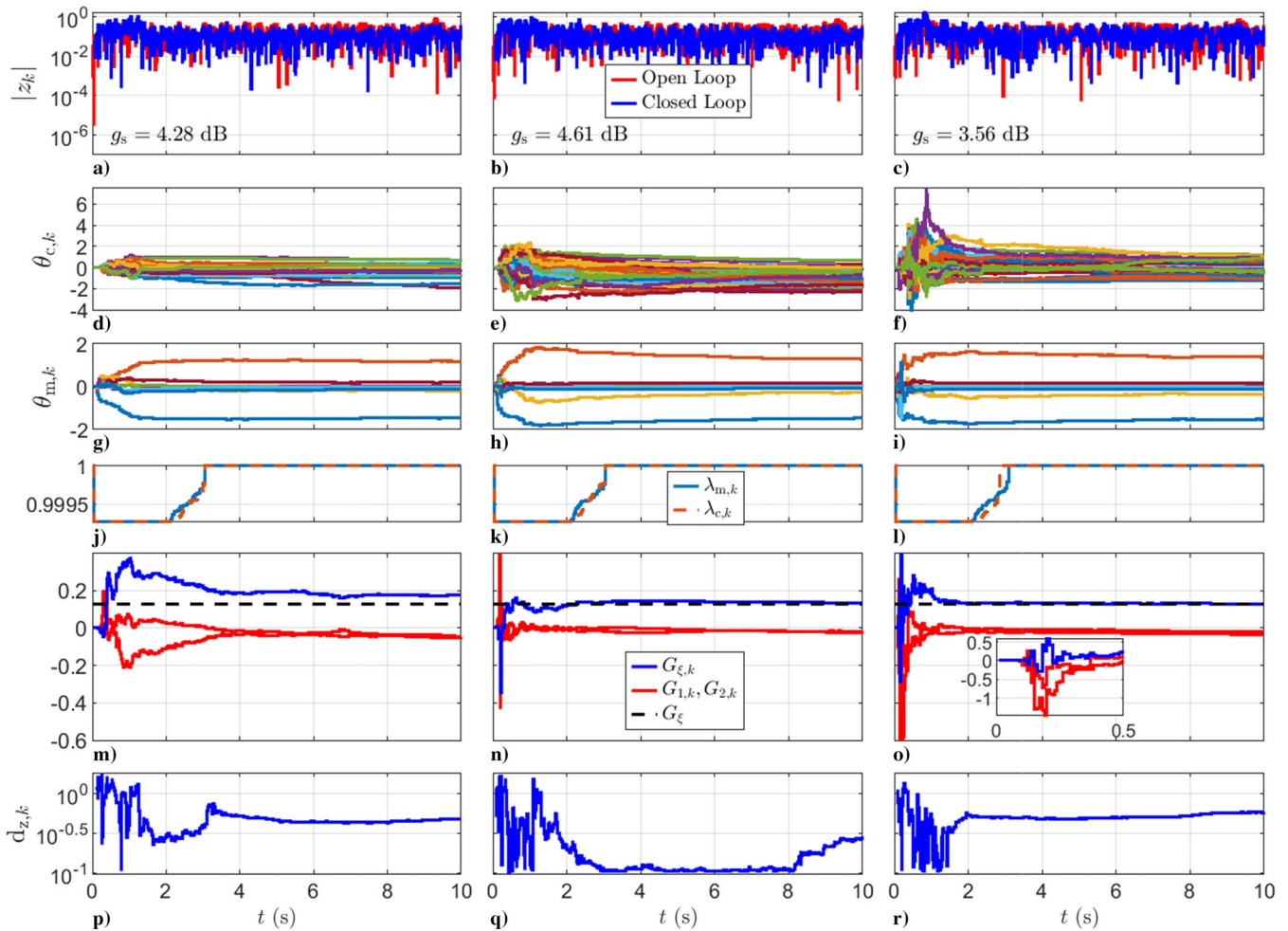


Fig. 19 Example 12: Columns 1–3 correspond to $p_{c,0} = 10$, $p_{c,0} = 10^2$, $p_{c,0} = 10^3$. The inset in (o) shows the full range of the transient response.

Downloaded by UNIV OF MICHIGAN on January 12, 2022 | http://arc.aiaa.org | DOI: 10.2514/1.6005778

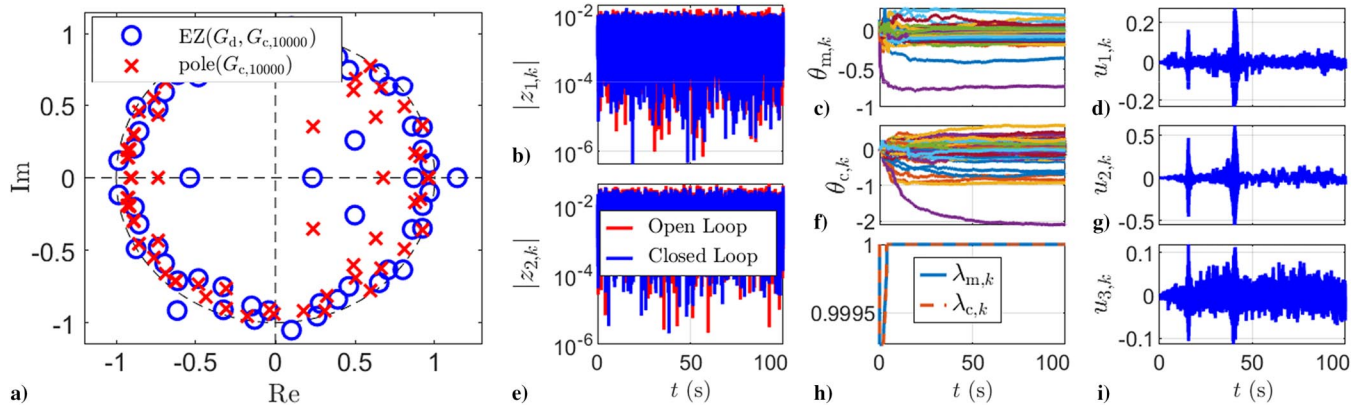


Fig. 20 Example 13: Example 4.7 revisited using DDRCAC. Unlike Example 4.7, no NMP cascade zeros are cancelled by the controller.

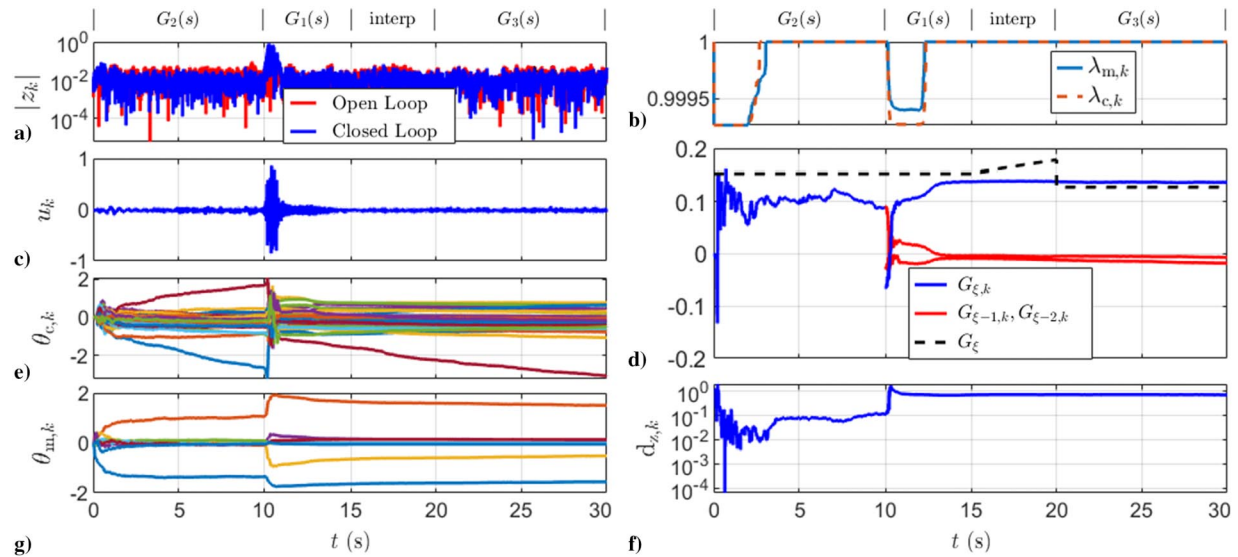


Fig. 21 Example 14: Disturbance rejection for Eq. (136). The relative degree changes from 1 to 3 at $t = 10$ s, and, during $t \in [15, 20]$ s, the discretization of Eq. (136) transitions from one real NMP zero to two complex NMP zeros.

unknown transition from MP to NMP dynamics, ii) pitch-rate control of a flexible aircraft, iii) flutter suppression, and iv) normal-acceleration control a nonlinear planar missile. For consistency in applying DDRCAC, an exactly proper model structure is used for RLSID for all of the examples in this section. Furthermore, the signal-to-noise ratio (SNR) between y_k and v_k is computed for all of the subinterval steps of each example. Note that the first three examples are linear, whereas the last example is nonlinear.

Example 15: Roll control of a hypersonic aircraft with an unknown transition from MP to NMP dynamics. Consider the linearized lateral dynamics of a hypersonic aircraft [42–44], given by Eqs. (1) and (2) with

$$A(t) \triangleq \begin{bmatrix} -0.0771 & 0.269 & -0.9631 & 0.0397 \\ \ell(t, -25.6, -108.8) & 0.0218 & 0.0995 & 0 \\ \ell(t, 0.6160, 0.4107) & 0.0376 & -0.2687 & 0 \\ 0 & 1 & -0.4202 & 0.0058 \end{bmatrix},$$

$$B(t) = B_w(t) \triangleq \begin{bmatrix} -0.0002 \\ 2.519 \\ \ell(t, -0.0222, -0.0665) \\ 0 \end{bmatrix} \quad (138)$$

$$C \triangleq [0 \ 0 \ 0 \ 1], \quad D = 0,$$

$$\ell(t, a, b) \triangleq \begin{cases} a, & t < 80 \text{ s}, \\ a + \frac{t-80}{20}(b-a), & 80 \leq t \leq 100 \text{ s}, \\ b, & t > 100 \text{ s} \end{cases} \quad (139)$$

where the components of $x(t) \triangleq [\beta(t) \ \bar{p}(t) \ \bar{r}(t) \ \phi(t)]^T$ are sideslip angle in rad, body x -axis angular velocity in rad/s, body z -axis angular velocity in rad/s, and roll angle in rad, and the dynamics transition from MP to NMP. Note that, in the case of full-state feedback, that is, $C = I_4$, Eqs. (138) and (139) possess no zeros and thus no NMP zeros. For this example, however, output feedback is assumed, and thus Eqs. (138) and (139) may have NMP zeros. In addition, the measurements of the roll angle $\phi(t)$ are assumed to be noisy. The roll-angle command is given by

$$r_k = \begin{cases} 10 \sin 0.28T_s k \text{ deg}, & t < 250 \text{ s}, \\ 12 \sin 0.21T_s k \text{ deg}, & 250 \leq t < 400 \text{ s}, \\ -10 \text{ deg}, & 400 \leq t < 450 \text{ s}, \\ 10 \text{ deg}, & 450 \leq t < 500 \text{ s}, \\ -10 \text{ deg}, & t > 550 \text{ s} \end{cases} \quad (140)$$

which is a harmonic signal that abruptly changes frequency, followed by a sequence of step commands. The instantaneous poles and zeros

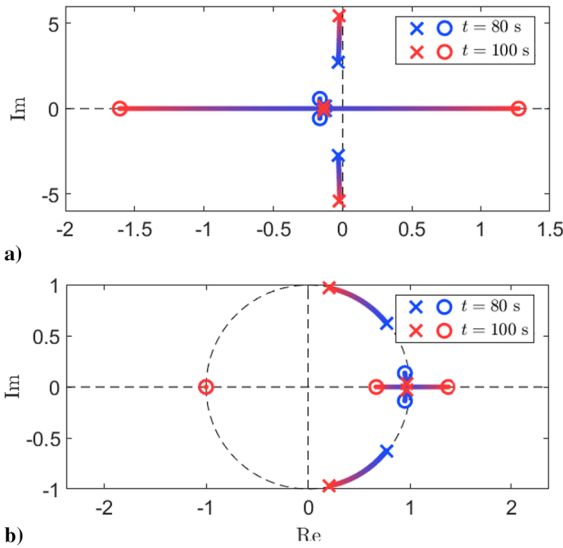
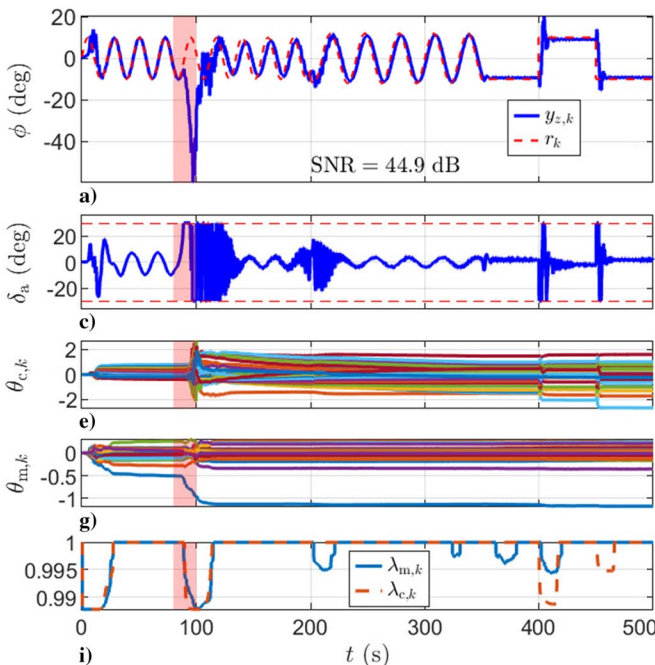


Fig. 22 Example 15: Instantaneous a) continuous- and b) discrete-time poles and zeros of the hypersonic aircraft during the transition from 80 to 100 s. The details of the transition are assumed to be unknown.

of $EG_u(s)$ and $EG_d(\mathbf{q})$ as functions of t are shown in Figs. 22a and 22b, respectively. The dynamics (138) and (139) and their discretization transition from MP to NMP.

The signal $u(t) = \delta_a(t)$ represents the asymmetric deflection of the split flaps in radians. The actuator rate-saturation and magnitude-saturation limits are 300 deg/s and 30 deg, respectively. Let $\bar{w}_{k,i}$ be Gaussian white noise with standard deviation 0.01 and mean 0.02, and let v_k be zero-mean, Gaussian white noise with standard deviation 0.001. The onset, duration, and time-dependence of the transition from MP to NMP dynamics, which occurs during [80, 100] s, are assumed to be unknown to the control algorithm.

Adaptive control is applied with $E = 1$, $T_s = 0.25$ s/step, $\bar{y}_k \triangleq z_k$, $p_{c,0} = 10$, $\eta = 12$, $n_c = 12$, $E_z = 1$, $E_u = 0$, $E_{\Delta u} = 0.1$, $\varepsilon = 0.01$, $\tau_n = 60$, $\tau_d = 300$, and $\bar{u} = 30$ deg. The response to the command (141) in the presence of disturbance is shown in Fig. 23. By adapting to the unknown, changing dynamics in $80 \leq t < 100$ s, RLSID and RLSAC are able to follow commands.



Example 16: Pitch-rate control of a flexible aircraft. Consider the pitch dynamics of a flexible aircraft [45] given by

$$G_u(s) = -0.417 \frac{s(s - 0.0143)(s - 0.4) \prod_{i=1}^4 (s^2 + 2\bar{\zeta}_i \bar{\omega}_i s + \bar{\omega}_i^2)}{\prod_{i=1}^6 (s^2 + 2\zeta_i \omega_i s + \omega_i^2)} \quad (141)$$

where $\bar{\zeta}_1 = 0.0423$, $\bar{\zeta}_2 = 0.147$, $\bar{\zeta}_3 = 0.0136$, $\bar{\zeta}_4 = 0.0125$, $\bar{\omega}_1 = 4.883$, $\bar{\omega}_2 = 17.79$, $\bar{\omega}_3 = 22.04$, $\bar{\omega}_4 = 23.59$, $\zeta_1 = 0.0951$, $\zeta_2 = 0.0358$, $\zeta_3 = 0.0374$, $\zeta_4 = 0.149$, $\zeta_5 = 0.021$, $\zeta_6 = 0.0136$, $\omega_1 = 0.0551$, $\omega_2 = 1.830$, $\omega_3 = 12.40$, $\omega_4 = 18.03$, $\omega_5 = 21.25$, and $\omega_6 = 22.04$. This system represents a flexible aircraft cruising at Mach 0.6 at 5000 ft, and includes aeroelastic effects. The transfer function (141) is lightly damped, asymptotically stable, and MP. This transfer function relates the elevator deflection δ_e in degrees to the pitch rate \bar{q} measured at the cockpit in rad/s. The actuator rate-saturation and magnitude-saturation limits are 300 deg/s and 30 deg, respectively.

Assume that $G_u(s) = G_w(s)$ and let $\bar{w}_{k,i}$ and v_k be zero-mean, Gaussian white noise with standard deviations 0.1 and 0.001, respectively. The pitch-rate command is

$$r_k = \begin{cases} 4 \text{ deg/s}, & t < 30 \text{ s}, \\ 0 \text{ deg/s}, & 30 \leq t < 60 \text{ s}, \\ -4 \text{ deg/s}, & 60 \leq t < 90 \text{ s}, \\ 0 \text{ deg/s}, & 90 \leq t < 120 \text{ s}, \\ 4 \text{ deg/s}, & 120 \leq t < 150 \text{ s}, \\ 0 \text{ deg/s}, & t \geq 150 \text{ s} \end{cases} \quad (142)$$

For this example, the adaptive controller is configured for command feedforward by defining

$$\bar{y}_k \triangleq \begin{bmatrix} z_k \\ r_k \end{bmatrix} \quad (143)$$

Adaptive control is applied with $T_s = 0.1$ s/step, $E = 1$, $p_{c,0} = 10^4$, $\eta = 8$, $n_c = 30$, $E_z = 1$, $E_u = 0$, $E_{\Delta u} = 0.01$, $\varepsilon = 0.02$, $\tau_n = 60$, $\tau_d = 240$, and $\bar{u} = 30$ deg. The response to a sequence

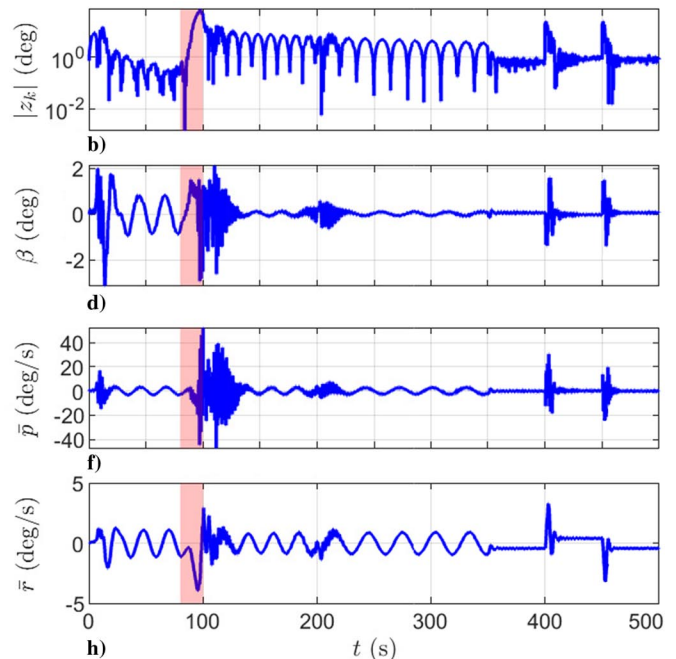


Fig. 23 Example 15: Response of the lateral dynamics of a hypersonic aircraft to harmonic and step commands with an unknown transition from MP to NMP dynamics, which occurs within the shaded regions.

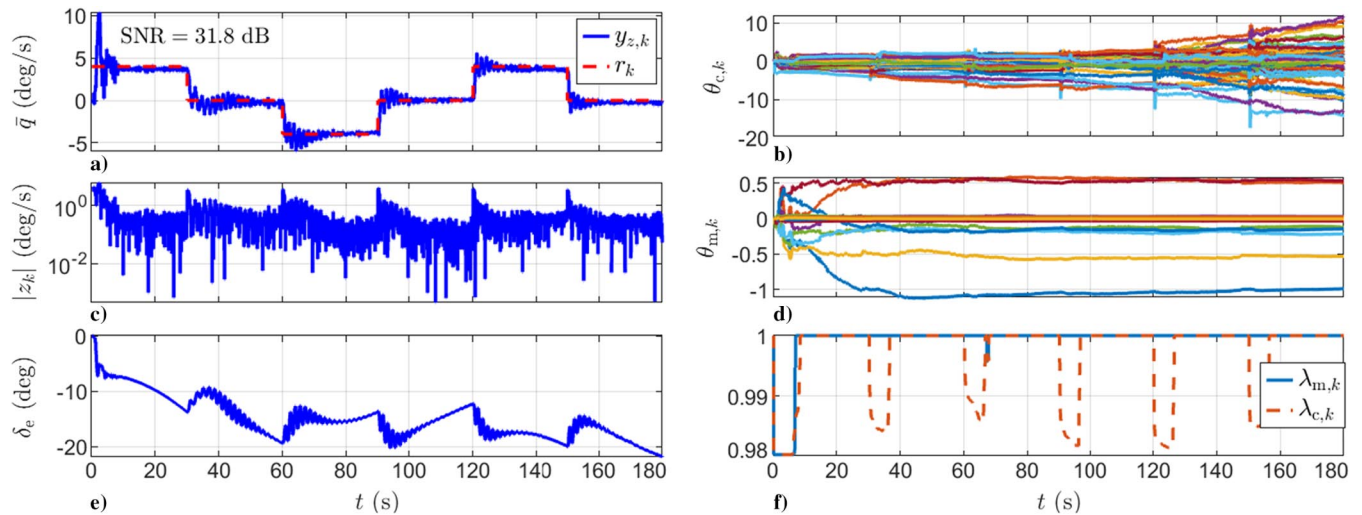


Fig. 24 Example 16: Response of the flexible aircraft to a sequence of pitch-rate step commands.

of step commands in the presence of zero-mean, Gaussian white-noise disturbance is shown in Fig. 24. \diamond

Example 17: Flutter suppression. Consider the Benchmark Active Control Technology (BACT) for Active Control Design Applications [46,47], which represents a wind-tunnel mounted wing that can translate vertically and pitch, and has a trailing edge flap as a control surface, as shown in Fig. 25. Various control techniques have been used to demonstrate flutter suppression in BACT [48–52]. The BACT model incorporates a vertical spring and damper to model vertical aerodynamic forces, as well as a rotational spring and damper to model aerodynamic torques.

Accelerometers mounted on the leading and trailing edges of the wing measure the leading-edge normal acceleration a_{LE} and trailing-edge normal acceleration a_{TE} , respectively. The flutter-suppression objective is to drive a_{LE} and a_{TE} to 0 using the control surface deflection δ_{TE} , in the presence of turbulence. Second-order actuator dynamics and a second-order Dryden wind turbulence model are included in BACT. The disturbance $\bar{w}_{k,i}$ represents the input to the second-order Dryden wind-turbulence model. BACT is an eighth-order, two-output-one-input, continuous-time, unstable, NMP, linear time-varying system with direct feedthrough, whose state-space matrices are functions of the freestream velocity U_0 . For this example the freestream velocity is varied as

$$U_0 = \begin{cases} 300 \text{ ft/s}, & t < 2 \text{ s}, \\ 300 + 25(t-2) \text{ ft/s}, & 2 \leq t < 6 \text{ s}, \\ 400 \text{ ft/s}, & t \geq 6 \text{ s} \end{cases} \quad (144)$$

The onset, duration, and time-dependence of the change of free-stream velocity, which occurs during [2, 6] s, are assumed to be

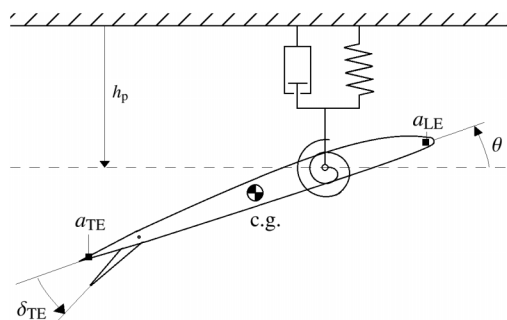


Fig. 25 Example 17: BACT wing. Leading- and trailing-edge accelerometers measure a_{LE} and a_{TE} . The wing can plunge and pitch. The actuator is a trailing-edge control surface with deflection δ_{TE} .

unknown to the control algorithm. The details of BACT are found in [47].

Let $\bar{w}_{k,i}$ and v_k be zero-mean, Gaussian white noise with standard deviations 1 and 0.05, respectively. Adaptive control is applied with $T_s = 0.02$ s/step, $E = I_2$, $\bar{y}_k \triangleq z_k$, $r_k = [0 \ 0]^T$, $p_{c,0} = 100$, $\eta = 2$, $n_c = 12$, $E_z = I_2$, $E_u = 1$, $E_{\Delta u} = 0$, $\varepsilon = 0.01$, $\tau_n = 40$, $\tau_d = 200$, and $\bar{u} = 12$ deg. The open- and closed-loop responses to a zero-mean, Gaussian white-noise disturbance are shown in Fig. 26. As noted in Fig. 26, the signal-to-noise ratio between the sampled noisy acceleration measurements and the sensor noise is approximately 13 dB. Therefore, the root-mean-squared level of the sensor noise is approximately 23% as large as the root-mean-squared level of the acceleration measurements. \diamond

Example 18: Normal-acceleration control of a nonlinear planar missile. Consider a tail-controlled interceptor missile, which is equipped with a strapdown accelerometer placed d_a meters forward of the center of mass of the missile, where the distance d_a is unknown. The missile [53–55] considered in this paper represents a missile in planar flight whose dynamics are given by

$$\dot{V} = \frac{1}{m} [f_d(C_{X\alpha} \cos \alpha + C_{Z\alpha} \sin \alpha) + T \cos \alpha - \bar{m}g \sin \gamma] + \frac{1}{m} f_d \sin(\alpha) C_{Z\delta} \delta \quad (145)$$

$$\dot{\alpha} = \frac{1}{mV} [f_d(C_{Z\alpha} \cos \alpha - C_{X\alpha} \sin \alpha) - T \sin \alpha + \bar{m}V\bar{q} + \bar{m}g \cos \gamma] + \frac{1}{mV} f_d \cos(\alpha) C_{Z\delta} \delta + w \quad (146)$$

$$\dot{\bar{q}} = \frac{d}{I_{yy}} f_d(C_{M\alpha} + C_{Mq}\bar{q}) + \frac{d}{I_{yy}} f_d C_{M\delta} \delta \quad (147)$$

$$\dot{\gamma} = \frac{1}{mV} [f_d(C_{X\alpha} \sin \alpha - C_{Z\alpha} \cos \alpha) + T \sin \alpha - \bar{m}g \cos \gamma] - \frac{1}{mV} f_d \cos(\alpha) C_{Z\delta} \delta \quad (148)$$

$$\dot{h} = V \sin \gamma \quad (149)$$

where arguments of t are omitted for brevity, $V(t)$ is the missile speed in m/s, T is the thrust in N, g is the acceleration due to gravity in m/s^2 , $\alpha(t)$ is the angle of attack in rad, $\bar{q}(t)$ is the y -axis angular velocity in rad/s, $\gamma(t)$ is the flight-path angle in rad, $h(t)$ is the altitude in m, $\delta(t)$ is the applied fin angle in rad, $f_d \triangleq \frac{1}{2} \rho V(t)^2 S$ is the dynamic force in N, $\rho(t) = \rho(h(t))$ is the air density in kg/m^3 at an altitude $h(t)$ m given by the International Standard Atmosphere

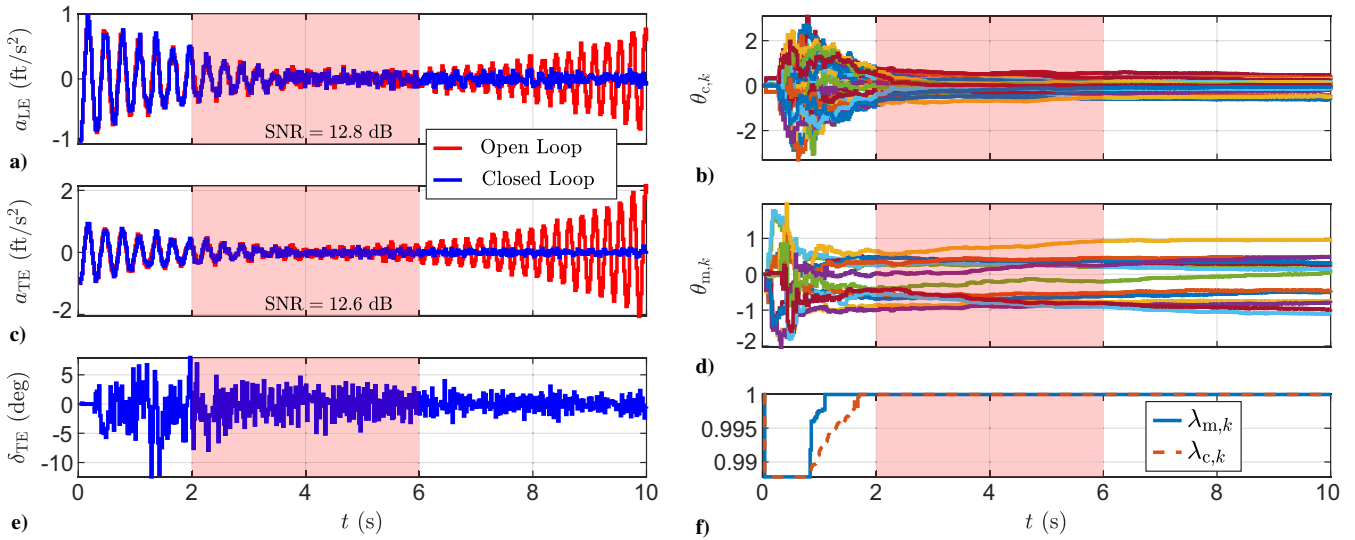


Fig. 26 Example 17: Open- and closed-loop responses of a_{LE} and a_{TE} . The freestream velocity U_0 is varied in the shaded region.

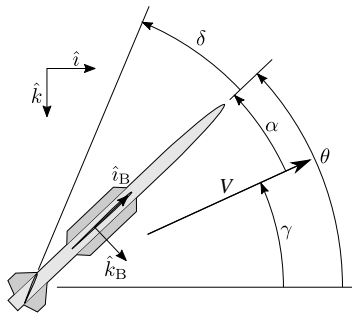


Fig. 27 Example 18: (\hat{i}, \hat{k}) and (\hat{i}_B, \hat{k}_B) are Earth-fixed and body-fixed unit vectors, δ is the fin deflection, α is the angle of attack, V is the missile velocity vector, γ is the flight-path angle, and θ is the pitch angle.

model, S is the reference surface area in m^2 , d is the reference length in m , \bar{m} is the mass of the missile in kg , and I_{yy} is the moment of inertia of the missile relative to its center of mass and around a transverse axis in $kg \cdot m^2$. The angles α , γ , θ , and δ_f are shown in Fig. 27. The values of the aerodynamic coefficients and parameter values are given in Tables 3 and 4, respectively.

Note that the aerodynamic coefficients are nonlinear functions of the missile speed $V(t)$, angle of attack $\alpha(t)$, and the local speed of sound a_s , which depends on the altitude $h(t)$.

The applied fin angle $\delta(t)$ is related to the requested fin angle $u_k = \delta_r(kT_s)$ by means of second-order actuator dynamics with natural frequency 150 rad/s , damping ratio 0.7 , and magnitude and rate

limits 30 deg and 500 deg/s , respectively. The gravity-corrected normal acceleration measured by an accelerometer placed at a distance d_a forward of the center of mass of the missile is given by

$$n_z = f_d(\mu C_{Z\alpha} - \mu_y C_{M\alpha} - \mu_y C_{Mq\bar{q}}) + f_d(\mu C_{Z\delta} - \mu_y C_{M\delta})\delta \quad (150)$$

where $\mu = (1/\bar{m})$, and $\mu_y = (dd_a/I_{yy})$. A noisy measurement $y_k = n_z(kT_s) + v_k$, of the normal acceleration $n_z(t)$, is used by the controller. The output equation (150) shows that there is a direct feedthrough of the applied fin $\delta(t)$ to the normal acceleration used by the controller.

For this example, the adaptive controller is configured for command feedforward by defining

$$\tilde{y}_k \triangleq \begin{bmatrix} z_k \\ r_k \end{bmatrix} \quad (151)$$

where the normal-acceleration command is $r_k = 100 \sin 0.025k^{1.2} \text{ m/s}^2$. Let $\bar{w}_{k,i}$ and v_k be zero-mean, Gaussian white noise with standard deviations 0.01 and 0.1 , respectively. Furthermore, let $V(0) = 985.7 \text{ m/s}$, $\alpha(0) = 0 \text{ rad}$, $\bar{q}(0) = 0 \text{ rad/s}$, $\gamma(0) = (\pi/4) \text{ rad}$, and $h(0) = 3000 \text{ m}$. Adaptive control is applied with $T_s = 0.05 \text{ s/step}$, $E = 1$, $p_{c,0} = 10^3$, $\eta = 4$, $n_c = 4$, $E_z = 1$, $E_u = 0$, $E_{\Delta u} = 0.005$, $\epsilon = 0.5$, $\tau_n = 20$, $\tau_d = 60$, and $\bar{u} = 30 \text{ deg}$. The command-following response of the nonlinear planar missile is shown in Fig. 28. After an initial transient, the command-following error is less than 5 g . Note that, starting with no prior knowledge of the nonlinear dynamics (145–149), the adaptive controller converges to a controller that facilitates command following.

Table 3 Aerodynamic coefficients

Aerodynamic coefficient	Value	Unit
$C_{X\alpha}$	-0.3005	---
$C_{Z\alpha}$	$9.717 \left(\frac{V}{3a_s} - 2 \right) \alpha - 31.023\alpha \alpha + 19.373\alpha^3$	---
$C_{M\alpha}$	$2.922 \left(\frac{8V}{3a_s} - 7 \right) \alpha - 64.015\alpha \alpha + 40.440\alpha^3$	---
$C_{Z\delta}$	-1.948	---
$C_{M\delta}$	-11.803	---
C_{Mq}	-1.719	s

α is the angle of attack in rad, V is the missile speed in m/s , and $a_s = a_s(h)$ is the local speed of sound given by the Internal Standard Atmosphere model at the altitude h .

Table 4 Parameter values for the nonlinear planar missile

Parameter	Value	Unit
\bar{m}	204.0227	kg
I_{yy}	247.4366	$kg \cdot m^2$
g	9.81	m/s^2
S	0.0409	m^2
d	0.2286	m
T	1000	N
d_a	0.5	m

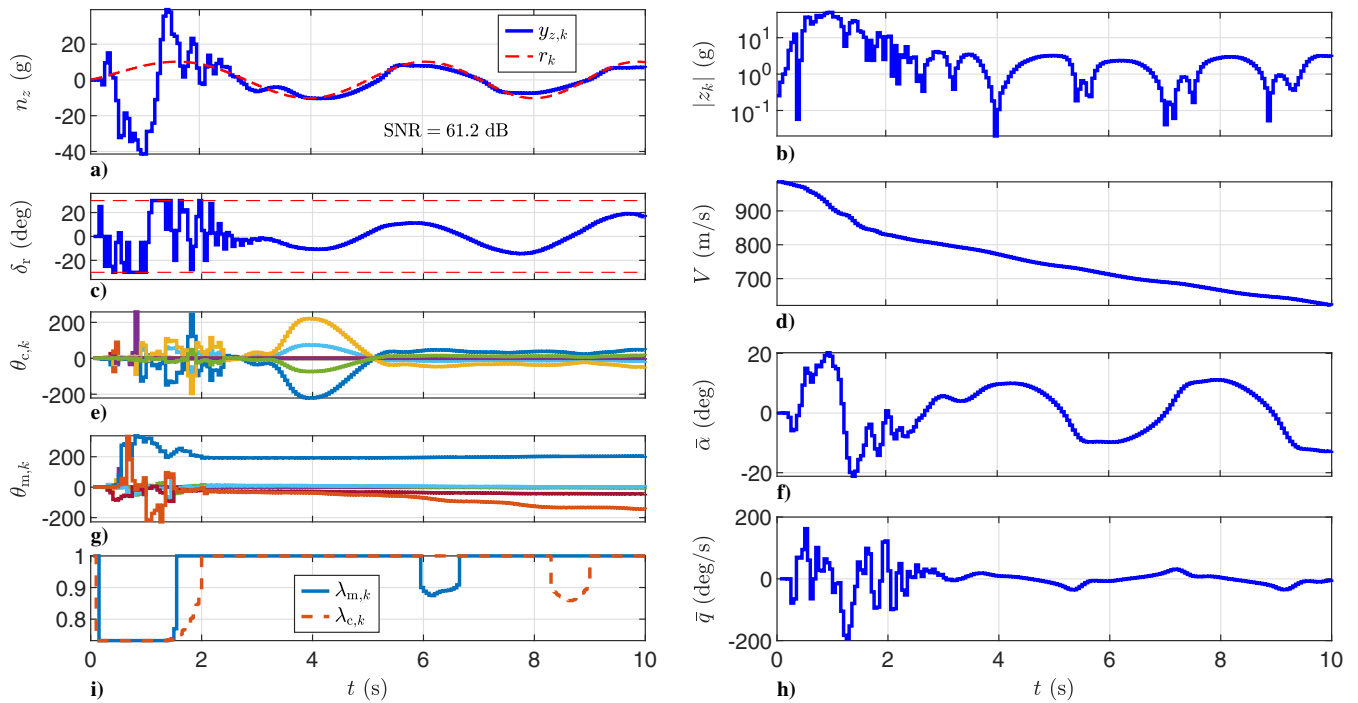


Fig. 28 Example 18: Normal-acceleration command-following response of the nonlinear planar missile.

VII. Conclusions

In the presence of sensor noise and actuator magnitude and rate limits, DDRCAC was shown to be effective for plants with a priori unknown NMP zeros, in contrast with standard output-feedback adaptive control methods, which are confined to MP systems. DDRCAC was also shown to avoid cancellation of NMP squaring zeros, which are created due to the cascade of a nonsquare system and a controller. Using RLS with VRF, DDRCAC was found to provide self-generated persistency, thus facilitating system identification. Furthermore, although closed-loop identification can entail parameter-estimate bias, it was found that, in DDRCAC, identification and control interact so as to reduce the effect of bias. Finally, flight-control examples showed that DDRCAC is effective for both linear and nonlinear applications as either a standalone embedded controller or as a simulation-based offline tuning technique for assessing achievable performance without requiring explicit knowledge of the underlying equations of motion.

Appendix A: Products of MIMO Transfer Functions and Pole-Zero Cancellations

This appendix considers pole-zero cancellation in products of MIMO transfer functions as these are present during control of MIMO systems.

Definition 5: Let $P \in \mathbb{R}[\mathbf{z}]^{l_1 \times l_2}$. Then the normal rank of P is defined by

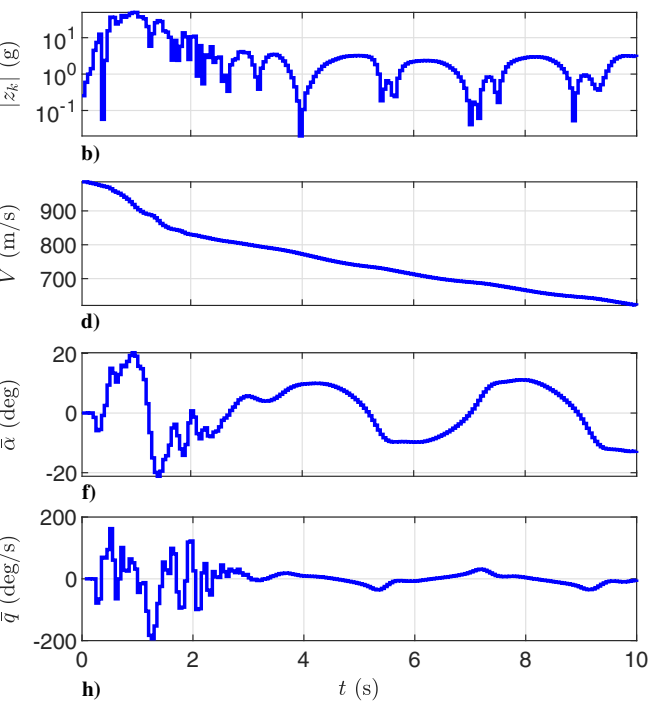
$$\text{rank} P \triangleq \max_{\mathbf{z} \in \mathcal{C}} \text{rank} P(\mathbf{z}) \quad (\text{A1})$$

Definition 6: Let (A, B, C, D) be a realization of $G \in \mathbb{R}(\mathbf{z})_{\text{prop}}^{l_1 \times l_2}$, where $A \in \mathbb{R}^{n \times n}$. Then the Rosenbrock system matrix $\mathcal{R}_{(A,B,C,D)} \in \mathbb{R}[\mathbf{z}]^{(n+l_1) \times (n+l_2)}$ of (A, B, C, D) is the polynomial matrix

$$\mathcal{R}_{(A,B,C,D)}(\mathbf{z}) \triangleq \begin{bmatrix} \mathbf{z}I - A & B \\ C & -D \end{bmatrix} \quad (\text{A2})$$

and $\mathbf{z}_0 \in \mathcal{C}$ is an invariant zero of (A, B, C, D) if

$$\text{rank} \mathcal{R}_{(A,B,C,D)}(\mathbf{z}_0) < \text{rank} \mathcal{R}_{(A,B,C,D)} \quad (\text{A3})$$



If, in addition, (A, B, C, D) is minimal, then $\mathcal{R}_{(A,B,C,D)}$ is denoted by \mathcal{R}_G , and $\mathbf{z}_0 \in \mathcal{C}$ is a transmission zero of G if

$$\text{rank} \mathcal{R}_G(\mathbf{z}_0) < \text{rank} \mathcal{R}_G \quad (\text{A4})$$

Definition 7: Let (A, B, C, D) be a realization of $G \in \mathbb{R}(\mathbf{z})_{\text{prop}}^{l_1 \times l_2}$. Then $\text{IZ}(A, B, C, D)$ is the multiset of invariant zeros of (A, B, C, D) , and $\text{TZ}(G)$ is the multiset of transmission zeros of G .

Definition 8: Let $G_1 \in \mathbb{R}(\mathbf{z})_{\text{prop}}^{l_1 \times l_2}$ and $G_2 \in \mathbb{R}(\mathbf{z})_{\text{prop}}^{l_2 \times l_3}$ with minimal realizations (A_1, B_1, C_1, D_1) and (A_2, B_2, C_2, D_2) , respectively. Define $G_{12} \triangleq G_1 G_2$, and consider its realization

$$\begin{aligned} A_{12} &\triangleq \begin{bmatrix} A_1 & B_1 C_2 \\ 0 & A_2 \end{bmatrix}, & B_{12} &\triangleq \begin{bmatrix} B_1 D_2 \\ B_2 \end{bmatrix}, \\ C_{12} &\triangleq \begin{bmatrix} C_1 & D_1 C_2 \end{bmatrix}, & D_{12} &\triangleq D_1 D_2 \end{aligned} \quad (\text{A5})$$

Then $\mathbf{z}_0 \in \mathcal{C}$ is a cascade zero of $G_1 G_2$, if, counting repetitions, it is an invariant zero of Eq. (A5) but not a transmission zero of either G_1 or G_2 . The multiset of cascade zeros of $G_1 G_2$ is denoted by

$$\text{CZ}(G_1, G_2) \triangleq \text{IZ}(A_{12}, B_{12}, C_{12}, D_{12}) \setminus [\text{TZ}(G_1) \cup \text{TZ}(G_2)] \quad (\text{A6})$$

Related results are found in [56,57]. Squaring is discussed in [58–60] and used in [61] to eliminate NMP zeros. The following result shows that cascade zeros of square transfer functions $G_1 G_2$ exist only in the case $l_1 \leq l_2$.

Proposition 6: Let $G_1 \in \mathbb{R}(\mathbf{z})_{\text{prop}}^{l_1 \times l_2}$ and $G_2 \in \mathbb{R}(\mathbf{z})_{\text{prop}}^{l_2 \times l_1}$ with minimal realizations (A_1, B_1, C_1, D_1) and (A_2, B_2, C_2, D_2) , respectively, where $A_1 \in \mathbb{R}^{n_1 \times n_1}$ and $A_2 \in \mathbb{R}^{n_2 \times n_2}$, and assume that G_1 and G_2 have full normal rank. Define $G_{12} \triangleq G_1 G_2$ and consider its realization (A5). If $\text{CZ}(G_1, G_2)$ is not empty, then $l_1 < l_2$.

Proof: Suppose that $l_1 \geq l_2$, and let $\mathbf{z} \in \text{CZ}(G_1, G_2)$. Since \mathbf{z} is not a transmission zero of either G_1 or G_2 , G_1 has full column rank, and G_2 has full row rank, it follows from ([62] Proposition 16.10.3) that

$$\text{rank} \begin{bmatrix} \mathbf{z}I_{n_1} - A_1 & B_1 \\ C_1 & -D_1 \end{bmatrix} = n_1 + l_2 \quad (\text{A7})$$

$$\text{rank} \begin{bmatrix} \mathbf{z}I_{n_2} - A_2 & B_2 \\ C_2 & -D_2 \end{bmatrix} = n_2 + l_2 \quad (\text{A8})$$

Next, note that

$$\begin{aligned} \mathcal{R}_{(A_{12}, B_{12}, C_{12}, D_{12})}(\mathbf{z}) &= \begin{bmatrix} \mathbf{z}I_{n_1} - A_1 & -B_1C_2 & B_1D_2 \\ 0 & \mathbf{z}I_{n_2} - A_2 & B_2 \\ C_1 & D_1C_2 & -D_1D_2 \end{bmatrix} \\ &= N_1(\mathbf{z})N_2(\mathbf{z}) \end{aligned} \quad (\text{A9})$$

where

$$N_1(\mathbf{z}) \triangleq \begin{bmatrix} \mathbf{z}I_{n_1} - A_1 & 0 & -B_1 \\ 0 & I_{n_2} & 0 \\ C_1 & 0 & D_1 \end{bmatrix} \in \mathbb{R}[\mathbf{z}]^{(n_1+n_2+l_1) \times (n_1+n_2+l_2)} \quad (\text{A10})$$

$$N_2(\mathbf{z}) \triangleq \begin{bmatrix} I_{n_1} & 0 & 0 \\ 0 & \mathbf{z}I_{n_2} - A_2 & B_2 \\ 0 & C_2 & -D_2 \end{bmatrix} \in \mathbb{R}[\mathbf{z}]^{(n_1+n_2+l_2) \times (n_1+n_2+l_1)} \quad (\text{A11})$$

It follows from Eqs. (A7) and (A8) that

$$\text{rank} N_1(\mathbf{z}) = \text{rank} N_2(\mathbf{z}) = n_1 + n_2 + l_2 \quad (\text{A12})$$

Next, Sylvester's inequality ([62] pp. 292, 294) implies

$$\begin{aligned} \text{rank} N_1(\mathbf{z}) + \text{rank} N_2(\mathbf{z}) - n_1 - n_2 - l_2 &\leq \text{rank} N_1(\mathbf{z})N_2(\mathbf{z}) \\ &\leq \min\{\text{rank} N_1(\mathbf{z}), \text{rank} N_2(\mathbf{z})\} \end{aligned} \quad (\text{A13})$$

It follows from Eqs. (A9–A13) that

$$\text{rank} \mathcal{R}_{(A_{12}, B_{12}, C_{12}, D_{12})}(\mathbf{z}) = n_1 + n_2 + l_2 \quad (\text{A14})$$

which shows that there are no values of \mathbf{z} such that $\text{rank} \mathcal{R}_{(A_{12}, B_{12}, C_{12}, D_{12})}(\mathbf{z}) < \text{rank} \mathcal{R}_{(A_{12}, B_{12}, C_{12}, D_{12})}$, and thus, $\mathbf{z} \notin \text{CZ}(G_1, G_2)$, which is a contradiction. \square

Definition 9: Let $G_1 \in \mathbb{R}(\mathbf{z})_{\text{prop}}^{l_1 \times l_2}$ and $G_2 \in \mathbb{R}(\mathbf{z})_{\text{prop}}^{l_2 \times l_3}$. Then the product $G_1 G_2 \in \mathbb{R}(\mathbf{z})_{\text{prop}}^{l_1 \times l_3}$ is down squared if $l_1 < l_2$ and up squared if $l_1 > l_2$.

Definition 10: Let $G_1 \in \mathbb{R}(\mathbf{z})_{\text{prop}}^{l_1 \times l_2}$ and $G_2 \in \mathbb{R}(\mathbf{z})_{\text{prop}}^{l_2 \times l_3}$ with minimal realizations (A_1, B_1, C_1, D_1) and (A_2, B_2, C_2, D_2) , respectively. Define $G_{12} \triangleq G_1 G_2$, and consider its realization (A5). Then $\mathbf{z}_0 \in \mathcal{C}$ is an evanescent zero of $G_1 G_2$, if, counting repetitions, it is a cascade zero of Eq. (A5) but not a transmission zero of G_{12} . The multiset of evanescent zeros of Eq. (A5) is denoted by

$$\text{EZ}(G_1, G_2) \triangleq \text{CZ}(G_1, G_2) \setminus \text{TZ}(G_{12}) \quad (\text{A15})$$

Example 19: Cascade and evanescent zeros. Consider the transfer functions

$$G_1(\mathbf{z}) = \frac{1}{\mathbf{z}(\mathbf{z}-3)} [\mathbf{z} \quad -1], \quad G_2(\mathbf{z}) = \frac{1}{\mathbf{z}(\mathbf{z}-4)} \begin{bmatrix} \mathbf{z}-1 \\ 4\mathbf{z}-6 \end{bmatrix} \quad (\text{A16})$$

which have minimal realizations (A_1, B_1, C_1, D_1) and (A_2, B_2, C_2, D_2) , respectively, where

$$A_1 \triangleq \begin{bmatrix} 0 & 0 \\ 1 & 3 \end{bmatrix}, \quad B_1 \triangleq \begin{bmatrix} 0 & -1 \\ 1 & 0 \end{bmatrix}, \quad C_1 \triangleq [0 \quad 1], \quad D_1 \triangleq [0 \quad 0] \quad (\text{A17})$$

$$A_2 \triangleq \begin{bmatrix} 4 & 0 \\ 1 & 0 \end{bmatrix}, \quad B_2 \triangleq \begin{bmatrix} 2 \\ 0 \end{bmatrix}, \quad C_2 \triangleq \begin{bmatrix} 0.5 & -0.5 \\ 2 & -3 \end{bmatrix}, \quad D_2 \triangleq \begin{bmatrix} 0 \\ 0 \end{bmatrix} \quad (\text{A18})$$

The Rosenbrock system matrices for (A_1, B_1, C_1, D_1) and (A_2, B_2, C_2, D_2) are

$$\begin{aligned} \mathcal{R}_{G_1}(\mathbf{z}) &\triangleq \begin{bmatrix} \mathbf{z} & 0 & 0 & -1 \\ -1 & \mathbf{z}-3 & 1 & 0 \\ 0 & 1 & 0 & 0 \end{bmatrix}, \\ \mathcal{R}_{G_2}(\mathbf{z}) &\triangleq \begin{bmatrix} \mathbf{z}-4 & 0 & 2 \\ -1 & \mathbf{z} & 0 \\ 0.5 & -0.5 & 0 \\ 2 & -3 & 0 \end{bmatrix} \end{aligned} \quad (\text{A19})$$

which show that $\text{rank} \mathcal{R}_{G_1}(\mathbf{z}) = \text{rank} \mathcal{R}_{G_1}$ and $\text{rank} \mathcal{R}_{G_2}(\mathbf{z}) = \text{rank} \mathcal{R}_{G_2}$, and thus $\text{TZ}(G_1)$ and $\text{TZ}(G_2)$ are empty. Next, consider the product $G_{12} \triangleq G_1 G_2$ with the realization (A5), which has the Rosenbrock system matrix

$$\mathcal{R}_{(A_{12}, B_{12}, C_{12}, D_{12})}(\mathbf{z}) \triangleq \begin{bmatrix} \mathbf{z} & 0 & 2 & -3 & 0 \\ -1 & \mathbf{z}-3 & -0.5 & 0.5 & 0 \\ 0 & 0 & \mathbf{z}-4 & 0 & 2 \\ 0 & 0 & -1 & \mathbf{z} & 0 \\ 0 & 1 & 0 & 0 & 0 \end{bmatrix} \quad (\text{A20})$$

It can be shown that $\text{rank} \mathcal{R}_{(A_{12}, B_{12}, C_{12}, D_{12})}(\mathbf{z}) < \text{rank} \mathcal{R}_{(A_{12}, B_{12}, C_{12}, D_{12})}$ (2) $< \text{rank} \mathcal{R}_{(A_{12}, B_{12}, C_{12}, D_{12})}$ (3) $< \text{rank} \mathcal{R}_{(A_{12}, B_{12}, C_{12}, D_{12})}$. Since $\text{TZ}(G_1)$ and $\text{TZ}(G_2)$ are empty, it follows that $\mathbf{z} = 2$ and $\mathbf{z} = 3$ are elements of $\text{CZ}(G_1, G_2)$. Next, consider the product of the transfer functions in Eq. (A16)

$$G_{12}(\mathbf{z}) \triangleq G_1(\mathbf{z})G_2(\mathbf{z}) = \frac{(\mathbf{z}-2)(\mathbf{z}-3)}{\mathbf{z}^2(\mathbf{z}-3)(\mathbf{z}-4)} = \frac{\mathbf{z}-2}{\mathbf{z}^2(\mathbf{z}-4)} \quad (\text{A21})$$

where the cascade zero at 3 is cancelled by a pole of G_1 , and thus $\mathbf{z} = 3$ is not an element of $\text{TZ}(G_{12})$. Therefore, $\mathbf{z} = 3$ is an element of $\text{EZ}(G_1, G_2)$. \diamond

Appendix B: Discrete-Time Filtering

This appendix reviews notation and terminology for discrete-time filtering in terms of the forward-shift operator \mathbf{q} . Define the proper discrete-time filter

$$G(\mathbf{q}) \triangleq D(\mathbf{q})^{-1}N(\mathbf{q}) \quad (\text{B1})$$

where $N(\mathbf{q}) = N_0\mathbf{q}^n + \dots + N_n \in \mathbb{R}[\mathbf{q}]^{p \times m}$ and $D(\mathbf{q}) = I_p\mathbf{q}^n + D_1\mathbf{q}^{n-1} + \dots + D_n \in \mathbb{R}[\mathbf{q}]^{p \times p}$ are polynomial matrices and $\det D(\mathbf{q}) \neq 0$.

Definition 11: The output $(y_k)_{k=-n}^\infty \subset \mathbb{R}^p$ of Eq. (B1) with input $(u_k)_{k=-n}^\infty \subset \mathbb{R}^m$ is given by the data filter

$$y_k + D_1 y_{k-1} + \dots + D_n y_{k-n} = N_0 u_k + \dots + N_n u_{k-n} \quad (\text{B2})$$

For convenience, Eq. (B2) is written as either

$$D(\mathbf{q})y_k = N(\mathbf{q})u_k \quad (\text{B3})$$

or

$$y_k = G(\mathbf{q})u_k \quad (\text{B4})$$

Example 20: Data filtering. Let $N(\mathbf{q}) = 2\mathbf{q} + 3$ and $D(\mathbf{q}) = \mathbf{q}^2 + 4\mathbf{q} + 5$, which yields the input-output difference equation

$$y_k = -4y_{k-1} - 5y_{k-2} + 2u_{k-1} + 3u_{k-2} \quad (\text{B5})$$

With the data $(u_k)_{k=-2}^0 = (6, 7, 8)$ and $(y_k)_{k=-2}^{-1} = (10, 11)$, Eq. (B4) yields

$$y_0 = -4y_{-1} - 5y_{-2} + 2u_{-1} + 3u_{-2} = -62 \quad (\text{B6})$$

$$y_1 = -4y_0 - 5y_{-1} + 2u_0 + 3u_{-1} = 230 \quad (\text{B7})$$

◇

Definition 8 is now extended to the case where the input u_k is a function of an independent variable x_k .

Definition 12: Let $D_1, \dots, D_n \in \mathbb{R}^{p \times p}$, let $N_0, \dots, N_n \in \mathbb{R}^{p \times m}$, let $y_{k-n}, \dots, y_{-1} \in \mathbb{R}^p$ be initial output data, let $(x_k)_{k=-n}^\infty \subset \mathbb{R}^r$, and, for all $k \geq -n$, let $u_k: \mathbb{R}^r \rightarrow \mathbb{R}^m$. Then, the FIA sequence $(y_k(x_k))_{k=0}^\infty$ is given by the fixed-input-argument (FIA) filter

$$\begin{aligned} y_k(x_k) + D_1 y_{k-1}(x_{k-1}) + \dots + D_n y_{k-n}(x_{k-n}) \\ = N_0 u_k(x_k) + \dots + N_n u_{k-n}(x_k) \end{aligned} \quad (\text{B8})$$

where, for all $k \in [-n, -1]$, $y_k(x_k) \triangleq u_k$.

Note that, at each step k , the arguments of u_{k-n}, \dots, u_k in Eq. (B8) are fixed at the current input value x_k over the interval $[k-n, k]$. In contrast, the left-hand side defines the current output $y_k(x_k)$, which depends on the past output values $y_{k-n}(x_{k-n}), \dots, y_{k-1}(x_{k-1})$. For convenience, Eq. (B8) is written as either

$$D(\mathbf{q})y_k(x_k) = N(\mathbf{q})u_k(x_k) \quad (\text{B9})$$

or

$$y_k(x_k) = G(\mathbf{q})u_k(x_k) \quad (\text{B10})$$

As a special case, note that

$$u_{k+r}(x_k) = \mathbf{q}^r u_k(x_k) \quad (\text{B11})$$

Example 21: FIA filtering. Let $N(\mathbf{q}) = 2\mathbf{q} + 3$ and $D(\mathbf{q}) = \mathbf{q}^2 + 4\mathbf{q} + 5$, and for all $k \geq -n$, define

$$u_k(x) \triangleq z_k x + 1 \quad (\text{B11})$$

The corresponding FIA filter is thus given by

$$\begin{aligned} y_k(x_k) = -4y_{k-1}(x_{k-1}) - 5y_{k-2}(x_{k-2}) + 2(z_{k-1}x_k + 1) \\ + 3(z_{k-2}x_k + 1) \end{aligned} \quad (\text{B12})$$

With the data $(z_k)_{k=-2}^0 = (14, 15, 16)$, $(x_k)_{k=0}^1 = (19, 20)$, and $(y_k)_{k=-2}^{-1} = (10, 11)$, Eq. (B12) yields

$$y_0(x_0) = -4y_{-1} - 5y_{-2} + 2(z_{-1}x_0 + 1) + 3(z_{-2}x_0 + 1) = 1279 \quad (\text{B13})$$

$$y_1(x_1) = -4y_0(x_0) - 5y_{-1} + 2(z_0x_1 + 1) + 3(z_{-1}x_1 + 1) = -3626 \quad (\text{B14})$$

◇

Acknowledgments

This research was supported by Office of Naval Research under Basic Research Challenge grant N00014-18-1-2211, and Air Force Office of Scientific Research under grant FA9550-20-1-0028 and Dynamic Data Driven Applications Systems grant FA9550-18-1-0171. The authors wish to thank John Burken and Tim Cox for providing the lateral aircraft dynamics model used in Example 15, Antai Xie for helpful discussions on the retrospective performance variable decomposition, Sneha Sanjeevini for discussions on the appendix, and Muneeza Azmat for discussions on filtering.

References

- [1] Parikh, A., Kamalapurkar, R., and Dixon, W. E., "Integral Concurrent Learning: Adaptive Control with Parameter Convergence Using Finite Excitation," *International Journal of Adaptive Control and Signal Processing*, Vol. 33, No. 12, 2019, pp. 1775–1787. <https://doi.org/10.1002/acs.2945>.
- [2] Gaudio, J. E., Annaswamy, A. M., Lavretsky, E., and Bolender, M. A., "Fast Parameter Convergence in Adaptive Flight Control," *AIAA Sci-Tech*, AIAA Paper 2020-0594, 2020. <https://doi.org/10.2514/6.2020-0594>.
- [3] Ioannou, P., and Fidan, B., *Adaptive Control Tutorial*, SIAM, Philadelphia, PA, 2006, p. 261. <https://doi.org/10.1137/1.9780898718652>.
- [4] Ioannou, P., and Sun, J., *Robust Adaptive Control*, Dover, New York, 2013, Chap. 9. https://doi.org/10.1007/978-1-4471-5102-9_118-1.
- [5] Tao, G., *Adaptive Control Design and Analysis*, Wiley, Hoboken, NJ, 2003, p. 17. <https://doi.org/10.1002/0471459100>.
- [6] Ilchmann, A., "Non-Identifier-Based Adaptive Control of Dynamical Systems: A Survey," *IMA Journal of Mathematical Control and Information*, Vol. 8, No. 4, 1991, pp. 321–366. <https://doi.org/10.1093/imamci/8.4.321>.
- [7] Hovakimyan, N., Cao, C., Kharisov, E., Xargay, E., and Gregory, I. M., "L1 Adaptive Control for Safety-Critical Systems," *IEEE Control Systems Magazine*, Vol. 31, No. 5, 2011, pp. 54–104. <https://doi.org/10.1109/MCS.2011.941961>.
- [8] Wiese, D. P., Annaswamy, A. M., Muse, J. A., Bolender, M. A., and Lavretsky, E., "Adaptive Output Feedback Based on Closed-Loop Reference Models for Hypersonic Vehicles," *AIAA Journal of Guidance, Control, and Dynamics*, Vol. 38, No. 12, 2015, pp. 2429–2440. <https://doi.org/10.2514/1.G001098>.
- [9] Tao, G., "Multivariable Adaptive Control: A Survey," *Automatica*, Vol. 50, No. 11, 2014, pp. 2737–2764. <https://doi.org/10.1016/j.automatica.2014.10.015>.
- [10] Hou, Z.-S., and Wang, Z., "From Model-Based Control to Data-Driven Control: Survey, Classification and Perspective," *Information Sciences*, Vol. 235, Aug. 2013, pp. 3–35. <https://doi.org/10.1016/j.ins.2012.07.014>.
- [11] Gao, W., Jiang, Z., and Ozbay, K., "Data-Driven Adaptive Optimal Control of Connected Vehicles," *IEEE Transactions on Intelligent Transportation Systems*, Vol. 18, No. 5, 2017, pp. 1122–1133. <https://doi.org/10.1109/TITS.2016.2597279>.
- [12] den Hof, P. V., and Schrama, R. J. P., "Identification and Control—Closed-Loop Issues," *Automatica*, Vol. 31, No. 12, 1995, pp. 1751–1770. [https://doi.org/10.1016/0005-1098\(95\)00094-X](https://doi.org/10.1016/0005-1098(95)00094-X).
- [13] Gevers, M., "Towards a Joint Design of Identification and Control?" *Essays on Control*, edited by H. L. Trentelman, and J. C. Willems, Vol. 14, Progress in Systems and Control Theory, Birkhäuser, Boston, MA, 1993, pp. 111–151. https://doi.org/10.1007/978-1-4612-0313-1_5.
- [14] Hjalmarsson, H., "From Experiment Design to Closed-Loop Control," *Automatica*, Vol. 41, No. 3, 2005, pp. 393–438. <https://doi.org/10.1016/j.automatica.2004.11.021>.
- [15] Feldbaum, A. A., "Dual Control Theory," *Avtomatika i Telemekhanika*, Vol. 22, No. 1, 1961, pp. 3–16.
- [16] Wittenmark, B., "Adaptive Dual Control Methods: An Overview," *Adaptive Systems in Control and Signal Processing*, edited by C. Bányász, Vol. 28, IFAC Postprint Volume, Pergamon, Oxford, 1995, pp. 67–72. <https://doi.org/10.1016/B978-0-08-042375-3.50010-X>.
- [17] Filatov, N. M., and Unbehauen, H., *Adaptive Dual Control: Theory and Applications*, Springer-Verlag, Berlin, 2004, p. 14. <https://doi.org/10.1007/b96083>.
- [18] Santillo, M. A., and Bernstein, D. S., "Adaptive Control Based on Retrospective Cost Optimization," *AIAA Journal of Guidance, Control, and Dynamics*, Vol. 33, No. 2, 2010, pp. 289–304. <https://doi.org/10.2514/1.46741>.
- [19] Hoagg, J. B., and Bernstein, D. S., "Retrospective Cost Model Reference Adaptive Control for Nonminimum-Phase Systems," *AIAA Journal of Guidance, Control, and Dynamics*, Vol. 35, No. 6, 2012, pp. 1767–1786. <https://doi.org/10.2514/1.57001>.
- [20] Rahman, Y., Xie, A., and Bernstein, D. S., "Retrospective Cost Adaptive Control: Pole Placement, Frequency Response, and Connections with LQG Control," *IEEE Control Systems Magazine*, Vol. 37, No. 5,

- 2017, pp. 28–69.
<https://doi.org/10.1109/MCS.2017.2718825>.
- [21] Islam, S. A. U., Xie, A., and Bernstein, D. S., “Adaptive Control of Systems with Unknown Nonminimum-Phase Zeros Using Cancellation-Based Pseudo-Identification,” *Proceedings of the American Control Conference*, IEEE, New York, 2019, pp. 441–446.
<https://doi.org/10.23919/ACC.2019.8814620>
- [22] Islam, S. A. U., and Bernstein, D. S., “Recursive Least Squares for Real-Time Implementation,” *IEEE Control Systems Magazine*, Vol. 39, No. 3, 2019, pp. 82–85.
<https://doi.org/10.1109/MCS.2019.2900788>.
- [23] Bruce, A. L., Goel, A., and Bernstein, D. S., “Convergence and Consistency of Recursive Least Squares with Variable-Rate Forgetting,” *Automatica*, Vol. 119, March 2020, Paper 109052.
<https://doi.org/10.1016/j.automatica.2020.109052>.
- [24] Willems, J. C., Rapisarda, P., Markovsky, I., and De Moor, B. L. M., “A Note on Persistency of Excitation,” *Systems and Control Letters*, Vol. 77, No. 4, 2005, pp. 325–329.
<https://doi.org/10.1016/j.sysconle.2004.09.003>.
- [25] Goel, A., Bruce, A., and Bernstein, D. S., “Recursive Least Squares with Variable-Direction Forgetting: Compensating for the Loss of Persistency,” *IEEE Control Systems Magazine*, Vol. 40, No. 4, 2020, pp. 80–102.
<https://doi.org/10.1109/MCS.2020.2990516>.
- [26] Chowdhary, G., Mühlegg, M., and Johnson, E. N., “Exponential Parameter and Tracking Error Convergence Guarantees for Adaptive Controllers Without Persistency of Excitation,” *International Journal of Control*, Vol. 87, No. 8, 2014, pp. 1583–1603.
<https://doi.org/10.1080/00207179.2014.880128>.
- [27] Forsell, U., and Ljung, L., “Closed-Loop Identification Revisited,” *Automatica*, Vol. 35, No. 7, 1999, pp. 1215–1241.
[https://doi.org/10.1016/S0005-1098\(99\)00022-9](https://doi.org/10.1016/S0005-1098(99)00022-9).
- [28] Aljanaideh, K. F., and Bernstein, D. S., “Closed-Loop Identification of Unstable Systems Using Noncausal FIR Models,” *International Journal of Control*, Vol. 90, No. 2, 2017, pp. 168–185.
<https://doi.org/10.1080/00207179.2016.1172733>.
- [29] Sobolic, F., Aljanaideh, K. F., and Bernstein, D. S., “A Numerical Investigation of Direct and Indirect Closed-Loop Architectures for Estimating Nonminimum-Phase Zeros,” *International Journal of Control*, Vol. 93, No. 6, 2020, pp. 1251–1265.
<https://doi.org/10.1080/00207179.2018.1501609>.
- [30] Gilson, M., and den Hof, P. V., “Instrumental Variable Methods for Closed-Loop System Identification,” *Automatica*, Vol. 41, No. 7, 2005, pp. 241–249.
<https://doi.org/10.1016/j.automatica.2004.09.016>.
- [31] Chen, T., Tapn, T., and Francis, B., *Optimal Sampled-Data Control Systems*, Springer-Verlag, London, 1995, p. 11.
<https://doi.org/10.1007/978-1-4471-3037-6>.
- [32] Aljanaideh, K. F., and Bernstein, D. S., “Initial Conditions in Time- and Frequency-Domain System Identification: Implications of the Shift Operator Versus the Z and Discrete Fourier Transforms,” *IEEE Control Systems Magazine*, Vol. 38, No. 2, 2018, pp. 80–93.
<https://doi.org/10.1109/MCS.2017.2786419>.
- [33] Middleton, R., and Goodwin, G., *Digital Control and Estimation: A Unified Approach*, Prentice-Hall, Englewood Cliffs, NJ, 1990, Part I.
<https://doi.org/10.1002/rmc.4590040308>.
- [34] Islam, S. A. U., Xie, A., and Bernstein, D. S., “Closed-Loop Performance versus Target-Model Matching in Retrospective Cost Adaptive Control,” *Proceedings of the American Control Conference* (to be published).
- [35] Goel, A., and Bernstein, D. S., “Gradient-, Ensemble-, and Adjoint-Free Data-Driven Parameter Estimation,” *AIAA Journal of Guidance, Control, and Dynamics*, Vol. 42, No. 8, 2019, pp. 1743–1754.
<https://doi.org/10.2514/1.G004158>.
- [36] Hansen, P. C., and O’Leary, D. P., “The Use of the L-Curve in the Regularization of Discrete Ill-Posed Problems,” *SIAM Journal on Scientific Computing*, Vol. 14, No. 6, 1993, pp. 1487–1503.
<https://doi.org/10.1137/0914086>.
- [37] Golub, G. H., Hansen, P. C., and O’Leary, D. P., “Tikhonov Regularization and Total Least Squares,” *SIAM Journal on Matrix Analysis and Applications*, Vol. 21, No. 1, 1999, pp. 185–194.
<https://doi.org/10.1137/S0895479897326432>.
- [38] Cucker, F., and Smale, S., “Best Choices for Regularization Parameters in Learning Theory: On the Bias-Variance Problem,” *Foundations of Computational Mathematics*, Vol. 2, No. 4, 2002, pp. 413–428.
<https://doi.org/10.1007/s102080010030>.
- [39] Lu, S., Pereverzev, S. V., and Tautenhahn, U., “Regularized Total Least Squares: Computational Aspects and Error Bounds,” *SIAM Journal on Matrix Analysis and Applications*, Vol. 31, No. 3, 2010, pp. 918–941.
<https://doi.org/10.1137/070709086>.
- [40] Lai, B., Islam, S. A. U., and Bernstein, D. S., “Regularization-Induced Bias and Consistency in Recursive Least Squares,” *Proceedings of the American Control Conference* (to be published).
- [41] Islam, S. A. U., Nguyen, T. W., Kolmanovsky, I. V., and Bernstein, D. S., “Adaptive Control of Discrete-Time Systems with Unknown, Unstable Zero Dynamics,” *Proceedings of the American Control Conference*, IEEE, New York, 2020, pp. 1387–1392.
<https://doi.org/10.23919/ACC45564.2020.9147891>.
- [42] Rahman, Y., Aljanaideh, K., Sumer, E. D., and Bernstein, D. S., “Adaptive Control of Aircraft Lateral Motion with an Unknown Transition to Nonminimum-Phase Dynamics,” *Proceedings of the American Control Conference*, IEEE, New York, 2014, pp. 2359–2364.
<https://doi.org/10.1109/ACC.2014.6859178>.
- [43] Ansari, A., and Bernstein, D. S., “Adaptive Control of an Aircraft with Uncertain Nonminimum-Phase Dynamics,” *Proceedings of the American Control Conference*, IEEE, New York, 2015, pp. 844–849.
<https://doi.org/10.1109/ACC.2015.7170839>.
- [44] Islam, S. A. U., Bruce, A. L., Nguyen, T. W., Kolmanovsky, I., and Bernstein, D. S., “Adaptive Flight Control with Unknown Time-Varying Unstable Zero Dynamics,” *AIAA SciTech*, AIAA Paper 2020-0839, 2020.
<https://doi.org/10.2514/6.2020-0839>.
- [45] Waszak, M. R., and Schmidt, D. K., “Flight Dynamics of Aeroelastic Vehicles,” *Journal of Aircraft*, Vol. 25, No. 6, 1988, pp. 563–571.
<https://doi.org/10.2514/3.45623>.
- [46] Waszak, M. R., “Modeling the Benchmark Active Control Technology Wind-Tunnel Model for Application to Flutter Suppression,” *21st AIAA Atmospheric Flight Mechanics Conference*, AIAA, Reston, VA, 1996, pp. 1–13; also AIAA Paper 1996-3437, 1996.
<https://doi.org/10.2514/6.1996-3437>.
- [47] Waszak, M., and Center, L. R., Modeling the Benchmark Active Control Technology Wind-Tunnel Model for Active Control Design Applications, NASA Langley Research Center, NASA TP-1998-206270, 1998.
<https://doi.org/10.2514/6.1996-3437>.
- [48] Scott, R. C., and Pado, L. E., “Active Control of Wind-Tunnel Model Aeroelastic Response Using Neural Networks,” *Journal of Guidance, Control, and Dynamics*, Vol. 23, No. 6, 2000, pp. 1100–1108.
<https://doi.org/10.2514/2.4661>.
- [49] Mukhopadhyay, V., “Transonic Flutter Suppression Control Law Design and Wind-Tunnel Test Results,” *Journal of Guidance, Control, and Dynamics*, Vol. 23, No. 5, 2000, pp. 930–937.
<https://doi.org/10.2514/2.4635>.
- [50] Xing, W., and Singh, S. N., “Adaptive Output Feedback Control of a Nonlinear Aeroelastic Structure,” *Journal of Guidance, Control, and Dynamics*, Vol. 23, No. 6, 2000, pp. 1109–1116.
<https://doi.org/10.2514/2.4662>.
- [51] Waszak, M. R., “Robust Multivariable Flutter Suppression for Benchmark Active Control Technology Wind-Tunnel Model,” *Journal of Guidance, Control, and Dynamics*, Vol. 24, No. 1, 2001, pp. 147–153.
<https://doi.org/10.2514/2.4694>.
- [52] Haley, P., and Soloway, D., “Generalized Predictive Control for Active Flutter Suppression,” *Journal of Guidance, Control, and Dynamics*, Vol. 24, No. 1, 2001, pp. 154–159.
<https://doi.org/10.2514/2.4696>.
- [53] Nichols, R. A., Reichert, R. T., and Rugh, W. J., “Gain Scheduling for H-Infinity Controllers: A Flight Control Example,” *IEEE Transactions on Control System and Technology*, Vol. 1, No. 2, 1993, pp. 69–79.
<https://doi.org/10.1109/87.238400>.
- [54] Mracek, C. P., and Cloutier, J. R., “Full Envelope Missile Longitudinal Autopilot Design Using the State-Dependent Riccati Equation Method,” *Proceedings of the Guidance, Navigation, and Control Conference*, AIAA, Reston, VA, 1997, pp. 1697–1705; also AIAA Paper 1997-3767, 1997.
<https://doi.org/10.2514/6.1997-3767>.
- [55] Bennani, S., Willemsen, D., and Scherer, C., “Robust LPV Control with Bounded Parameter Rates,” *Proceedings of the Guidance, Navigation, and Control Conference*, AIAA, Reston, VA, 1997, pp. 1080–1089; also AIAA Paper 1997-3641, 1997.
<https://doi.org/10.2514/6.1997-3641>.
- [56] Vardulakis, A. I. G., “Zero Placement and the ‘Squaring Down’ Problem: A Polynomial Matrix Approach,” *International Journal of Control*, Vol. 31, No. 5, 1980, pp. 821–832.
<https://doi.org/10.1080/00207178008961085>.
- [57] Davison, E., “Some Properties of Minimum Phase Systems and ‘Squared-Down’ Systems,” *IEEE Transactions on Automatic Control*, Vol. 28, No. 2, 1983, pp. 221–222.
<https://doi.org/10.1109/TAC.1983.1103197>.

- [58] Saberi, A., and Sannuti, P., "Squaring Down of Non-Strictly Proper Systems," *International Journal of Control*, Vol. 51, No. 3, 1990, pp. 621–629.
<https://doi.org/10.1080/00207179008934088>.
- [59] Leventides, J., and Karcanias, N., "Structured Squaring Down and Zero Assignment," *International Journal of Control*, Vol. 81, No. 2, 2008, pp. 294–306.
<https://doi.org/10.1080/00207170701413843>.
- [60] Oara, C., Flutur, C., and Jungers, M., "Squaring Down with Zeros Cancellation in Generalized Systems," *Systems and Control Letters*, Vol. 92, 2016, pp. 5–13.
<https://doi.org/10.1016/j.sysconle.2016.02.019>.
- [61] Lavretsky, E., "Robust and Adaptive Output Feedback Control for Non-Minimum Phase Systems with Arbitrary Relative Degree," *AIAA SciTech*, AIAA Paper 2017-1490, 2017.
<https://doi.org/10.2514/6.2017-1490>.
- [62] Bernstein, D. S., *Scalar, Vector, and Matrix Mathematics: Theory, Fact, and Formulas*, Rev. ed., Princeton Univ. Press, 2018.
<https://doi.org/10.1515/9781400888252>